energies

MDPI

Review

Review and Analysis of Electro-Magnetohydrodynamic Flow and Heat Transport in Microchannels

Balaram Kundu * and Sujit Saha

Department of Mechanical Engineering, Jadavpur University, Raja S.C. Mallick Road, Kolkata 700032, India
* Correspondence: bkundu@mech.net.in; Tel.: +91-33-2457-2669

Abstract: This paper aims to develop a review of the electrokinetic flow in microchannels. Thermal characteristics of electrokinetic phenomena in microchannels based on the Poisson–Boltzmann equation are presented rigorously by considering the Debye–Hückel approximation at a low zeta potential. Several researchers developed new mathematical models for high electrical potential with the electrical double layer (EDL). A literature survey was conducted to determine the velocity, temperature, Nusselt number, and volumetric flow rate by several analytical, numerical, and combinations along with different parameters. The momentum and energy equations govern these parameters with the influences of electric, magnetic, or both fields at various preconditions. The primary focus of this study is to summarize the literature rigorously on outcomes of electrokinetically driven flow in microchannels from the beginning to the present. The possible future scope of work highlights developing new mathematical analyses. This study also discusses the heat transport behavior of the electroosmotically driven flow in microchannels in view of no-slip, first-order slip, and second-order slip at the boundaries for the velocity distribution and no-jump, first-order thermal-slip, and second-order thermal-slip for the thermal response under maintaining a uniform wall-heat flux. Appropriate conditions are conferred elaborately to determine the velocity, temperature, and heat transport in the microchannel flow with the imposition of the pressure, electric, and magnetic forces. The effects of heat transfer on viscous dissipation, Joule heating, and thermal radiation envisage an advanced study for the fluid flow in microchannels. Finally, analytical steps highlighting different design aspects would help better understand the microchannel flow's essential fundamentals in a single document. They enhance the knowledge of forthcoming developmental issues to promote the needed study area.

Keywords: electrokinetic flow; slip/jump; viscous dissipation; Joule heating; thermal radiation; electric fields; magnetic fields

Citation: Kundu, B.; Saha, S. Review and Analysis of Electro-Magnetohydrodynamic Flow and Heat Transport in Microchannels. *Energies* **2022**, *15*, 7017. https://doi.org/10.3390/en15197017

Academic Editor: Andrea Mariscotti

Received: 1 September 2022
Accepted: 19 September 2022
Published: 24 September 2022

1. Introduction

Microfluidics has become a more attractive research area nowadays. The major area of application is the miniaturization of the transport device, biotechnology, microelectromechanical system (MEMS), and drug delivery chip [1–5]. Electrical fields [6–11], electromagnetic fields [12], capillaries [13], bubbles [14,15], surface acoustic waves [16], electroosmotic pumps [9–11,17–19], etc. are possible design conditions. The tininess of the chemical system for sampling and handling processes using lab-on-a-chip devices [20–22] integrates into a compact form to produce mobile analysis. The main advantage of miniaturization is reducing the time and space for clinical testing in laboratories to implement heat transport and fluid motion in microchannels successfully. Micropumps and injectors [23,24], microfluidic devices [25,26], induced hydraulic pumps [27], fluid propulsion systems [28], etc., are the key applications of microfluidics.

Burgreen and Nakache [29] introduced the study of fluid flow by viewing electrokinetic effects in a very fine capillary microchannel with a rectangular cross-section. They determined the streaming potential and speed with an arbitrarily high ionic energy and

small electrokinetic circumstances. This model was developed mainly based on the electro-hydrodynamic pressure-driven flow for no-slip conditions analyzed using Navier–Stokes momentum equations. Early, several researchers investigated the effects of the liquid's ionic concentration on the solid surface's zeta potential to explore the streaming potential, speed distribution, friction factor, and volumetric flow rate in microchannels with the existence of the electrical double layer (EDL) [30–34]. The first-order slip for a pressure-driven electroosmotic flow could increase the flow rate [35]. Yang and Li [36] established a 2D model by implementing the product method and Green function approach with the help of the Debye–Hückel approximation for speed, steaming potential, volumetric discharge rate, and friction coefficient in rectangular microchannels. Later, many authors [37–43] developed their works in rectangular microchannels using the model of Yang and Li [36] to study the pressure-driven and electrokinetic effects.

Generally, the electric field due to the electroosmosis direct current (DC) causes the electroosmotic flow. In contrast, an alternating current (AC) electric field is associated with the time and frequency-dependent electroosmotic flow. Electroosmosis has a significant effect on fluid motion in the case of the AC electric field across the channels. Yang et al. [44] and Luo et al. [45] proposed a 2D model by describing the frequency and time-dependent electroosmotic flow in rectangular microchannels. Their results found that the sinusoidal electric field strongly depends on the frequency of the AC electroosmotic flow to analyze the flow pattern. Next, Yang and Kwok [46] and Kang et al. [47] introduced a time-dependent pressure-driven flow and electrokinetic slippage flow in a rectangular cross-sectional 2D channel, where the slippage and pressure-driven flow counteract the EDL effects. Consequently, an increase in the flow rate was noticed. The flow analysis and mixing in various microchannel geometries were extensively studied by Jayaraj et al. [48] with the help of different numerical simulations and experimental investigations under the electrokinetic driven flow.

The electro-magneto-hydrodynamics (EMHD)-driven micropump works with the principle of the Lorentz force, and the electric and magnetic fields imposed in microchannels are responsible for this phenomenon. The electrical current produced by the interaction of aqueous solutions sets a perpendicular magnetic field in channels. Therefore, the electromagnet or the permanent magnet can make the magnetic field. A high flow rate is achieved due to the pumping effect caused by the permanent magnet, and no moving parts are present [49–51]. Jang and Lee [52] reported the EMHD micropump acting along the flow of an electrically conducting liquid in the imposed electric and magnetic fields in the perpendicular direction. Jian et al. [53] studied the transient rotating electroosmotic flow through two infinite microparallel plates. They obtained the speed and volume flow rate by using the method of the separation of variables for both AC and DC electric and magnetic fields. Theoretically, DC EMHD micropumps have a more continuous flow speed.

However, if gas bubbles are generated, the flow speed declines. In the case of the AC EMHD micropumps, when a high current passes through the electrolyte solution, chemical reactions take place to oppose the formation of bubbles [54,55]. Recently, Xie and Jian [56] studied a transient rotating EMHD power-law fluid flow between two parallel plates in microchannels. The finite difference method was used to obtain velocity distributions with the variation of various fluid behavior indexes. Yang et al. [57] determined the thermal characteristics of EMHD flow in a two-dimensional rectangular microchannel by assessing the Debye-Huckel approximation [58]. Subsequently, the combined pressure-driven electroosmotic flow was influenced by the electric and magnetic fields. Finally, viscous dissipation and Joule heating effects are required to include in determining the velocity and temperature distributions at no-slip and no-jump conditions.

2. Fundamentals of Electrical Double Layers

Reuss [59] first conducted an experimental study of a water-clay mixture in the electroosmotic flow. Helmholtz [60] introduced the concept behind the electrical double layers formed between the charged metal surface and electrolyte solution. The EDL theory

demonstrated the flow velocity under the electrokinetic effect in capillary tubes. Then, Smoluchowski [61] extended Helmholtz's work [60] to investigate the electroosmotic speed. Gouy [62] and Chapman [63] introduced diffusive double layers on a flat surface, accumulating ions due to the Boltzmann distribution and extending it to a distance from the solid surface. For the theories mentioned above, Stern [64] proposed a model to include Helmholtz and the diffusive layer of Gouy and Chapman at the solid-fluid interface. The electrokinetic flow is a combination of electrophoresis, electroosmotic, streaming potential, and sedimental potential. However, both electrophoresis and electroosmotic flow create a motion by applying the electric field. In the electrophoresis phenomenon, charged particles travel in the stationary fluid. The electroosmotic ionized fluid moves toward the relatively more charged particles in static conditions [65–67].

When surfaces of the solid carry a net charge of the polar medium contacting with an aqueous solution, chemical associations or dissociations of ions attract or repel each other. Acids to alkynes pH (potential of hydrogen), clay, sand, the surface of the quartz, ceramics, etc. are examples of the negatively charged surface. The charged surface attracts the oppositely charged counter ions in the fluid, and the surface repels coions. The electrical double layer is formed by excess counterions closer to the interface in the solid-fluid environment. This phenomenon plays an enormous role in colloid science, polymer science, biophysics, medicine, and separation technologies, such as wastewater filtration, membrane filtration, protein, cell separation, etc., are examples of the application and importance of the electrical double layer [68,69]. The EDL develops two layers: the sterned layer (Helmholtz layer) and the diffused layer (Gouy-Chapman). The sterned layer is thin and stationery, which absorbs the opposite ions of the surface. However, the diffused layer is mobile and free to migrate from its surface; a plane forms between the sterned and diffused layers called a shear plane. When the electric field applies tangentially along the surface, the ions move due to an exerting force in the diffused electric layer. Fluid flows through the diffused layer, causing ion drag of the fluid in channels, and the motion of this type of flow is known as electroosmotic flow (EOF) [70–72]. Neale [73] stated one important electrokinetic phenomenon in the absence of the electric field where the mobile ions force the fluid to flow by applying an external pressure difference. So, EDL's mobile charge ions (counterions) move downstream and generate electrical currents in the pressure-driven flow direction. Wall [74] studied the brief history of electrokinetic flow, where the fluid movement is tangential from the charged surface. Lopez-García et al. [75] analyzed the Poisson–Boltzmann equation in electrical double layers consisting of a finite ion size in the aqueous electrolyte solution with the suspension of polarizable insulating spheres in fluids.

3. Pressure-Driven Electrokinetic Flow

Fluid delivery is a complex process in microfluidic systems when the operating pressure is very high. However, owing to their movable parts, there are complications in design and fabrication, and consequently, fatigue and fabrication involve mechanical failures [25]. Therefore, this system is not at all practicable in microfluidic applications. Alternatively, electroosmotic micropumps are favorable for creating a pumping effect in microfluidic devices as they have many advantages. There are no moving devices in electrokinetic flow systems, so the design is straightforward and easy to fabricate [76]. In addition, this type of micropumps possibly applies to a fluid with an extensive range of conductivity, and biomedical applications require this phonological aspect highly. The other beneficiary applications are pumping the solution in capillaries [77], micromachine in a chip [20], a process to control the injection of samples through microchips [78], and enhancement of the electroosmotic flow [79].

A slight pressure difference imposed in microchannels results in flow and thermal characteristics that depart from the purely electroosmotic flow [80]. However, the electroosmotic flow is always different from the conventional pressure-driven flow where the thermal transport mechanism is not the same. Velocity profiles in a channel strongly depend on the electroosmotic effect. The electroosmotic mobility and the voltage potential

in the flow direction are used to describe them. These situations affect the electroosmotically induced flow with the viscosity variation, wall zeta potential, dielectric constant, and velocity profile dependent on the Debye–Hückel parameter. The electroosmotically induced velocity highly influences the temperature distribution and heat transfer. Electroosmotically created electric current produces the Joule heat in fluids due to a volumetric heat generation. The heat generation has significantly influenced the temperature distribution and heat transfer [81,82]. Many studies were performed extensively on combined electrokinetic pressure-driven flow in microchannels for Newtonian [46,83–87] and non-Newtonian fluids [88–95]. The parametric conditions, namely, electrokinetic and pressure, electroosmotic and Poiseuille, etc., influence the velocity distribution. Electroosmotic [10] and pure electroosmotic [96] affect the velocity profile significantly with the influence of pressure and electric fields in microchannels.

4. Thermophysical Phenomena

4.1. Main Effects of Joule Heating

An electrokinetic flow in the presence of the Joule heating in microchannels was developed with axial and radial temperature gradients in channels [97]. The electrokinetic flow occurs due to volumetric heating by applying an electric field in conducting media. For example, the electric current flowing in the electrolyte solution produces heat by the ohmic resistance. However, Joule heating on the electrokinetic phenomenon depends on many factors, such as fluid specimen and channel wall [98,99]. Other factors that can cause an axial temperature gradient in microchannels and capillaries are elaborated below:

- Capillary electrophoresis and disruption in bubble formations [100].
- Thermal end effects of the electroosmotic flow occurred in cooling reservoirs by pulling the cold fluid from the inlet reservoir and pushing the hot fluid into the outlet reservoir [101].
- Non-uniform cross-section and length and non-uniform cooling or heating.
- The radial temperature gradient existed due to the radial non-uniformity of the geometry [101] and temperature variations for the conductivity effect [102].

Several researchers [81,98,103–107] studied the fully developed two-dimensional steady/unsteady electroosmotic flow and heat transport in microchannels with Joule heating to control and enhance the hybridization. They determined the temperature and Nusselt number as a function of the Joule heating parameter. Tang et al. [108] numerically analyzed Joule heating effects on heat transport in microchannels having an electrical double layer. The Joule heating affects the temperature distribution in axial and radial directions. Joule heating amplifies the fluid temperature and temperature gradient in the axial direction [109,110]. The temperature effect makes the fluid properties non-uniform; hence, the applied electric potential field's characteristics change on the flow field. The Joule heating phenomenon explains the impact of electric current flow in the electrolyte solution on the electrokinetic flow, as shown in Figure 1.

To construct Figure 1, data have been taken from the published papers [109,111]. The electric current passes through the buffer solution in the capillary, which strongly influences the Joule heating parameter. The results indicate that the presence of Joule heating increases 66.5% current compared to without Joule heating. Due to Joule heating, the temperature rises caused by current flow in the Buffer layer, which is the relationship as a function of the square of field strength in a lab-on-a-chip device [112–114]. A plug-like velocity profile was investigated for the electroosmotic flow in microfluidic channels [115]. By neglecting the thermal end effect in microchannels, the radial temperature gradient increases with the fluid temperature due to Joule heating [116–119]. Then, Mondal et al. [120] invented a combined electroosmotic and pressure-driven flow in plane microchannels considering the Joule heating aspect. However, their model analyzes when a positive Joule heating parameter is for surface heating, and the negative parameter is for surface cooling. Therefore, the temperature was an extremum at the wall and the lowest at the centerline. Tripathi et al. [121] and Noreen et al. [122] observed the electroosmotic transport of aqueous

nanofluid with Joule heating in two-dimensional microchannels. This model considered Brownian motion and thermophoresis effects on the complex waveform. Nayak et al. [123] and Shit et al. [124] developed a closed-form solution of the electroosmotic pressure-driven flow of power-law fluids through a hydrophobic microchannel. They found that the Joule heating parameter greatly influences the heat transfer in variable power-law index fluids in Bio-MEMS design aspects. In the electrokinetic flow, Joule heating effects are negligible. Such flow strongly depends on the thermal gradient, viscous force, and electric field. On the other hand, Sanchez et al. [125] discussed an interrupted flow pattern in microchannels. Vargas et al. [126] analyzed temperature-dependent viscosity, arbitrary zeta potential, and electrical conductivity with the Joule heating effect of electroosmotic mobility in microchannels.

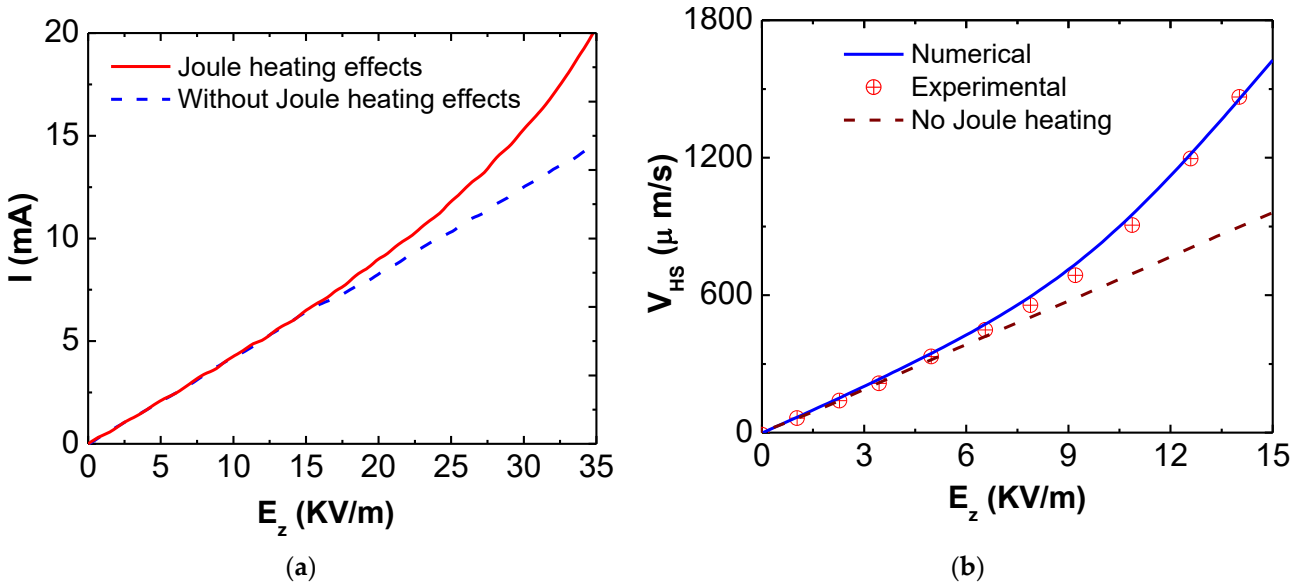

(**a**) (**b**)

Figure 1. Effects of variation of electric field on electric current and electroosmotic velocity. (**a**) I vs. Electric field E_z [109] (**b**) V_{HS} as a function of electric field (E_Z) at 15 s [111].

The Joule heating in the microcapillary amplified is at a high electric field [125]. Figure 1a shows that at 15 kV/m, 50% electroosmotic velocity increases in the existence of Joule heating compared to without Joule heating. The electric current increases the fluid temperature for the Joule heating, as shown in Figure 1b. The results show that the 66.5% current is increased in Joule heating compared to without Joule heating.

4.2. Primary Effects of Viscous Dissipation

Temperature-dependent fluid properties play a significant role in the temperature field's development, which alters the heat flux and velocity distributions. Many researchers investigated the viscous dissipation effects theoretically and experimentally [127–131]. It was found that a small value of the Brinkman number affects the bulk fluid temperature. For microchannels, the effect of the Brinkman number relates to the dynamic viscosity and increments the bulk fluid temperature. The above fact reduces the Brinkman number at the outlet by about 50% of its inlet value. It was observed that the axial variation of the Brinkman number affects the Nusselt number in microchannels and is called a "secondary effect." The temperature disparity for the viscous dissipation varies the thermo-physical properties of the fluid in microchannels. In the case of a liquid flow, the main effects of temperature-dependent fluid properties are mainly owing to the viscosity change with temperature. It notes that the temperature influences the viscosity, which modifies the velocity distribution in the channel's hot or cold parts. Viscous dissipation effects are negligible for microchannels with small hydraulic diameters. Therefore, the viscous dissipation

with the temperature-dependent viscosity revises the microchannel's temperature and velocity profiles.

Lawal and Mujumdar [132] investigated the heat transfer behavior of power-law fluids in different channel shapes. For viscous dissipation, degradation of mechanical energy into thermal energy alters the temperature distribution in a duct. Xu et al. [133] examined the effect of viscous dissipation on liquid flow in microchannels. Their study shows that pressure, velocity, and temperature strongly influence the viscous dissipation parameter (Brinkman number). Giudice et al. [128] and Nonino et al. [134,135] reported the thermally fully developed liquid flow in different straight microchannels. Their results highlight that the effects of the viscous dissipation parameter vary the temperature distribution. Many researchers [136–141] introduced the viscous energy dissipation on the fully developed laminar flow in circular ducts. They showed the effect of viscous dissipation on the axial distribution of wall heat flux for power-law fluids in a thermally developed region. Tso et al. [142] analyzed the viscous dissipation for hydro-dynamically and thermally fully developed laminar heat transfer of power-law fluids between two fixed plates. They showed that heat transfer depends on fluids' power-law index. Xuan et al. [111] studied the electroosmotic velocity with the Joule heating effect in a homogeneous capillary fluid. They developed fluorescence-based thermometry techniques to measure the liquid temperature and speed in a capillary tube. The volume flow rate increases at a high electric field by increasing the electroosmotic velocity, and consequently, it amplifies the Joule heating effect.

Koo and Kleinstreuer [143] investigated viscous dissipation effects in microtubes and microchannels. They analyzed the viscous dissipation effects on the fluid flow dependent on the Brinkman number. Morini and Spiga [129] reported scaling effects (axial heat conduction, viscous dissipation, conjugate heat transfer, wall roughness, etc.) for flows in microchannels. They demonstrated the viscous dissipation to be a function of the Brinkman number, aspect ratio, and hydraulic diameter, which are crucial parameters in determining the impact of viscous dissipation on the Nusselt number.

It can be noted that the viscous energy dissipation effect is negligible in microchannels for ordinary fluids having a small Prandtl number for a low value of hydraulic diameter [128,144,145]. Such fluids, hydrodynamic [143] and thermally fully developed [146] flow, heating, or cooling, begin at the thermal entrance length of the hot or cold regions. It starts forming the velocity and temperature boundary layers. Sheela-Francisca et al. [147] studied the effects of viscous dissipation on heat transfer at a constant wall heat flux under the steady, laminar, and both hydrodynamically and thermally fully developed pseudo-plastic fluid with a power-law index of Couette–Poiseuille flow. The importance of the effect of viscous dissipation on the fully developed forced convection in porous media for the temperature distribution in the transverse direction was studied extensively [148–150]. These works elaborate on the heat transfer characteristics and frictional heating effects. It was observed that the temperature distributions are a vital function for the Darcy friction factor and Brinkman number for both the cooling and heating processes. Recently, Mukherjee et al. [151] studied the fluid rheology and viscous dissipation effect on heat transfer in forced convection microchannels with different cross-sectional geometries. It highlights that for all the geometries, the Nusselt number inversely varies with the Brinkman number at a constant heat flux or wall temperature. The effects of viscous energy dissipation due to nanoparticle volume fractions in nanofluids were investigated by many researchers [148,152,153], and the energy dissipation, temperature distribution, and entropy generation were prominently affected due to the increase in irreversibility. Ting et al. [154] established a closed-form solution for the temperature considering with and without viscous dissipation in the energy equation. The study of the extended Graetz problem for the gaseous slip-flow with a heating section of a finite length of micropipes and parallel-plate microchannels subject to viscous dissipation and axial conduction was carried out by Haddout and Lahjomri [155].

The charge surface-induced EDL is directly associated with the flow behavior and heat transfer, such as viscous dissipation, axial conduction, etc. [156,157]. Şen and Darici [158] investigated effects on flow rarefaction, viscous dissipation, and axial conduction in tran-

sient conjugate circular microchannels. The finite difference method was employed to solve the momentum and energy equations under the slip velocity and the temperature jump boundary conditions. Lalami et al. [159] focused on evaluating the effects of viscous dissipation and Joule heating parameters for an imposed magnetic field to enhance heat transfer at the superhydrophobic surface of a nanofluid microchannel.

Figure 2 shows the influence of the Brinkman number on heat transfer in a triangular microchannel for thermally and hydrodynamically fully developed flow for power-law fluids with viscous heat generation at a constant wall heat flux [151]. At a particular Brinkman number (*Br*) and power index ($N = 0.8$) in forced convection, the shear thickening fluid has a lower development length than the shear-thinning fluid, irrespective of the thermal boundary conditions. The energy generation due to the viscous effect is more prominent in shear-thickening fluids than in shear-thinning fluids, with the same flow as illustrated in Figure 2a. Chen and Tso [138] investigated Nusselt number variation with Da for different Brinkman numbers for Newtonian and non-Newtonian fluids. They highlighted that for a Darcy factor $Da < 0.3$, the shear thickening fluid dominates over the shear-thinning fluid, while the reverse is true for Darcy factor $Da > 0.3$. The range of Darcy factor ($0.0001 < Da < 0.1$) becomes pronounced for the viscous dissipation in non-Newtonian fluids. However, Newtonian and non-Newtonian fluids have the same value when $Da = 0.2$, as shown in Figure 2b. For a small Br, viscous dissipation's effect is significant for a non-Newtonian fluid having a Da greater than 1.

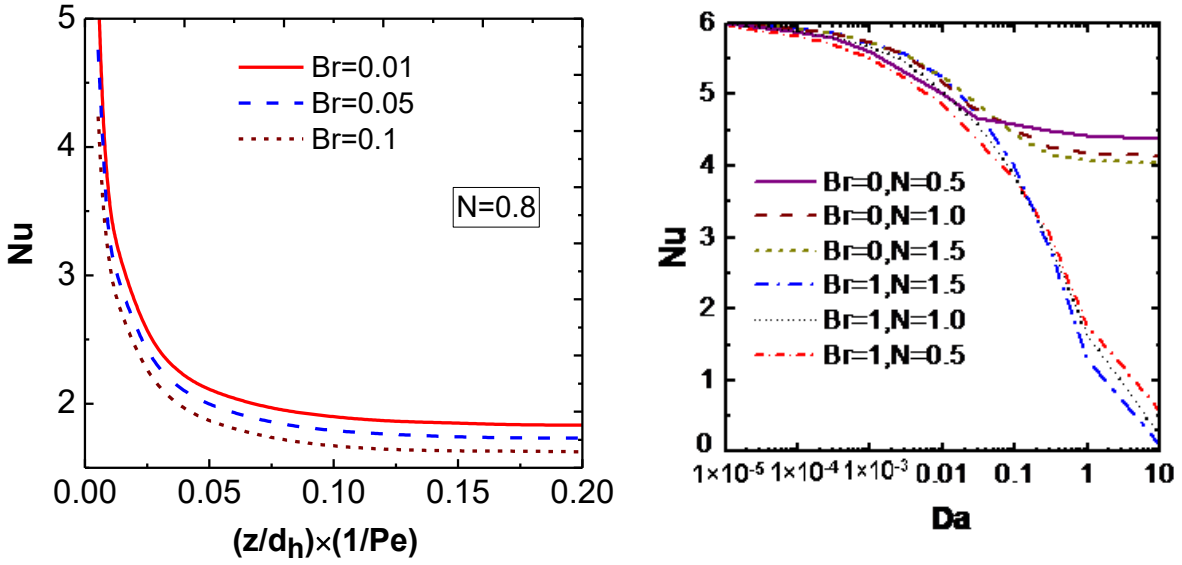

(**a**) (**b**)

Figure 2. Average Nusselt number as a function of Br and N. (**a**) *Nu* vs. (z/d_h) (1/Pe) [153] (**b**) *Nu* vs. Da [139].

4.3. Effects of Thermal Radiation

A slight temperature difference between the wall and the local temperature of the electrolytic solution largely influences the heat transfer in microchannels [160]. Notably, a temperature potential without the penetration of the incident radiation at the boundary wall of the channel employs in the involvement of the thermal aspects. It depends on the difference between the fourth power of the wall temperature and fluid temperature to approximate a linear function [161]. Nevertheless, electromagnetic interactions are present in micropumps, microelectronics, and micro heat exchangers [162], where the fluid is an essential medium for heat transfer. The molecular interaction of fluid due to the exchange of the radiation heat transfer in microchannels enhances the overall heat transfer at a constant wall temperature. Besides, nonlinear radiative term in the energy equation and conjugate

convection-radiation heat transfer at the boundary surface is more general for the heat transfer and fluid flow analysis in microchannels.

According to the Rosseland approximation [162], the radiative heat flux is $q_r = -\left(4\sigma^* \partial T^4\right)/(3k^* \partial y)$. It assumes the temperature difference in the flow system expressed a linear combination of the temperature. The term T^4 expands using the binomial theorem with the reference wall temperature in the following:

$$T^4 = T_w^4 + 4T_w^3(T - T_w) + 6T_w^2(T - T_w)^2 + 4T_w(T - T_w)^3 + (T - T_w)^4 \quad (1)$$

Neglecting the higher order terms, we have:

$$T^4 = 4T_w^3 T - 3T_w^4 \quad (2)$$

Gorla and Bakier [163] calculated the effect of radiation and natural convection on heat transfer in porous fins. The heat transfer in porous and solid fins was determined with and without radiation. Compared with both cases, it was found that the radiation parameter contributes to the heat transfer more than that of the convection solely. Lopez et al. [164] analyzed the entropy production and heat transport in a magneto-hydrodynamic nanofluid through a porous vertical microchannel with nonlinear thermal radiation. They performed the analysis numerically using the Runge–Kutta and shooting techniques. However, conjugated convective radiation involves heat transport by nonlinear-thermal radiation, viscous dissipation, and Joule heating. Kundu et al. [165] developed an appropriate model for calculating optimum heat transfer in different radiation porous fins. An extensive analysis of the Adomian decomposition method for energy transfer from a porous fin for three possible cases highlighting radiation mode was proposed by Kundu and Bhanja [166]. Recently, Das and Kundu [167] estimated the heat generation and magnetic field from the fin surface temperature information for heat transfer in radial porous fins exposed to radiation environments.

Radiation effects have significantly influenced blood flow; there are several practical applications in medical treatments, biomedical engineering, thermal therapeutic analyses, etc. Especially, the radiation effect treats muscle pain, muscle spasms, heat therapy, and permanent shortening of the muscle. He et al. [168] studied the human breast's blood flow, temperature distribution, and oxygen transport in tumors. Laser irradiation is an adjuvant method in treating cancer cells using one-dimensional pulsating flow.

In the case of polymer processing industries, the final quality product depends on heat transfer, where thermal radiation acts as a significant character in flow dynamics. In fluid flow and heat transfer, thermal radiation effects are essential for advanced thermal design systems. Under thermal radiation and ohmic dissipation, Pal and Mondal [169,170] determined the particle deposition from the development of thermophoresis. They found the transport phenomena that occurred under a magnetohydrodynamic field over a wedge. Sinha and Shit [171] reported a comprehensive analytical analysis of the electro-magneto-hydrodynamic energy transport of the blood fluid with thermal radiation. Nazeer et al. [172] deliberated the electroosmotic flow for a third-grade fluid in the presence of thermal radiation to determine the velocity and temperature distributions between two parallel plates in microchannels.

5. Hydrodynamic Slip and Thermal Jump at Boundaries

Molecular dynamic simulations usually examine the flow boundary conditions between two flat walls [173]. It always needs assumptions on the fluid motion at the solid interface. No-slip boundary condition is one of the most natural and simple boundary conditions, which denotes zero relative speed of the elemental fluid neighboring the solid surface. Slip and jump conditions represent a discontinuity of transportation variables crosswise the interface (as shown in Figure 3).

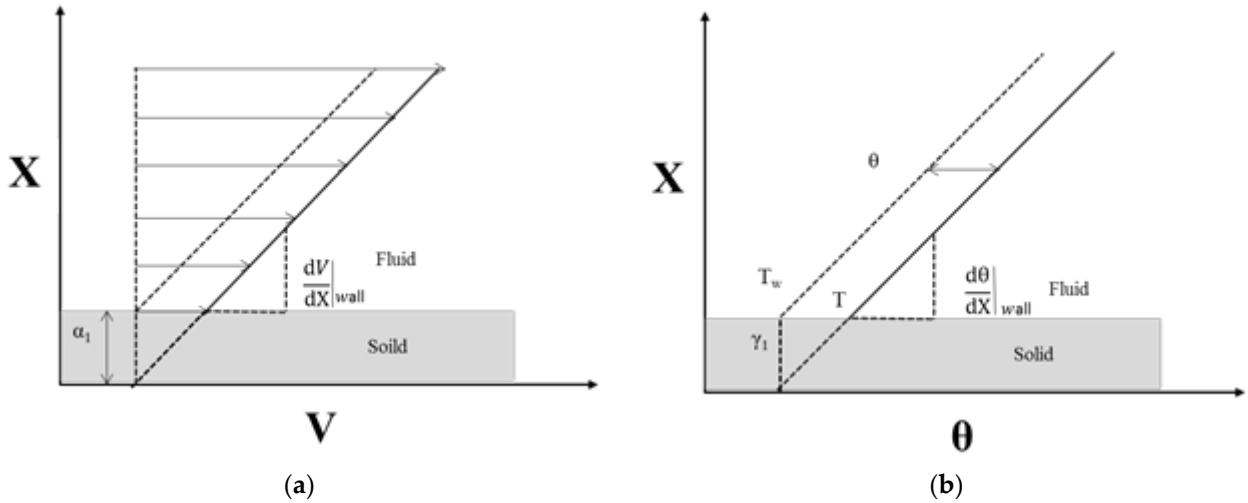

Figure 3. Slip and jump boundary conditions. (**a**) Velocity-slip boundary condition. (**b**) Temperature-jump boundary condition.

Helmholtz [174] discovered possibility of liquid slip by considering a small order of magnitude of molecular velocities. However, this situation nullifies the interfacial slip in a large-scale system. Microscale and nanoscale transport phenomena alter the macroscopic condition due to interactions of solid-liquid particles, which becomes more dominant for an elevated surface-to-volume ratio of fluid particles and for tiny length scales in the analysis. The boundary conditions are susceptible to the wetting properties, electrical properties, dissolved gases, shear rates, molecular roughness, pressure drop, friction at the solid surface, and fluid-structure near the wall [175]. The slip flow has a slip length, a non-physical quantity, and it measures the backward distance from the boundary wall where the slip speed extrapolates to zero [176]. Navier [177] proposed a first-order slip simple model to correlate tangential slip speed and shear rate at the solid interface as follows:

$$V = -\alpha_1 dV/dX \tag{3}$$

where α_1 is a dimensionless slip parameter, V is a dimensionless slip speed, and X is a dimensionless coordinate normal to the wall surface shown in Figure 3a. Poisson suggested the temperature jump similar to Equation (3) as:

$$\theta = -\gamma_1 d\theta/dX \tag{4}$$

where γ_1 is a non-dimensional first-order temperature jump parameter and X is a non-dimensional coordinate normal to the wall illustrated in Figure 3b.

It highlights that Navier slip conditions still exist when the local shear deformation rate at the interface is lower than the critical shear rate. The deviation of the fluid flow from the continuum depends on the Knudsen number (Kn) [96]. It is defined as the ratio of the mean free path (λ) of molecules to the characteristics length (dh) of the channel, and, reasonably, the flow regime of the Knudsen number varies from 0.001 to 0.1. In the slip flow regime, the solution of the momentum Navier–Stokes (N-S) equation needs to modify with slip conditions at the solid-liquid interface. Thompson and Troion [173] theoretically studied the degree of slip at the boundary. It depends on several interfacial parameters, including the strength of solid-liquid coupling, rarefaction, thermal roughness of the interface, etc. Two types of slip are analyzed for the Newtonian fluid flow: true slip and apparent slip. A true slip occurs for the actual slipping of the fluid molecules over the solid surface, whereas the apparent slip opposes the true slip. It refers to fluid sliding over a less viscous layer [178,179].

For non-Newtonian fluids, polymer dynamics explain the slip flow velocity, whereas, for Newtonian fluids, the shear-rate-dependent flow in channels [180] determines it ex-

perimentally. In the above cases, analyzing the flow in microchannels is very complex because the shear rate is a function of viscosity. A moving bulk fluid flow over the polymer grafted surface was critically analyzed in three slip regimes [178]—the bulk polymer was unchanged from the surface polymer in no-slip conditions with lower shear rates. At the critical shear rate, the detachment of the bound polymer begins from the scratched surface polymer, and consequently, a sliding between bulk and surface layers occurs. The slip reaches a peak upon complete dissociation until it becomes a constant. Then, the bulk flow effectively disconnects from the surface polymer layer.

Maxwell [181] first introduced the slip phenomena in gas molecules on a solid surface based on the kinematic theory of monoatomic gases: molecules, modeled as a rigid sphere, always strike and reflect from the solid surface and incessantly collide with each other. A hydrophobic surface absorbs and reflects entirely. For this surface, it assumes that the surface absorbs σ_v of the molecules due to the unevenness of the wall and remits with a velocity relative to those in still gas at the thermal wall state. The remaining molecules $(1-\sigma_v)$ reflect from the wall. Therefore, the non-dimensional coefficient σ_v is termed the tangential momentum accommodation coefficient. When σ_v = 0, it indicates the tangential momentum of incident molecules equal to reflected molecules and momentum transmitted to the wall vanishes. This type of reflection is known as specular reflection. However, the gas molecules transmit all their tangential momentum to walls for σ_v = 1. This type of reflection is termed diffuse refraction. The slip velocity can be expressed mathematically as:

$$v_{slip} = v_{gas} - v_{wall} = \frac{2-\sigma_v}{\sigma_v}\lambda(\partial v/\partial n)_w + \frac{3}{4}\frac{\mu}{\rho T_{gas}}(\partial v/\partial n)_w \quad (5)$$

where λ is a mean free path and $(\partial v/\partial n)_w$ is a velocity gradient normal to the wall. Smoluchowski [182] experimentally verified the hypothesis that the first-order temperature jump γ_1 relates to the mean free path λ. Like a slip velocity, the fraction σ_T is the molecules reflected from the wall and the wall adjusts their mean thermal energy. Therefore, the molecules reflect from the walls due to the temperature difference between the fluid and adjacent to the wall. The other fraction of molecules $(1-\sigma_T)$ reflects with their incident thermal energy. The dimensionless σ_T represents the thermal accommodation coefficient. From the energy balance at the wall, the temperature jump condition was as below:

$$T_g - T_w = \left(\frac{2-\sigma_T}{\sigma_T}\right)\left(\frac{2\gamma}{\lambda+1}\right)\left(\frac{\lambda}{\mathrm{Pr}}\right)\left(\frac{\partial T}{\partial n}\right)_w \quad (6)$$

where $\mathrm{Pr} = \mu c_p/k_T$ is the Prandtl number.

Several researchers have engaged to develop the slip flow model by extending to the continuum model. Recognizing the Taylor series expansions, the boundary conditions were derived by Deissler [183] as given in Equations (7) and (8), and the boundary conditions recommended by Karniadakis et al. [184] are in Equations (9) and (10):

$$v|_{x=0} = \left(\frac{2-\sigma_v}{\sigma_v}\right)\lambda\frac{\partial v}{\partial x} - \frac{9}{8}\lambda^2\left(\frac{\partial^2 v}{\partial x^2} + \frac{1}{2}\frac{\partial^2 v}{\partial y^2} + \frac{1}{2}\frac{\partial^2 v}{\partial z^2}\right) + v_c \quad (7)$$

$$T|_{x=0} - T_w = \left(\frac{2-\sigma_T}{\sigma_T}\right)\left(\frac{2\gamma}{\gamma+1}\right)\frac{\lambda}{\mathrm{Pr}}\frac{\partial T}{\partial x} - \frac{9}{128}\lambda^2\left(\frac{177\gamma-145}{\gamma+1}\right)\left[\frac{\partial^2 T}{\partial x^2} + \frac{1}{2}\frac{\partial^2 T}{\partial y^2} + \frac{1}{2}\frac{\partial^2 T}{\partial z^2}\right] \quad (8)$$

$$v|_{x=0} = \frac{(2-\sigma_v)}{\sigma_v}\left[\lambda\frac{\partial v}{\partial x} + \frac{\lambda^2}{2}\frac{\partial v^2}{\partial x^2}\right]_{x=0} + v_c \quad (9)$$

$$T|_{x=0} - T_w = \frac{(2-\sigma_T)}{\sigma_T}\left(\frac{2\gamma}{\gamma+1}\right)\frac{1}{Pr}\left[\lambda\frac{\partial T}{\partial x} + \frac{\lambda^2}{2}\frac{\partial^2 T}{\partial x^2}\right]_{x=0} \quad (10)$$

where γ is the specific heat ratio. The value of momentum and thermal accommodation coefficients ranges from 0 to 1.

Interfacial boundary conditions are not only the fundamental importance but also the physical modeling of modern applications involving MEMS, biology systems, colloid chemistry, etc. The fluid slip has a vital role in reducing flow resistance in microchannels; it associates with increased permeability of the porous medium. Microscale pumps use in both drug delivery and microelectronic cooling with varying degrees of slip [185,186]. In gaseous flow, the slipping phenomenon is crucial for the hard-disk driver at the head-disk interface. The kinetic theory framework describes the gas-solid slip. The existence of thermal resistance at the boundary or the equivalent temperature discontinuity is for the interfacial transport of phonons. Sound typically travels at a velocity at an order of magnitude higher in solids compared to that in liquids. An abrupt change in molecular structures mismatches acoustic properties from one medium to another by the large impedance [187–189]. The effect of the temperature jump reflects the energy disruption. By molecular dynamic simulation, the amount of temperature jump depends on the surface roughness and wettability of the surface. Kapitza [190] first discovered the temperature jump at the solid-liquid interface for superfluid helium at a temperature of 2 K.

Gad-el-Hak [191] studied a range of slip flow defined in the rarefied regime. When the Knudsen number is 0.1, the Navier–Stokes (N-S) equation is still valid. They are related to the Maxwell and Smoluchowski boundary conditions, which deal with the hydrodynamic slip and the thermal jump at the wall surface. Taylor's series expansion shows that velocity and temperature at the solid wall are directly proportional to their transverse gradients. When the Knudsen number increases to 0.1 or slightly above, a higher-order term of Taylor's series expansion is necessary. Colin et al. [192] studied the second-order slip flow in rectangular microchannels. They have found that the first-order slip is not valid at a higher value of the Knudsen number. Thus, the difference between the predicted model and the experimental data becomes significant. An increasing rarefication effect decreases outlet pressure, which significantly influences the difference between the no-slip and first-order slip or second-order slip from the experimental data.

Colin [193] analytically investigated the steady gaseous flow in rectangular microducts, satisfying the second-order slip boundary conditions. The mass flow rate is lower for no-slip states. However, a square cross-section of a microduct shows a prominent effect of the second-order slip. An increasing aspect ratio of geometry significantly differs between the second-order and first-order slip models. The maximum deviation of 13% (difference between the second- and first-order slips) occurs in an aspect ratio with the 0.08 Knudsen number. Some works for the velocity distribution [194] and the temperature distribution [195,196] were analyzed for steady laminar flow with the first-order slipping case in ducts with an arbitrary aspect ratio and Knudsen number in the absence of electrokinetic effects.

At a relatively low pressure, the pressure drop along the channel is a fraction of the absolute pressure, especially for long ducts. However, for the constant temperature wall condition, a change in density along the duct occurs, and subsequently, the variation of momentum flux is due to the compressibility effect [197]. For the density difference, solving N-S equations is complicated. For ease of analysis, the isothermal wall and fully developed flow to determine the velocity and pressure drop in rarefied gas flow through rectangular and annular ducts with the first-order slip are considered.

Slip/Jump on Electrokinetic Flow

The physical aspects of the electrokinetic phenomenon for the velocity slip need to comprehend the design and operation of microfluidic flow in MEMS. Yang and Kowk [198] and Park and Kim [199] established the fully developed laminar electrokinetic oscillating flow subjected to an external electric field with Navier's first-order slip condition. The results showed that actual and apparent zeta potentials differ by at least an order of magnitude for an electrolytic solution with the 1% slip. Later, Yang and Kwok [35,46] and Marcos et al. [200] introduced a time-dependent pressure-driven and electrokinetic

first-order slippage flow in a rectangular-cross section by developing a 2D model, where the slippage and the pressure-driven characteristics counteract the effect of the EDL.

In the above context, the liquid slip occurs over the hydrophobic surface [201] for the significant zeta potential in electrolyte solutions. By combining electrokinetic and pressure-driven with the first-order Navier's slip condition, the oscillating flow in rectangular [202–207] and circular [208–210] microchannels increased the flow efficiency. It was found that 10% slip length in a specific electrolyte solution enhances the flow rate by 20%. On the other hand, the voltage drop in an electrolyte solution reduces to 90%, having a 1% slip length and 99% for the 10% slip length.

Zhu et al. [211] analytically studied the thermal behavior with asymmetric heat fluxes in microchannels under the boundary conditions of the second-order slip velocity and temperature jump. Hooman et al. [212] determined a closed-form solution based on the perturbation technique for the hydro-dynamically and thermally fully developed flow through microchannels and micropipes. Their analysis employed the first-order velocity slip and the temperature jump to obtain the effect of viscous heating and variable thermal conductivity on thermal conditions. Hooman [213,214] investigated heat transfer and fluid flow analyses for hydro-dynamically and thermally fully developed rectangular microchannels. Their investigations focused on determining the effects of first-order slip and temperature jump on heat transfer rate. Ranjit et al. [215] analyzed the two-layer propulsion-driven flow in a varying microchannel with the first-order velocity slip and temperature jump at boundaries. They showed that viscous dissipation, Joule heating, and entropy generation strongly influence the velocity and temperature fields. Jiang et al. [216] experimentally analyzed a combined pressure-driven electroosmotic flow in T-shape microchannels.

6. Theory of Electro-Hydrodynamic (EHD) Flow

Electrohydrodynamic flow interacts with the charged particles in an electrolytic solution to enhance fluid flow rate. Such a fluid's electrical conductivity varies from an excellent insulator to a highly conducting fluid. Electrohydrodynamic interactions occur in the metrology field where the charge distribution in the air is very significant (thunderstorm). In the case of surface physics, the charge distribution at the interface is substantial [217]. The electrohydrodynamic pump is more advantageous than the conventional pump because there is no moving part.

Some critical applications of electrohydrodynamics are polyelectrolytes [218] and DNA molecules and proteins [219]. These are examples of polyelectrolytes. Electrohydrodynamic spraying techniques [220] are other applications in which liquid menisci deforms under the electric field [221]. In EHD pumps, the pumping motive source is the Coulomb force, where the zeta potential produces the fluid [222]. The organic solution's thermal conductivity is very low (ethanol, methanol, etc.). However, it is useful in medical and biological applications because it has high ionic aqueous solutions [223].

6.1. Effects of Electric Fields on Rectangular Microchannel Flow

The literature on microchannel flow has already reported many analytical and numerical studies of mixed electrokinetically pressure-driven flows and heat transfer behavior in Newtonian fluids through rectangular microchannels for combined effects of various factors with no-slip [30,38,40,44,81,84,103,106,224–229] and first-order slip [199,206,230,231] states.

The visco-elastic differential equations were derived using shear-thinning viscosity, normal stress, memory effects [232,233], saliva [234], fluids with simplified-Phan-Thien-Tanner (sPTT) [235,236], and nonlinear elastic-Peterlin (FENE-P) for microchannel flows. Analytical solutions were developed for microchannels' combined electroosmotic and pressure-driven flow to determine velocity and temperature fields with no-slip [237–248] and first-order slip [249–251]. Their investigations have described the sPTT model with the linear kernel and FENE-P model-based kinetic theory. Mukherjee et al. [252] studied the electroosmosis phenomenon during fluid flow between two parallel plate microchannels having finite-size ions. They considered the Navier slip conditions at the channel wall

by imposing an electric field. Bandopadhyay et al. [253] determined the velocity for time-periodic electroosmotically driven viscoelastic fluids for the modulated charge surface in microchannels. The time-dependent oscillating flow in rectangular microchannels in the presence of EDL was examined by Yang et al. [254] and Peralta et al. [255]. The dispersion coefficient described in the sPPT model of a passive solute in combined effects of hydrodynamic slip and non-uniform charge in a parallel plate microchannel was studied by Arcos et al. [256] and Hoshyargar et al. [257]. The fully developed flow in a polyelectrolyte layer grafted in a slit microchannel was deliberated by Sadeghi et al. [258] in the unsteady solute dispersion.

The augmentation in mixing in microdevices is not suitable for the low Reynolds number. In this case, the mixing velocity is relatively small; therefore, additional forces are required, such as an electrical and rotational actuation [45,259–261]. For the importance of a lab-on-a-CD (compact disk) type device in biological and medical systems, the system analysis is done based on the Coriolis force components rotating about an axis perpendicular to the axis in microchannels [262,263]. Velocity profiles for the transient electroosmotic flow of Maxwell fluid in rotating [264] and rectangular [265,266] microchannels were systematically investigated at the no-slip boundary condition. Several authors [267–274] studied analytical solutions for the transient electroosmotic flow in rotating microchannels. Siginer et al. [275] analyzed the velocity and temperature distributions in unsteady rotating rectangular microchannels using the second-order slip without electrokinetic phenomena. Shit et al. [276] examined the rotating electroosmotic Newtonian fluid in a gradually varying shape of a microchannel with a high zeta potential using the finite difference method. The rotating combined electroosmotic and pressure-driven flow of power-law fluids in two infinitely microparallel plates at a high zeta potential was developed by Yavari et al. [277] and Xie and Jian [278]. By applying the finite difference method, they computed the flow field's velocity profile, which depends on the power-law behavior index, Coriolis force, and thermal physical parameters.

As most bio-fluids, such as blood, shampoo, foams, polymer melts, etc., are under electroosmotic actions, the accurate analysis of thermal characteristics of fluids is required to design lab-on-a-chip devices. Previous studies showed that the electroosmotic fully developed flow behaves similar to non-Newtonian power-law fluids [89,91,92,94,156,279–285]. A Poisson–Boltzmann equation [93,206] determines the velocity profile of fully developed flow in micro (or nano) channels predict electrokinetic effects. The available literature highlights the analysis connected with the thermal transport of mixed electroosmotic and pressure-driven fully developed flow between two parallel plate microchannels subject to constant heat flux and wall temperature with Joule heating and viscous dissipation effects [76,107,286]. Furthermore, Dey et al. [287] studied an extended steric impact along with mentioned conditions. Based on the high zeta potential, several researchers investigated the velocity and temperature distribution for the combined pressure and electroosmotically driven flow in microchannels [104,120,288–291]. Shojaeian and Koşar [292] presented the perturbation technique to determine the heat transfer for hydrodynamically fully developed and thermally fully developed power-law fluids for the flow in the parallel plate and circular microchannels under the constant heat flux and slip boundary conditions. Saravani and Kalteh [293] investigated the effect of the nanoparticle volume fraction and first-order velocity slip at the boundary to study the thermal characteristics of nanofluid flow in a microchannel. Gaikwad et al. [294,295] showed the combined effects of viscous dissipation and Joule heating, including slip effects on heat transfer with the principle of entropy generation in asymmetrically heated microchannels. Nayak et al. [123] examined the electroosmotic pressure-driven flow of non-Newtonian power-law fluids in a hydrophobic channel. They derived a closed-form solution for the flow velocity and heat transfer with Joule heating and radiation effects.

Many researchers [296,297] focused on the combined pressure-driven electroosmotic flow with axial conduction, viscous dissipation, and Joule heating effects. They determined heat transfer in two semi-infinite regions in the microchannel at a low Peclet number. The periodic flow [298] in microfluidic devices plays a vital role in EDL effects. Hosh-

yargar et al. [299] analyzed the osmotic flow of an electrolyte solution for a uniform charge surface in rectangular microchannels by applying the finite element method. Zhu et al. [300] evaluated power-law fluids' velocity, friction factor, and volumetric flow rate through a periodic rectangular microchannel. Jimenez et al. [301] analyzed the two-dimensional electroosmotic flow of the Maxwell fluid with a high zeta potential in rectangular microchannels. They reported the oscillating behavior of the velocity profile. Later, Wang et al. [302] extended the work [301] for the first-order velocity slip at the solid-liquid interface for the rotating electroosmotic flow in a parallel plate microchannel. A combined steric and viscoelectric effect on a hydrodynamic-electroosmotic flow in a microchannel under the high zeta potential was examined by Jimenez et al. [303]. Xing and Jiang [304] focused on steric and first-order slip effects in soft nanochannels for electroosmotic flow. Based on the lubrication theory, Ramos et al. [305] presented a perturbation analysis for the non-isothermal electroosmotic flow in rectangular microchannels to obtain the dependency of thermal parameters. Koushik and Chakraborty [306] and Jiang et al. [307] presented a start-up transient 2D flow of viscoelastic fluid by developing an Oldroyd-B model. However, the rotational flow [308] in rectangular microchannels was analyzed from an extended work [306]. Using the finite difference method, Liang et al. [309] explored the rotational electroosmotic flow of the Oldroyd-B fluid in microchannels with the first-order velocity slip.

The electroosmotic first-order slip flow of the fractional second-grade fluid in a parallel plate microchannel was investigated by Wang et al. [310] and Dey and Shit [311]. Huang and Yang [312] studied the electrokinetic streaming potential in squeezing liquid flow to evaluate the flow velocity and energy conversion efficiency. Matin [313] studied the electroviscous effects of the EDL at the solid-liquid interface on the fluid flow and heat transfer between two parallel plates in microchannels to portray the impact of the velocity slippage, viscous dissipation, and Joule heating. Sadeghi et al. [314] evaluated the Nusselt number for the thermally fully developed mixed electroosmotic pressure-driven flow in rectangular microchannels maintained at a constant wall heat flux or wall temperature in viscous dissipation and Joule heating conditions.

Zhao et al. [315] established the Buongiorno model of nanofluid flow and heat transfer between two parallel plates' microchannels. The influence of Joule heating on heat transfer in a slowly varying microchannel having Navier slip was reported by Mondal and Shit [316]. This flow system with the no-slip situation was analyzed by Nadeem et al. [317]. Using the finite volume method, Bag and Bhattacharyya [318] studied the electroosmotic flow of non-Newtonian fluid. They found a significant effect on the rheological behavior of flow patterns. Chen and Jian [319] and Qi and Ng [320] deliberated the rotating electroosmotic flow in the microchannel in detail. They obtained analytical solutions for the electrokinetic energy conversion efficiency, streaming potential, and velocity in a microparallel channel, considering the rotational influence. The electroosmotic flow of power-law fluid in curved microchannels was investigated by Nekoubin [321]. He showed that at a high zeta potential, the reduction in flow behavior index increases the axial velocity and volume flow rate. Kamali et al. [322] investigated the effect of roughness on the 2D electroosmotic flow in a flat microchannel using the Lattice–Boltzmann method (LBM). Sadek and Pinho [323] studied the oscillating flow with small amplitude by adopting the multimode upper convected Maxwell (UCM) model of viscoelastic fluid in microchannels.

6.2. Effects of Electric Fields on Flow in Non-Rectangular Microchannels

Rice and Whitehead [324] scrutinized a fully developed electrokinetic flow for the Newtonian fluid in a narrow cylindrical capillary. Using the Bessel function of the first kind, they obtained the velocity and streaming potential with the Debye–Hückel linearization approach at a low zeta potential. Later, Levine et al. [325] extended the work of Rice and Whitehead [324] by a semi-analytical analysis with a high zeta potential. A transient electroosmotic flow in a cylindrical capillary was analyzed by Kang et al. [326], solving a complete Poisson–Boltzmann equation for anarbitrary zeta potential. After that, many researchers concentrated on the heat transfer characteristics in microtubes.

Maynes and Webb [327] investigated the electroosmotically generated convective transport in a parallel plate and circular microtube subject to maintaining a constant heat flux and wall temperature. Najjaran et al. [328] investigated the induced charge electrokinetic phenomenon to intensify microchannels' convective heat transfer and mixing process. Liechty et al. [329] examined the hydrodynamically and thermally fully developed electroosmotic-microtube flow for the high zeta potential at the wall. They reported that the wall zeta potential and Joule heating significantly affect the heat transfer. Some studies involved the fully developed electrokinetic analysis for the heat transfer in circular shape microchannels with constant heat flux and wall temperature at no-slip/jump boundary conditions [80,143,146,330,331]. These works analyzed the hydrodynamic-electrokinetic driven flow in an annulus to evaluate the electrical potential and velocity profile [85,332–334].

Most studies have addressed microchannels' electrical double layer and fluid interaction under steady-state conditions. Some studies have concentrated on the time-dependent phenomenon without the electrical double layers in flow through microchannels. The time-dependent electrokinetic flow in microchannels by applying an electric field was reported with the no-slip [335–337] and first-order slip [210]. Zhao et al. [338] reviewed Oldroyd-B fluids in a straight pipe with a circular cross-section. The blood flow in a tapered microvessel was demonstrated by Prakash et al. [339], whereas Hsu et al. [340] engaged the steady-state analysis in elliptical microchannels. Deng et al. [341] concentrated on the two-layer mixed electroosmotic pressure-driven flow with power-law fluids in circular microchannels. A mathematical model for peristaltic pumping flow in a wavy microchannel with the first-order velocity slip and first-order temperature jump was developed by Prakash et al. [342]. Narla et al. [343] conducted the transient 2D flow analysis in wavy microchannels under low zeta potential. It is noteworthy that the electroosmosis phenomenon improves the fluid motion in microchannels.

Ren and Li [344] and Masilamani et al. [345] examined the electroosmotic flow at a high zeta potential in cylindrical microchannels. Chakraborty [346], Azari et al. [347], and Matías et al. [348] determined a closed-form solution of thermally fully developed flow in microtubes. They focused mainly on combined influences of electroosmotic flow, imposed pressure gradient, and Joule heating effects with no-slip conditions. In contrast, Azari et al. [349] paid attention to the Graetz problem in a circular microchannel. Chang et al. [350] investigated a perturbation technique for the electroosmotic microtubes with slightly corrugated walls. Monazami and Manzari [351] developed a finite element method-based analysis for the two-dimensional pressure-driven electroosmotic flow in a square microchannel. Electroviscous effects in the two sections with different zeta potentials on the pressure-driven flow through a microchannel were determined by Cetin et al. [352]. Using the finite difference method, Bharti et al. [353] studied electroviscous effects in a cylindrical microchannel with a non-uniform zeta potential in power-law fluids. Deng [354] attempted the analysis of the electroosmotic flow in power-law fluids at a high zeta potential in a cylindrical microchannel. This study shows that the flow behavior index, zeta potential, and electrokinetic width play a significant role in velocity and volumetric flow rate distributions.

Sun et al. [355] analyzed the combined electroosmotic and pressure-driven flow considering the finite Debye length through an insulated sharp straight microchannel under a direct current. Moghadam [356] developed a solution for AC electrokinetic flow in circular microchannels. The electroosmotic mixing flow in an optimized geometry was studied numerically by Basati et al. [357]. In a time-periodic electric field, they determined the flow velocity using the combined Green function and modified Bessel function of the first kind. Peralta et al. [358] deliberated the time-periodic electroosmotic flow through an annulus microchannel for the Maxwell fluid. Cho et al. [359] reviewed the electrokinetically driven flow in microchannels with wavy surfaces. In contrast, Guo and Qi [360] established an analytical method for electroosmotic fractional Jeffrey's fluid flow in microchannels. Cho et al. [361] performed microchannels' combined electroosmotic and pressure-driven flow characteristics. The results highlight that the flow characteristics depend on the flow behavior index of the non-Newtonian fluids, as described by the power-law model.

Ng and Zhou [362] observed the dispersion of a neutral non-reacting solute under the combined effect of hydrodynamic slip and non-uniform charge in a circular microchannel. An electroosmotic-oscillatory flow of power-law fluid in hydrophobic slit microchannels was demonstrated extensively by Banos et al. [363]. They determined the fluid rheology and mass transport with the first-order slip. Karabi and Moghadam [364] interpreted the effects of non-Newtonian electroosmotic flow in a semi-microtube under the influence of a constant wall heat flux. Peralta et al. [365] studied the asymmetric zeta potential for the electroosmotic-viscoelastic biofluid flow in parallel plate microchannels, where an electric field was applied to pulsatility for fluid motion. The Joule heating effect strongly influences the thermal behavior of electroosmotic flow in circular microannulus [366] and elliptical microchannels [367]. Srinivas [368] used the electroosmotic flow of a power-law fluid in an elliptical microchannel and compared the flow characteristics with that in the circular microchannel. Yavari et al. [366] showed that the heat transfer at constant heat flux depends on the ratio of annulus radii in the flow field. Using the Lattice-Boltzmann method (LBM), Kamali et al. [322] investigated a dynamic 2D model for the electroosmotic flow, taking an overlapped EDL. Zhao et al. [369] investigated a microtube's electroosmotic nanofluid flow thermal transport characteristics. This study concluded that the first-order slip condition and nanoparticle volume fraction have a significant role in heat transfer augmentation. Due to the rapid development of electroosmotic flow in circular microchannels, many researchers have devoted a lot of effort to studying various non-Newtonian flow models, such as Erying fluid [370,371], binary fluid [372,373], and Bingham fluid [374–376] with/without slip boundary conditions. Rojas et al. [377] analyzed the electroosmotic-pulsatile fluid flow in circular microchannels with slippage at the wall surface.

7. Theory of Electro-Magneto-Hydrodynamic (EMHD) Flow

Magnetohydrodynamics (MHD) is one of the key areas, thus attracting many researchers. It is the study of flow for electrically conducting liquids in the presence of electric and magnetic fields [378]. Ritchie [379] studied liquid flow due to the magnetic field imposed in the transverse direction. In general, an electro-magnetohydrodynamic (EMHD) micropump works based on the Lorentz force exerted. The Lorentz force is a motive to pump a medium, aqueous solution in biological applications. The MHD micropump has remarkable advantages, such as flow control, flow pumping, thermal reactor, microcooler, fluid mixing, no moving part, low operation voltage, forward and reverse flow, chemical process, simple fabrication, etc. [50,52,380–382]. The MHD pump not only works for the flow control and pumping, but also induces the complex secondary fluid, producing chaotic convections and help of mixing [383,384] and string [51,385,386]. Applying electromagnetic force to the pump to control the flow is a super specialty of microfluidics, which deals with converting electromagnetic energy into mechanical energy [387,388].

The magnetohydrodynamic flow involves the interaction of free currents and magnetic fields in a fluid. Magnetohydrodynamics has many practicable applications in science and engineering, namely pumping of liquid metals, orientation and confinement of scorching ionized gases, electric power generation from ionized gases, fission reactions, and space propulsion resulting from the electromagnetic acceleration of ionized gases. The electric field has been employed in electrophoretic separation, portability, reduced power consumption, less waste material, electroosmotic pumping, and dielectrophoretic trapping [381,389,390]. Even a tiny scale improves the sensitivity as an example of a micro total analysis system (μTAS) which aims to contribute to multiple laboratory systems in one single-handed device [391]. Such a system could remodel chemical analysis in environmental monitoring, genomics, medical diagnostics, and drug delivery. Many microfluidic devices are often essential to propel fluids from one portion to another for controlling, separating, mixing, etc. [392]. Thus, the electrostatic force uses to flow around the microchannel uniformly. However, it may be challenging to have a high flow rate in the case of high electrical potential, and the solution becomes affected significantly due to generating heat.

The advantages of the external magnetic field in microfluidic channels are due to the absence of direct contact with the fluid. In biochemistry, biomolecules can be isolated from a sample using a small magnet; therefore, they are recovered by an external magnetic field. In this case, the magnetic force is never utilized by manipulated magnetic objects, such as magnetic particles, magnetically labeled cells, plugs of ferrofluids inside microchannels, etc.

Effects of Both Electric and Magnetic Fields

It has already been highlighted that a combined electro-magneto-hydrodynamic (EMHD) effect potentially develops an EDL to increment the flow rate in microchannels. Jang and Lee [52] experimentally studied that the flow rate enhances substantially using micropumps at a low magnitude magnetic field. Verardi et al. [385] investigated a rectangular microchannel for the two-dimensional magnetohydrodynamic flow to analyze using the finite element method (FEM). Electromagnetohydrodynamic transport characteristics on the hydrodynamically and thermally fully developed flow on heat transfer under a combined influence of force and pressure gradients in microchannels have been reported in the existing literature [393–396]. The Debye–Hückel approximation with the no-slip velocity and no-jump temperature boundary conditions has been employed at a constant wall temperature and heat flux conditions. Using the separation of variables, Zhao et al. [397–399] investigated the MHD flow of generalized Maxwell fluids in a rectangular micropump under the AC electric field. In another study, the finite-size ion (steric) affects the streaming potential and heat transfer on an electrokinetic flow with viscous dissipation, and Joule heating was discussed for power-law fluids [400,401] and Newtonian fluids [402] under the influence of superimposed magnetic fields.

Jian et al. [53] studied the effect of transient EMHD micropumps in two infinite parallel plates. The flow depends on the Lorentz force for the AC and DC EMHD pumps. Subsequently, Ganguly et al. [403] analyzed the thermally developing mixed electroosmotic transport and pressure-driven nanofluid flow with the viscous dissipation and Joule heating in a microchannel under the imposition of both the electric and magnetic fields. They estimated velocity, temperature, and Nusselt number in the presence of the volume fraction of dispersed nanoparticles and particle agglomerations with the no-slip speed and no-jump temperature boundary conditions. Under the combined influences of electric and magnetic fields in non-conducting Phan-Thein-Tanner (PTT) fluids, many investigations were involved in determining the distribution of velocity, temperature, and entropy generation [396,404]. The effect of fluid rheology on rotating electroosmotic flow was discussed for Jeffrey fluid by Liu and Jian [401]. The power-law fluid was studied by Patel et al. [405] in soft (Polyelectrolyte grafted) microchannels. Li et al. [406] analyzed Jeffrey fluid's transient AC electroosmotic flow in a soft nanochannel. Hoshyargar et al. [407] determined the velocity and concentration profiles in fully developed electroosmotic flow in slit microchannels occurring dispersion effects. After that, Sun et al. [408], Yang et al. [57], Sarkar et al. [409], and Qi and Wu [410] presented the rotating electroosmotic and pressure-driven flow in rectangular microchannels. Their analyses adopted the Debye–Hückel approximation to estimate the velocity and temperature distributions at a constant wall temperature and wall heat flux in the electric and magnetic fields. Vargas et al. [411] combined electroosmotic-magnetohydrodynamic flow for the influence of hydrodynamic dispersion in a parallel plate microchannel. Their results showed that the varying zeta potential induced pressure gradient modifies the flow field in the channel.

Next, an attempt was made on the electro-magneto-hydrodynamic and electrokinetic effects in a micropump. Mirza et al. [412] theoretically studied a transient electro-magneto-hydrodynamic two-phase blood flow through a capillary vessel, existing the pressure gradient, joule heating effect with constant heat flux, and no-slip boundary condition. Their study ignored the impact of viscous dissipation, EDL, and imposed electric and magnetic fields, determining the thermal transport characteristics of fluid flow through cylindrical microchannels. Using the Debye–Hückel linearization at a low zeta potential, Xie et al. [413] determined the velocity, temperature distributions, and Nusselt number under the constant

wall temperature, viscous dissipation, and Joule heating with the no-slip and no-jump boundary conditions. Later, Chen et al. [414] extended Xie et al.'s work [413] for the first-order velocity slip and no-jump temperature at the boundary. Zhao et al. [415] calculated the heat transfer for thermally fully developed nanofluid flow in porous microtubes at a constant heat flux. They accounted for a small wall potential to determine the velocity and temperature distributions by applying the electric and magnetic fields. They also showed that the Nusselt number and entropy generation closely relates to the Hartmann number, Brinkman number, and Joule heating parameter in the presence of an EDL thickness. Ali et al. [416] investigated the unsteady electroosmotic flow of Walters'-B fluid to analyze the heat and mass transfer in a magnetic field.

Tso and Sundaravadivelu [417] analyzed the influence of the electromagnetic field on the surface tension-driven flow in a parallel plate microchannel. Their study considered the transverse electric field by interacting with an externally applied magnetic field, neglecting EDL effects. Duwairi and Abdullah [418] and Shit et al. [419] studied the two-dimensional velocity and temperature distributions of electro-magneto-hydrodynamic (EMHD) micropump. They addressed Joule heating effects without viscous dissipation, thermal radiation, and EDL effects with the applied electromagnetic field. Buren et al. [420] and Fengqin et al. [421] extended their works [418,419] to analyze a microchannel flow with slightly corrugated walls. Munshi and Chakraborty [422] analytically studied the energy conversion efficiency under an external magnetic field in a narrow fluidic channel. Das et al. [423] and Jian and Chang [424] investigated an EMHD micropump using the Lorentz force in the presence of a spatially nonuniform magnetic field to determine the velocity profile in narrow fluidic channels. Using the finite difference method, Moghaddam [425] investigated the transient MHD micropumps of a two-dimensional power-law fluid in rectangular microchannels without EDL effects. Jian [426] reported the transient MHD flow in a parallel plate microchannel with mixed electroosmotic and pressure-driven impact and took into account the influence of Joule heating and viscous dissipation. Shit et al. [427] and Ranjit and Shit [428] developed mathematical models for the peristaltic flow of a coupled stress fluid with electric and magnetic fields. Kiyasatfar and Pourmahmoud [429] studied the MHD non-Newtonian electroosmotic flow in a square microchannel using a numerical technique based on the finite difference method in the presence of viscous dissipation and Joule heating effects.

Liu et al. [430] and Mondal et al. [431] calculated the velocity and heat transfer of EMHD flow through a curved rectangular microchannel in the presence of the vertical electric field and radial magnetic field. They highlighted that the entropy generation rate strongly depends on the velocity and temperature distributions. Ranjit and Shit [432] and Ramesh et al. [433] carried out a mathematical model in coupled stress-fluid driven by the influence of pressure gradient, peristaltic pumping with electric and magnetic fields subjected to the first-order velocity slip and temperature jump boundary conditions. They observed that the electroosmotic flow in the entropy generation and Joule heating dramatically depends on the velocity and temperature distributions. The effect of Joule heating, dissipation of energy, the volume fraction of nanoparticles, entropy generation, and mixed convection in EMHD nanofluids through an asymmetric channel was discussed by Noreen et al. [434]. Ghosh [435] studied the pressure-driven electrokinetic flow interaction between electrical double layer and electromagnetic fields in confined non-linear Phan-Thein-Tanner (PTT) fluids. Wang et al. [436] proposed the unsteady transient EMHD flow in a fractional Oldroyd-B fluid under a microchannel's electroosmotic and pressure gradient mix. They derived the velocity distribution by employing the Laplace and Fourier cosine transforms for the slip at the boundaries. Elmaboud [437] introduced the transient Caputo-Fabrizio time fractional of an electroosmotic generalized Burgers' fluid flow through a microannulus. Using the finite Hankel and Fourier transform, Khan et al. [438] theoretically analyzed the flow dynamics of the generalized Burgers' fluid in a cylindrical domain.

Turkyilmazoglu [439] studied the heat and mass transfer characteristics of magnetohydrodynamic flow for the velocity slip and thermal slip on a permeable stretching

surface and observed the influence of viscous dissipation and Joule heating effects. Furthermore, Turkyilmazoglu [439] extended his work to multiple solutions for the viscoelastic fluid [440,441]. Chamka et al. [442] determined the heat transfer of MHD nanofluids in a rotating system between two surfaces subjected to thermal radiation and viscous dissipation. The MHD effects enhance the skin friction coefficient for a sheet with stretching was investigated by Turkyilmazoglu [443,444]. Using the Fourier transform, Turkyilmazoglu [445] analyzed the heat transfer in MHD flow in microchannels. He observed that the MHD significantly controls fluid motion and circulation rate. Sheikholeslami et al. [446] investigated the nanofluid flow with influences of the magnetic field between two pipes. The effect of the Hartmann number on the velocity and temperature profiles in a parallel plate microchannel was extensively discussed by Salehi et al. [447] and Hosseinzadeh et al. [448]. Sheikholeslami and Ganji [449] studied magnetohydrodynamics in a nanofluid flow between two parallel plate sheets. Their study took into account the viscous dissipation and Joule heating. The impact of the magnetic field on the nanofluid for buoyancy flow over an expending sheet was discussed by Dogonchi and Ganji [450]. They showed that the velocity and temperature reduce with an increase in thermal radiation. Mahapatra and Bandopadhyay [451] combined the electroosmotic and pressure-driven Oldroyd-B fluid in microchannels. They highlighted the velocity slip flow at a high zeta potential in the presence of thin EDL.

8. Enhancing Microchannel Mixing and Separation

Various experimental and theoretical pieces of research identified mixing processes in microfluidic systems. Most of them focused on enhancing mixing efficiency by passive or active methods. For passive mixing, complex channel geometries play a vital role in increasing the interaction between two fluids to achieve complete mixing with a short transport distance [452]. However, active mixing methods introduce external energy into the mixing process to enhance the mixing efficiency. Generally, an external force does not apply in passive micromixers, and mixing is achieved only in twisted flow geometry. In the case of the laminar flow, the mixing is due to molecular diffusion. One of the strategies to improve efficiency is to increase the interface of the two fluids and reduce the diffusion path between them [453]. Therefore, active methods have broad applications, such as droplet-based mixing [454], time-periodic mixing [455], multi-step mixing [456], etc. Due to their easy fabrication and integration, passive micromixers engage widely. Passive mixers are popular in chemical [457] and biological [458] microfluidics. Moreover, micromixer chips can mix samples with enzymes, and thereby, detect the concentration of excessive pesticide residues in food with less cost and high sensitivity [459]. Several methods have been beneficial for high production requirements, such as low-cost device fabrication, high mixing performance, and ease of operation [460]. In addition, studies have been on improving the mixing efficiency and controlling the fluid motion in the EOF. Active micromixers improve mixing by magnetically [392], mechanically [461], electrically [462], and acoustically swirling [463] fluid streams. Passive micromixers have two common types. One is lamination-based mixers [464] and the other types are chaotic advection-based mixers [465], 3D serpentine mixers [466], zigzag or waveform mixers [467], micromixers with patterned blocks [468], obstacles [469], staggered herringbones [470], etc. For lamination-based mixers, T-shaped and Y-shaped are the broadly investigated devices, in which their main inlet channels can be split into several sub-streams and then recombined to form the main stream [471,472].

The particle diffusion in microchannels was heavily affected by the wall roughness. Wang et al. [473] presented the effects of sidewall roughness on the mixing performance of zigzag microchannels increased by 1.208% compared to the smooth microchannel. The mixing performance of a passive-type microchannel with variously shaped obstacles, including rectangular, triangular, and cylindrical designs, was presented by Seo et al. [474]. Comparing the outcomes for various flow scenarios highlights concentration distributions demonstrated the maximum efficiency for the rectangular obstacle to be the most effective.

Nazari et al. [475] proposed an induced charge electrokinetic-micromixer with conductive surfaces which can produce vortices. Different mixing chamber geometries were compared, such as square, triangular, rhomboid, and circular. They found that, among the other situations, the rhomboid mixing chamber exhibits the best mixing efficiency at 95%. According to Vasista et al. [476], mixing efficiency increases with the slip and zeta potential parameters in heterogeneous surfaces. The effect of the magnetic field on the flow, which can significantly improve the mixing efficiency, was studied by Dallakehnejad et al. [392]. The numerical results show that applying a magnetic field to a flow can increase mixing efficiency by 70% to 90%. In a trapezoidal micromixer, Alipanah et al. [477] explored non-Newtonian power law fluids. By increasing the applied electric field, they found that mixing efficiency for both Newtonian and shear-thinning fluid increases. In comparison, the mixing effectiveness in shear thickening fluid reduces with increasing the electric field. Other applications of microfluidic channels have been used for particle separation by applying a variety of approaches, including dielectrophoresis [478], elasto-inertial [479], and acoustic [480].

Recently, it has become widespread to employ microfluidic devices to separate infectious pathogens from body fluids, such as malformed cells, fungus, sepsis, etc. With complete effectiveness, the machine can separate magnetic particles (MPs) from human blood under various circumstances. The biological entities are identified using magnetic particles and separated by magnetophoresis technology. It is frequently used to direct [481], capture [482], accumulate [483], and disaggregate [484] particles by the motion of magnetic particles in a magnetic field. Das et al. [485] studied the efficient separation from the continuous flow using an external magnetic field in fluorescence-tagged magnetic microbeads driven by electroosmotic flow. Alipanah et al. [486] presented an on-demand microfluidic separator with an adjustable magnetic field to provide the required magnetic strength based on the particle size through electroosmotic flow. The separation of species in oscillating flows under the effect of an oscillatory pressure gradient was studied by Teodoro et al. [487]. Cao et al. [488] investigated the mass separation of Oldroyd-B fluid of the rotating electroosmotic flow of two-layer fluid in a parallel microchannel.

The pie chart shown in Figure 4 highlights extensive works done analytically in microchannels utilizing various analytical methods under the influence of an electric field. It may be observed that several researchers have developed either numerical methods or hybrid techniques (both analytical and numerical) to determine the velocity and temperature distributions in electrokinetic flow. On the other hand, fewer works identify the flow in microchannels with the electric and magnetic fields investigated analytically for the fully developed flow. Mainly, hybrid techniques have been employed for Newtonian and non-Newtonian fluids to estimate the mean temperature distribution.

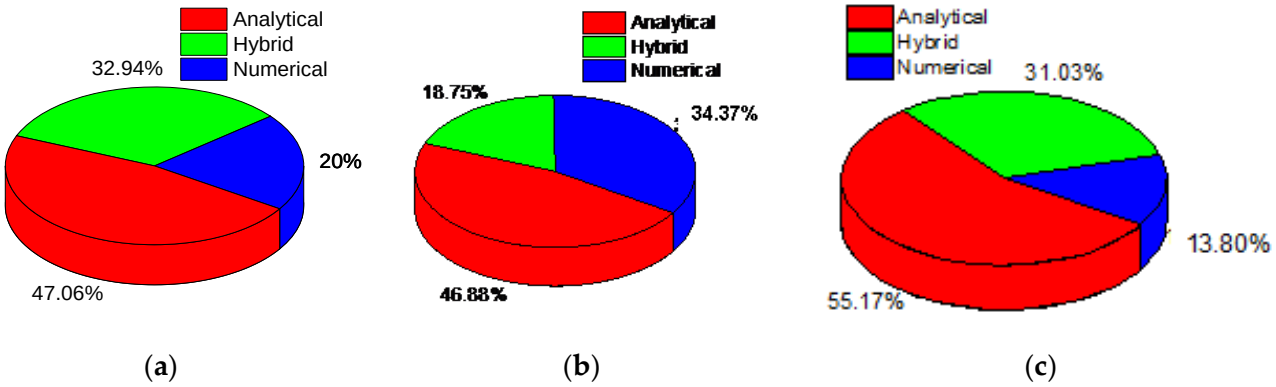

Figure 4. Different analyses employed in percentage to analyze electrokinetic flow in microchannels based on the existing literature. (**a**) Rectangular channel with electric field applied; (**b**) Non-rectangular channel with electric field applied; (**c**) Both electric and magnetic fields applied.

This study provides an enormous overview of microchannels' flow and heat transfer characteristics and their applications. Firstly, imposed pressure gradient, electric field, and magnetic field based on the Navier–Stokes and energy equations in different geometries of microchannels are discussed thoroughly. Secondly, we elaborate on the various analytical and numerical methods to determine the distributions of EDL potential, velocity and temperature, and Nusselt number, which affect the microfluid characteristics due to the viscous dissipation, Joule heating, and thermal radiation. Thirdly, no-slip and no-jump boundary conditions are taken in microchannels considering both the Newtonian and non-Newtonian fluids. Then, it is extended to the first-order velocity slip and a temperature jump on a hydrophobic surface. The above literature works observed that most researchers considered their work with no-slip conditions, neglecting the thermal radiation, viscous dissipation, and Joule heating parameters. However, they determined the Nusselt number using the finite difference method. The study related to the analytical works regarding the determination of the Nusselt number along with the radiation, viscous dissipation, and Joule heating parameter, with the second-order slip for both the velocity and temperature distributions in EMHD flow through rectangular microchannels being scattered and incomplete. The present review paper aims to determine the exact analytical solution of combined pressure-driven EMHD flow through a rectangular microchannel assuming the Debye–Hückel (DH) approximation. The thermal characteristics at a constant heat flux are studied with the second-order slip velocity and temperature jump boundary conditions. It found that the effect of radiation, viscous dissipation, and Joule heating parameters plays a prominent role in heat transfer. The velocity distribution, temperature distribution, and Nusselt number results in electro-magneto-hydrodynamic pressure-driven electroosmotic flow through a rectangular microchannel making a difference with the first-order slip, second-order slip, and no-slip conditions; and the first-order jump, second-order jump, and no-jump conditions are compared. Additionally, this review paper discusses how effectively separation and mixing can occur in microchannels.

Microfluidics has become a more attractive research area nowadays. The microchannel has gained popularity in the last decade to increase heat transfer. Various applications include textile fabrics [489], rechargeable batteries [490], small-scale cooling [491], military hardware [492], microdosing system [493], cancer therapy [494,495], etc. Miniaturization has many advantages, such as fast response, accurate results, affordability of mobile monitoring, compassionate analysis, etc. Therefore, the present study has some merits in performing novel research to improve real-world system analyses.

9. Mathematical Modeling and Governing Equations

9.1. Physical Formulation

The present physical problem is to combine pressure-driven electroosmotic flow under the effect of electric and magnetic fields in rectangular microchannels. The flow takes place in the microchannel between the two parallel plates at a constant channel height. Figure 5 shows a schematic geometry of a microchannel. The width of the channel W and length L is separated by a distance $2a$. The x and y axes are perpendicular and parallel to the channel wall, respectively. For very small aspect ratio, i.e., $W \gg\gg 2a$, and assuming the length L is much larger than both height $2a$ and width W, i.e., $L \gg\gg 2a$, and $L \gg\gg W$, one can then ignore the end effects and treat the microchannel as infinite parallel plates. The mathematical analysis is present only on the upper half $0 \leq y \leq a$ of the channel because of its symmetry about the y-axis. The microchannel fills with the incompressible electrolyte solution of the dielectric constant (ε). The plates charge uniformly with the zeta potential. The channel is subjected to constant heat flux q_w and constant wall temperature T_w. The pressure gradient in the axial direction $P_y = -dp/dy$ is applied in the flow field. There is electric field (E_y) acting along the y axis, whereas the electric field (E_z) acts along the z-direction (lateral direction) of the flow. The magnetic field (B_x) acts in the transverse direction (positive x-direction).

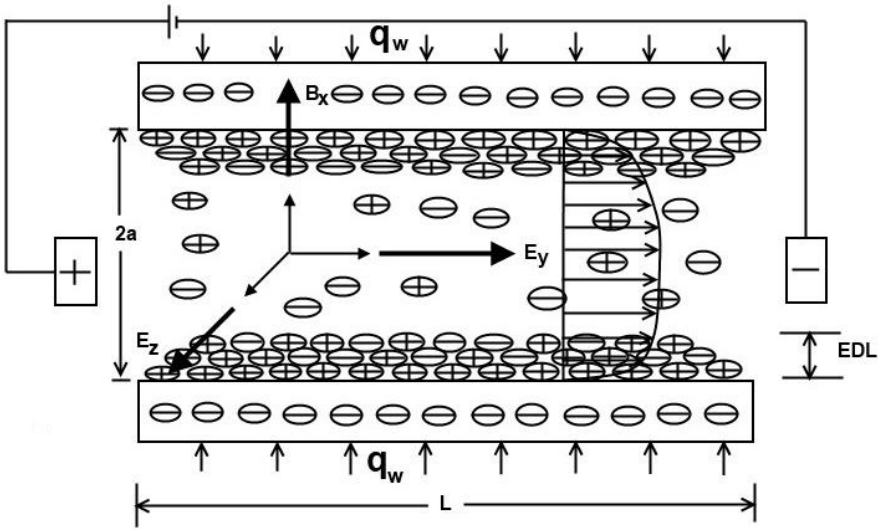

Figure 5. Schematic diagram of a rectangular microchannel showing EDL with coordinate system taken to establish the present study.

9.2. Determination of Electrical Double Layer Potential

Some important assumptions are taken to present a mathematical analysis to establish the steps required for the theoretical estimation:

- Streamline, incompressible, and developed flow.
- Constant thermo-physical properties.
- The channel walls satisfy a constant heat flux.
- The symmetric condition $(\omega_+ = \omega_- = \omega)$ with respect to the center axis for the geometry rectangular microchannel.
- Low zeta potential value for the applicability of the Debye–Hückel linearization approximation.
- The charge of the EDL follows the Boltzmann distribution.

According to Gouy [62] and Chapman [63], the electrical double layer potential distribution (ψ) with a non-variable permittivity can be expressed as a function of a uniform charge density (ρ_e) and is governed by the Poisson equation as:

$$\nabla^2\psi = -\rho_e/(\varepsilon\,\varepsilon_0) \tag{11}$$

where ε is the permittivity of the medium, ε_0 is the permittivity of free space, and ρ_e is the density of net charge per unit volume. One can express ρ_e as:

$$\rho_e = e(\omega_+ n_+ - \omega_- n_-) \tag{12}$$

where e represents the ionic-charge density of electrons, $\omega_\pm$ represents the valency, and $n_\pm$ is the ionic number density of positively and negatively charged species, respectively. ω is the symmetric electrolyte having an equal amount of charge valency, where both coions and counter ions have the same charged value. The ionic species are considered to be point charges. The ionic number densities obey the Boltzmann distribution as given by Hunter [66] in the following:

$$n_\pm = n_0 \exp\left(\frac{\omega_\mp e\,\psi}{k_B T}\right) \tag{13}$$

where n_0 denotes the bulk ionic concentration, k_B represents the Boltzmann constant, and T is the temperature in absolute scale. Substituting Equation (13) into Equation (12) gives:

$$\rho_e = -2n_0 ze\sinh(e\,\omega\psi/k_B T) \tag{14}$$

Combining Equations (11) and (14) yields:

$$\nabla^2\psi = (2n_0 e\ \omega/\varepsilon\ \varepsilon_0)\sinh(e\ \omega\ \psi/k_B T) \tag{15}$$

Equation (15) is highly non-linear. However, the zeta potential (electrical potential at the wall) is generally very low in comparison to the thermal potential. In this situation, $\sinh(e\omega\psi/k_B T) \approx (e\omega\psi/k_B T)$ results in Equation (15), converted into a linear equation. This approximation is called Debye–Hückel linearization approximation. The mathematical expression $\left(2n_0 e^2\omega^2/\varepsilon\varepsilon_0 k_B T\right)^{-1/2}$ is known as Debye length (λ_D) and $(a\ /\lambda_D)$ is the ratio of half-length channel height to Debye length. Equation (15) is in dimensionless form as:

$$d^2\overline{\psi}/dX^2 - \left(K^2/\overline{\zeta}\right)\ \sinh\left(\overline{\psi}\ \overline{\zeta}\right) = 0 \tag{16}$$

The dimensionless parameters used to express Equation (16) in a dimensionless form are as follows:

$$\overline{\zeta} = e\ \omega\zeta/k_b T_{av};\ X = x/a;\ \overline{\psi} = \psi/\zeta;\ K = R\times\ a\ ;\ \text{and}\ R = 1/\lambda_D \tag{17}$$

Using the Debye–Hückel linearization approximation, Equation (16) changes into:

$$d^2\overline{\psi}/dX^2 - K^2\overline{\psi} = 0 \tag{18}$$

For the microchannel flow, the boundary wall maintains a constant zeta potential, the effect of it gradually reduces from the wall to the fluid, and it is a minimum at the center of the channel. Therefore, the mathematical expressions of the boundary conditions for the zeta potential are:

$$\text{at}\ X = 1,\ \overline{\psi} = \overline{\zeta} \tag{19}$$

and

$$\text{at}X = 0,\ d\overline{\psi}/dX = 0 \tag{20}$$

Applying the boundary conditions (Equations (19) and (20)), the dimensionless EDL potential distribution is:

$$\overline{\psi} = \overline{\xi}\cosh(KX)/\cosh(K) \tag{21}$$

Therefore, the local volumetric net charge density is used to evaluate, using Equations (11), (14), and (21) as:

$$\rho_e = -\left(K^2\varepsilon\varepsilon_0\ \overline{\xi}/a^2\right)\cosh(KX)/\cosh(K) \tag{22}$$

9.3. Velocity Profile in Microchannel Flow

In the flow field, the governing continuity and Navier–Stokes' equations are in vector notations, respectively, as:

$$\text{div}\ \mathbf{U} = 0 \tag{23}$$

and

$$\rho(\mathbf{U}\cdot\nabla\ \mathbf{U}) = -\nabla P + \mu\ \ \nabla^2\ \mathbf{U} + \mathbf{F} \tag{24}$$

where $\mathbf{U}\left(= \hat{\mathbf{i}}\ u + \hat{\mathbf{j}}\ \ v + \hat{\mathbf{k}}\ w\right)$ is the induced velocity vector and μ is the fluid viscosity. The net body force acting on the fluid element is due to the electric field and magnetic field applied and it is called Lorentz force. The electromagnetic body force can be defined as:

$$\mathbf{F} = \rho_e\ \mathbf{E} + \mathbf{J}\times\mathbf{B} \tag{25}$$

where $\mathbf{E} = \hat{\mathbf{j}}\, E_y + \hat{\mathbf{k}}\, E_z$ is the applied electric field and $\mathbf{J}$ is the current density vector, which can be expressed from the Ohm's law as:

$$\mathbf{J} = \sigma(\mathbf{E} + \mathbf{U} \times \mathbf{B}) \tag{26}$$

where σ is the electrical conductivity of the fluid and $\mathbf{B} = \hat{\mathbf{i}}\, B_x$, which is the magnetic field acting in the x-direction. The momentum balance in the electromagnetic hydrodynamic flow field in the y-direction simplifies to:

$$-dP/dy + \mu d^2v/dx^2 + \rho_e E_y + \sigma E_z B_x - \sigma v B_x^2 = 0 \tag{27}$$

where v is a y-component flow velocity. To solve Equation (27), the boundary condition considers the second-order slip [179,325] written in a dimensionless form as:

$$\text{at} X = 1,\ V = -\alpha_1 dV/dX + \alpha_2 d^2V/dX^2 \tag{28}$$

where $V = v/v_{HS}$, v_{HS} is a reference electro-osmotic velocity known as the Helmholtz–Smoluchowski velocity. Due to the symmetric velocity with respect to the axis of the channel, the boundary condition for the velocity at the axis is satisfied as:

$$\text{at} X = 0,\ dV/dX = 0 \tag{29}$$

Now, Equation (27) is in dimensionless form by combining Equation (11) as:

$$d^2V/dX^2 - Ha^2V + SHa + \Omega + K^2\cosh(KX)/\cosh(K) = 0 \tag{30}$$

where $Ha = aB_x\sqrt{\sigma/\mu}$ is the Hartmann number, $\Omega = \left(P_y a^2\right)/\left(\mu v_{HS}\right)$ is a dimensionless pressure gradient, and $S = \left(E_z a\sqrt{a}\right)/\left(v_{HS}\sqrt{\mu}\right)$ is a non-dimensional parameter representing the strength of the transversed electric field.

The closed-form solution for the non-dimensional velocity distribution is obtained by solving Equation (30) with the help of boundary conditions in Equations (28) and (29) as:

$$V = A_1 + A_4\cosh(HaX) - A_3\cosh(KX) \tag{31}$$

where:

$$\begin{gathered} A_1 = (SHa + \Omega)/Ha^2;\ A_2 = K^2/\left(K^2 - Ha^2\right);\ A_3 = A_2/\cosh(K); \\ A_4 = \frac{A_2 - A_1 + KA_3\alpha_1\sinh(K) - K^2\alpha_2 A_2}{\cosh(Ha) + \alpha_1 Ha\sinh(Ha) - \alpha_2 Ha^2\cosh(Ha)} \end{gathered} \tag{32}$$

9.4. Temperature Profile

This study is to delineate the thermal transport behavior in the electro-magneto-hydrodynamic environment for the Newtonian fluid in microchannels. For this, the energy equation for the temperature response is [57,164,325]:

$$\rho c_p v\frac{\partial T}{\partial y} = k_T\left(\frac{\partial^2 T}{\partial x^2} + \frac{\partial^2 T}{\partial y^2}\right) - \frac{\partial q_r}{\partial x} + \mu\left(\frac{\partial v}{\partial x}\right)^2 + S_J \tag{33}$$

where c_p is the specific heat at constant pressure, T is the local temperature, and S_J is the heat generation rate per unit volume due to the Joule heating. The thermal boundary condition at the wall in dimensionless forms is with the second-order jump [173] as follows:

$$\text{at } X = 1,\ \theta = -\gamma_1 d\theta/dX + \gamma_2 d^2\theta/dX^2 \tag{34}$$

where the non-dimensional temperature θ is defined as $\theta = k_T(T - T_w)/q_w a$ for the thermally fully developed flow and T_w is the wall temperature of the channel. Due to the

symmetric variation of the temperature distribution with respect to the X-coordinate, the temperature boundary condition at the center is:

$$\text{at } X = 0,\ d\theta/dX = 0 \tag{35}$$

As the flow becomes thermally fully developed:

$$\partial T/\partial y = dT/dy = dT_M/dy = C \tag{36}$$

The above condition gives $\partial^2 T/\partial y^2 = 0$. The average flow velocity of the channel is $v_{av} = \frac{1}{a}\int_0^a v dx$. The non-dimensional average velocity, $V_{av} = v_{av}/v_{HS}$ is obtained from Equation (31):

$$V_{av} = A_1 + A_5 \sinh(Ha) - A_6 \sinh(K) \tag{37}$$

where:

$$A_5 = A_4/Ha \text{ and } A_6 = A_3/K \tag{38}$$

The viscous energy dissipation is obtained with the following expression:

$$\beta = \int_0^1 (dV/dX)^2 dX \tag{39}$$

Equation (39) is integrated using Equation (31):

$$\beta = F_1 \sinh(2Ha) + F_2 \sinh(2K) - F_3 - F_4 \sinh(Ha)\cosh(K) + F_5 \sinh(K)\cosh(Ha) \tag{40}$$

where:

$$F_1 = A_7^2/4Ha;\ F_2 = A_8^2/4K;\ F_3 = \left(A_7^2/2 + A_8^2/2\right);\ F_4 = 2A_7A_8K/\left(K^2 - Ha^2\right);\ F_5 = 2A_7A_8Ha/\left(K^2 - Ha^2\right);\ A_7 = HaA_4;\ A_8 = KA_3 \tag{41}$$

The energy balance on the elemental control volume with the length of the channel (dy) is:

$$dT_M/dy = \left[q_w(1+Nr) + S_J a + \left(\mu v_{HS}^2/a\right)\int_0^1 (dV/dX)^2 dX\right] \Big/ \left(\rho c_p v_{av} a\right) \tag{42}$$

where $Nr = 16T_3^3\sigma^*/3k^*k_T$ is a dimensionless thermal radiation parameter [162,357]. The non-dimensional energy equation can be written from Equations (33), (36), (37), and (40) in the following form:

$$\frac{d^2\theta}{dX^2} = \frac{V}{V_{av}}\left[1 + \frac{g_1}{(1+Nr)} + \frac{Br\beta}{(1+Nr)}\right] - \frac{g_1}{(1+Nr)} - \frac{Br}{(1+Nr)}\left(\frac{dV}{dX}\right)^2 \tag{43}$$

where g_1 is the non-dimensional Joule heating parameter, $\left(S_J a\right)/q_w$, which represents the ratio of the Joule heating to the applied wall heat flux, and Br is the Brinkman number; it represents the ratio of Joule heating to the applied wall heat flux.

Equation (43) has been solved to determine the dimensionless temperature by applying the boundary conditions (Equations (34) and (35)):

$$\theta = H_1X^2 + H_2\cosh(HaX) - H_3\cosh(KX) - H_4\cosh(2HaX) - H_5\cosh(2KX) + H_6\sinh(HaX)\sinh(KX) - H_7\cosh(HaX)\cosh(KX) + H_8\sinh(HaX)\sinh(KX) + C_1 \tag{44}$$

where:

$$C_1 = -\gamma_1(A_{10} + A_{11}\sinh(Ha) - A_{12}\sinh(K) - A_{13}\sinh(2Ha) - A_{14}\sinh(2K) + A_{15}\sinh(Ha)\cosh(K) - A_{16}\cosh(Ha)\sinh(K)) + \gamma_2(A_{10} + A_{17}\cosh(Ha) - A_{18}\cosh(K) - A_{19}\cosh(2Ha) - A_{20}\cosh(2K) + A_{21}\sinh(Ha)\sinh(K)) - H_1 - H_2\cosh(Ha) + H_3\cosh(K) + H_4\cosh(2Ha) + H_5\cosh(2K) - H_6\sinh(Ha)\sinh(K) + H_7\cosh(Ha)\cosh(K) - H_8\sinh(Ha)\sinh(K) \quad (45)$$

$$A_9 = \frac{1+\frac{g_1}{1+Nr}+\frac{Br\beta}{1+Nr}}{V_{av}};\ A_{10} = \left(A_1A_9 - \frac{g_1}{1+Nr} + \frac{F_3Br}{1+Nr}\right);\ A_{11} = \frac{A_9A_4}{Ha};\ A_{12} = \frac{A_3A_9}{K};$$
$$A_{13} = \frac{BrA_5^2}{4Ha(1+Nr)};\ A_{14} = \frac{A_6^2Br}{4K(1+Nr)};\ A_{15} = \frac{2A_5A_6KBr}{(K^2-Ha^2)(1+Nr)};\ A_{16} = \frac{2A_5A_6HaBr}{(K^2-Ha^2)(1+Nr)};$$
$$A_{17} = A_{11}Ha;\ A_{18} = A_{12}K;\ A_{19} = 2HaA_{13};\ A_{20} = 2KA_{14};\ A_{21} = KA_{15};\ A_{22} = HaA_{15};\ A_{23} = KA_{16};$$
$$A_{24} = HaA_{16};\ H_1 = \frac{A_1A_9}{2} - \frac{g_1}{2(1+Nr)} + \frac{F_3Br}{2(1+Nr)};$$
$$H_1 = \frac{A_1A_9}{2} - \frac{g_1}{2(1+Nr)} + \frac{F_3Br}{2(1+Nr)};\ H_2 = \frac{A_9A_4}{Ha^2};\ H_3 = \frac{A_3A_9}{K^2};$$
$$H_5 = \frac{BrA_6^2}{8K^2(1+Nr)};\ H_6 = \frac{2A_5A_6K^2Br}{(K^2-Ha^2)^2(1+Nr)};\ H_7 = \frac{4A_5A_6KBrHa}{(K^2-Ha^2)^2(1+Nr)};\ H_8 = \frac{2A_5A_6Ha^2Br}{(K^2-Ha^2)^2(1+Nr)} \quad (46)$$

To calculate the average temperature in the flow field, it needs the following integration with the help of Equations (31) and (44):

The dimensionless bulk-mean temperature is obtained from the following mathematical expression:

$$\begin{aligned}\int_0^1 V\theta dX = {} & \frac{A_1H_1}{3} + \frac{A_1H_2}{Ha}\sinh(Ha) - \frac{A_1H_3}{K}\sinh(K) - \frac{A_1H_4}{2Ha}\sinh(2Ha) - \frac{A_1H_5}{2K}\sinh(2K) \\ & + (A_1H_6 + A_1H_8)\left[\frac{K}{(K^2-Ha^2)}\sinh(Ha)\cosh(K) - \frac{Ha}{(K^2-Ha^2)}\cosh(Ha)\sinh(K)\right] \\ & - (A_1H_7 + A_4H_3 + A_3H_2)\left[\frac{K}{(K^2-Ha^2)}\cosh(Ha)\sinh(K) - \frac{Ha}{(K^2-Ha^2)}\sinh(Ha)\cosh(K)\right] \\ & + A_1C_1 + A_4H_1\left[\frac{\sinh(Ha)}{Ha} - \frac{2}{Ha^2}\cosh(Ha) + \frac{2}{Ha^3}\sinh(Ha)\right] + \frac{A_4H_2}{2}\left[1 + \frac{\sinh(2Ha)}{2Ha}\right] \\ & - A_4H_4\left[\frac{2}{3Ha}\cosh(Ha)\sinh(2Ha) - \frac{1}{3Ha}\sinh(Ha)\cosh(2Ha)\right] \\ & - \left(A_4H_5 - \frac{A_3H_7}{2}\right)\left[\frac{2K}{(4K^2-Ha^2)}\cosh(Ha)\sinh(2K) - \frac{Ha}{(4K^2-Ha^2)}\sinh(Ha)\cosh(2K)\right] \\ & + \left(\frac{A_4H_6}{2} + \frac{A_4H_8}{2}\right)\left[\frac{K}{(K^2-4Ha^2)}\sinh(2Ha)\cosh(K) - \frac{2Ha}{(K^2-4Ha^2)}\cosh(2Ha)\sinh(K)\right] \\ & - \left(\frac{A_4H_7}{2} - A_3H_4\right)\left[\frac{2Ha}{(4Ha^2-K^2)}\cosh(K)\sinh(2Ha) - \frac{K}{(4Ha^2-K^2)}\sinh(K)\cosh(2Ha)\right] \\ & - \frac{A_4H_7}{2K}\sinh(K) + \frac{A_4C_1}{Ha}\sinh(Ha) - A_3H_1\left[\frac{\sinh(K)}{K} - \frac{2}{K^2}\cosh(K) + \frac{2}{K^3}\sinh(K)\right] \\ & + \frac{A_3H_3}{2}\left[1 + \frac{\sinh(2K)}{2K}\right] + A_3H_5\left[\frac{2}{3K}\cosh(K)\sinh(2K) - \frac{1}{3K}\sinh(K)\cosh(2K)\right] \\ & - \left(\frac{A_3H_6}{2} + \frac{A_3H_8}{2}\right)\left[\frac{Ha}{(Ha^2-4K^2)}\sinh(2K)\cosh(Ha) - \frac{2K}{(Ha^2-4K^2)}\cosh(2K)\sinh(Ha)\right] \\ & + \frac{A_3H_7}{2Ha}\sinh(Ha) - \frac{A_3C_1}{K}\sinh(K)\end{aligned} \quad (47)$$

$$\theta_m = \int_0^1 V\theta dX \Big/ \int_0^1 V dX \quad (48)$$

The Nusselt number (Nu) based on the hydraulic mean diameter is:

$$Nu = hd_h/k_T = -4/\theta_m \quad (49)$$

where h is the convective heat transfer coefficient. Here, it highlights the analytical expression of the Nusselt number established by considering the second-order slip and second-order jump, which are not yet available in the existing literature. Therefore, the

closed-form analysis presented has significant merit. The results have been newly generated in the present study, and the results are discussed in the following sections.

10. Results and Discussion

This study deals with a compressive literature survey for fluid flow in microchannels. It also develops a closed-form analytical solution of EMHD rectangular microchannels combined with the pressure-driven electroosmotic flow. The present analysis helps to determine the non-dimensional velocity, temperature, and Nusselt number by taking second-order velocity slip and temperature jump boundary conditions along with the effects of viscous dissipation, Joule heating, and thermal radiation parameters. The non-dimensional physical parameters are in the physically permissible range based on the practicable design aspects. Therefore, the normalized different physical parameters are in connection with the externally applied magnetic field, transverse electric field, electrokinetic width, viscous dissipation, and other parameters. In this work, the magnitude of Hartmann number (Ha) varies from 0.01 to 0.1 for the permissible EMHD micropumps (10 for the maximum permissible range), $a \sim 100$ μm , $\sigma \sim 10$ S/m, the range of externally imposed magnetic field (B_x) is 1 to 100 T, S varies from 0 to 10 (100 for the maximum permissible limit), $v_{HS} \sim 100$ μm/s , $\mu \sim 10^{-3}$ Pa-s, $O(E_z) \sim 1$ V/m, $O(S) \sim 10$, Brinkman number (Br) is 0–0.01, K = 10, $\Omega = 1$, and $Nr = 0 - 2$, which are taken from the published literature with physical acceptability [58,125,393].

In order to validate the present analysis, Figure 6a is depicted the velocity distribution determined by the present study and the published work [393] with the different magnitudes of Hartman number (Ha), ignoring the electric field and no-slip boundary conditions $(\alpha_1 = 0, \alpha_2 = 0)$. The exact matching of results indicates the correctness of the velocity distribution predicted by the present study. It highlights from this figure that an increase in Hartman number declines the electroosmotic flow velocity.

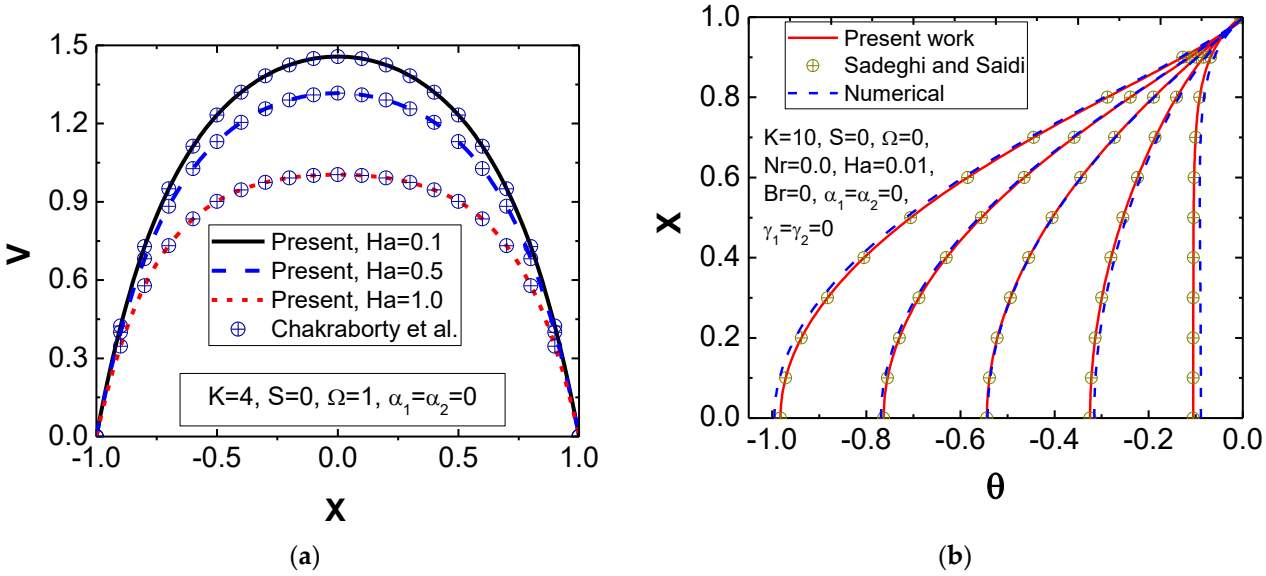

Figure 6. Validation of the present analysis for velocity and temperature distributions in microchannels. (**a**) Velocity distribution determined by present analysis and published work [393]; (**b**) Temperature distribution determined by present analytical and numerical analyses and published work [76].

The finite difference method employs to determine the non-dimensional velocity, non-dimensional temperature, and Nusselt number to establish the correctness of the present analytical analysis with the slip boundary conditions. Equations (30) and (43) are discretized with second-order accuracy. The Gauss–Seidel iterative method was used for the solution with the second-order velocity slip and the second-order temperature jump boundary condition. Figure 6b depicts the temperature distribution evaluated by

the present analysis and the numerical method based on the finite-difference approach for the pure electroosmotic flow. Here, pressure gradient, transverse electric field, thermal radiation, and viscous dissipation $(\Omega = 0, S = 0, Nr = 0, Br = 0)$ have been considered in no-jump boundary conditions, with a small magnetic field $(Ha = 0.01)$ employed to maintain the generality of the analysis. The results determined by Sadeghi and Saidi [76] are also plotted in the same figure for the comparative information. A good agreement of results among the different prediction methods shows the authentication of the present analytical results in rectangular microchannels. Therefore, using a reasonable range of the non-dimensional flow parameters, the results of the present study, including velocity, temperature, and Nusselt number with the influence of the electric and magnetic fields for the second-order slip conditions, are discussed in the forthcoming sections.

The influence of electric and magnetic fields on velocity distribution is depicted in Figure 7 with the no-slip, first-order slip, and second-order slip boundary conditions. It can be noted that the transverse electric field (S) applied by a small value of Hartman number (Ha) causes the influence of the flow velocity for the interaction of body forces (i.e., Lorentz forces). With a small value of *Ha*, the fluid velocity appears to a maximum at the axis of the channel. However, the velocity increases with an increase in Hartman number, as shown in Figure 7a for the second-order slip boundary condition. The flow aiding component and the flow opposing component significantly increase the velocity by increasing the Hartmann number. From the physical aspect, the flow aiding component and the flow opposing character can be defined as the order of magnitude in which $\sigma E_z B_x$ acts as a driving pressure gradient and $\sigma v B_x^2$ is a retarding axial pressure gradient, as described in Equation (27). Now, in the presence of a transverse electric field (S = 10), the flow aiding component plays a significant role in the flow system. It shows in Figure 7a. The flow adding component is larger than the flow opposing component owing to the revised influence of electromagnetic body forces, so the velocity of the flow confinement usually increases. Nevertheless, this is to the fact that, due to the stagnation of the uniform inlet velocity at the wall of the microchannel for the continuum flow $(Kn < 0.001)$, no-slip velocity is valid, and first- and second-order slip parameters α_1 and α_2 are zero. Figure 7b is plotted for a comparison of different slip boundary conditions to realize the influence of the electric field (S) on the transport phenomenon under different values of *Ha* for the first-order slip ($\alpha_1 = 0.12$ and $\alpha_2 = 0$) and the second-order slip ($\alpha_1 = 0.12$ and $\alpha_2 = 0.0048$). Now, in the existence of an electric field (S), the Hartman number (*Ha*) increases the electroosmotic velocity in microchannels. It reveals that the Knudsen number (Kn) is the key factor for the slip condition and a high value of *Kn* has always a tendency with the slipping situation. Generally, a slip-flow occurs for the Knudsen number varying in a range of $0.001 \leq Kn \leq 0.1$. Obviously, an increasing Knudsen number always amplifies the slip flow. Therefore, it is natural that an increasing mean free path of molecules causes to decrease in the collision that happens between them because molecules travel a longer distance without colliding with each other at a fixed characteristic length. However, in the presence of the wall, a few molecules colloid with it and travel a longer distance until momentum reduces due to collision. At the solid-fluid interface, absorption of fluid molecules on the solid surface occurs, and as a result, the wall slip affects velocity gradients adjacent to the wall. It can be mentioned that such a phenomenon raises the advection transport of moving ions in the EDL. Hence, in the presence of first-order velocity slip, the bulk fluid flow increases due to increased velocity at the confined wall, as depicted in Figure 7b. For the slip condition, more fluid comes near the wall, and this aspect can be understood in Figure 3a. The second-order slip condition is to partially transmit and pull the wall due to the slip condition of the fluid in the slip flow regime for the Knudsen number (*Kn*) in the range of $0.01 \leq Kn \leq 0.1$. Furthermore, a comparison of velocity distributions for the magnetic field (*Ha* = 1) with the influence of the transverse electric field shown in Figure 7b depicts that for $Kn = 0.08$, the second-order slip gives an intermediate velocity between that of the no-slip and first-order slip. However, the second-order slip model has

opposite effects compared to the first-order slip velocity. Therefore, the opposite sign of the second-order slip causes a decrease in the velocity.

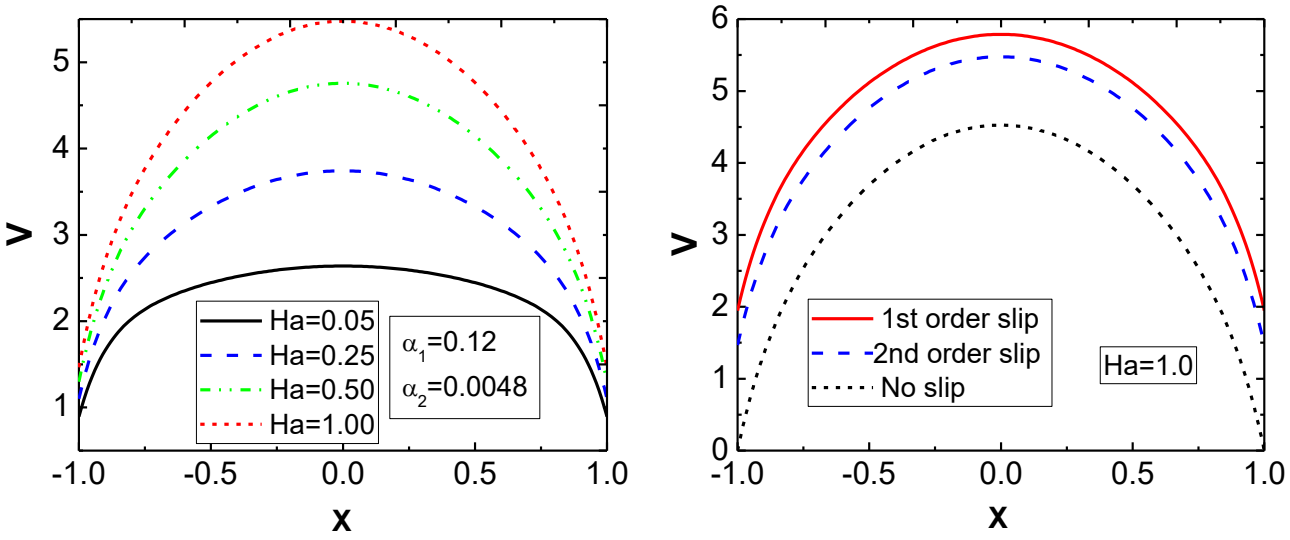

(**a**) (**b**)

Figure 7. Effects of slip-conditions on flow-velocity in microchannels for $K = 10$, $S = 10$, and $\Omega = 1$. (**a**) Second-order slip; (**b**) Comparison of no-slip, first-order, and second-order slips.

Figure 8 delineates the velocity distribution of an electro-magneto-hydrodynamic flow as a function of the transverse electric field (S) in the presence of Hartmann number (*Ha*). This study focuses on the effect of the transverse electric field (S) on the velocity distribution for different slip boundary conditions. It is noticeable that the velocity increases significantly with the transverse electric field, as shown in Figure 8a for the second-order slip. However, a slight indentation for the velocity distribution for $S = 0$ is found at the middle section of the rectangular microchannel. The reason explains that in the absence of a transverse electric field (S = 0), the flow-adding force vanishes, and the opposing force is only the dominating in the magnetic field to decrease the trend of velocity distributions in the flow field. Rarefaction and mass flow rate are the main parameters affected by changing the velocity distribution of the microchannel. In the case of the no-slip condition, rarefaction is zero, and the velocity distribution is depicted in Figure 8b. It is evident that the slip boundary condition increases the fluid flow velocity compared to the no-slip case. This nature occurs due to the influence of the surface and molecular interactions adjacent to the solid surface called the Knudsen layer. Therefore, an increase in the value of the Knudsen number (rarefaction) amplifies fluid mass flow rate through microchannels. A straightforward comparison of the velocity pattern in microchannels under the possible boundary conditions is displayed in Figure 8b.

Figure 9 depicts the temperature distribution in a microchannel along the x-direction for different values of *Ha*. Figure 9a plots for the second-order jump. A lower value of *Ha* uses to draw these figures in the absence of a transverse electric field. The nonexistence of the electric field nullifies the flow aiding component; therefore, the flow-opposing component is only present. Thus, the flow velocity in this design condition is moderately dependent upon the Hartmann number. The reduction in flow velocity is due to an increase in the magnitude of *Ha*, which influences the increase in fluid temperature. The advective transport thermal energy also reduces the speed of the fluid in channels. For these reasons, the numerator and denominator parts in the non-dimensional temperature reduce separately. However, the reduction in denominator becomes more compared to the numerator at a lower value of *Ha*, and the magnitude of the dimensionless temperature amplifies at a higher *Ha*. The same trend is noticed for the no-jump, the first order, and the second-order jump. Moreover, variation of the temperature distribution in channels

for the jump condition at the boundary slightly increments compared to that for the no jump. This difference is due to more thermal energy transferred to the fluid in the case of the jump situation. Figure 9b compares the temperature distribution for the different jump conditions at a constant *Ha*.

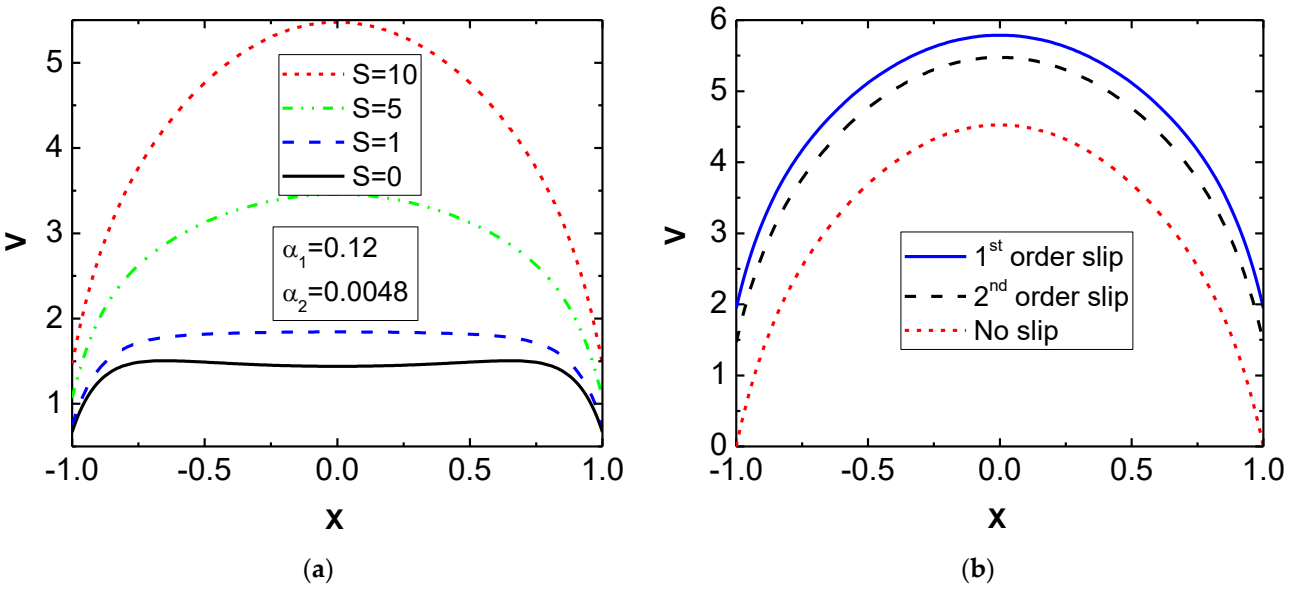

(**a**) (**b**)

Figure 8. Influences of on velocity distributions in microchannels for $K = 10$, $Ha = 1$, and $\Omega = 1$. (**a**) Second-order slip; (**b**) Comparison of no-slip, first-order, and second-order slips at S = 10.

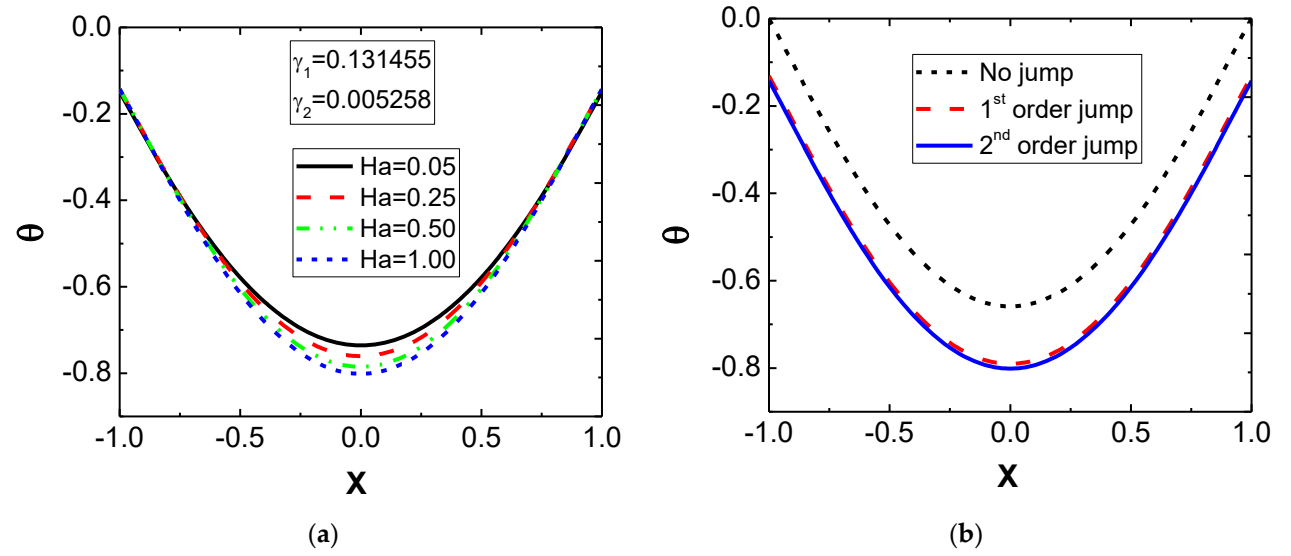

(**a**) (**b**)

Figure 9. Effects of Hartmann number on temperature distributions in microchannel flow at $K = 10$, $S = 0$, $Br = 0.01$, $g_1 = 1$, $\Omega = 1$, $Nr = 1$, $\alpha_1 = 0.12$, and $\alpha_2 = 0.0048$. (**a**) Second-order jump; (**b**) Comparison of no-jump, first-order jump, and second-order jump at *Ha* = 1.0.

Figure 10a depicts the variation of the non-dimensional temperature distribution in the transverse direction for different values of *Ha* for *Ha* > 1, whereas Figure 10b plots a comparison of the temperature distribution due to the other possible boundary conditions adopted to obtain the actual impact of the thermal energy carried out. For maintaining a constant heat flux at the boundary, the advective transport of thermal energy is the crucial parameter to change the local temperature of fluid significantly. An increase in *Ha* promotes the heat transfer by the fluid. For this reason, the non-dimensional temperature decreases with the Hartmann number. Nevertheless, in the presence of the transverse electric field

(S = 10), the flow-aiding force and opposing force take part in a significant role in the flow field. For smaller values of the Hartmann number (*Ha*~0.05–1), the flow velocity increases near the center as compared to near the wall. Therefore, the reduction of thermal energy's advective transport increases the fluid's local fluid temperature under the constant wall heat flux condition.

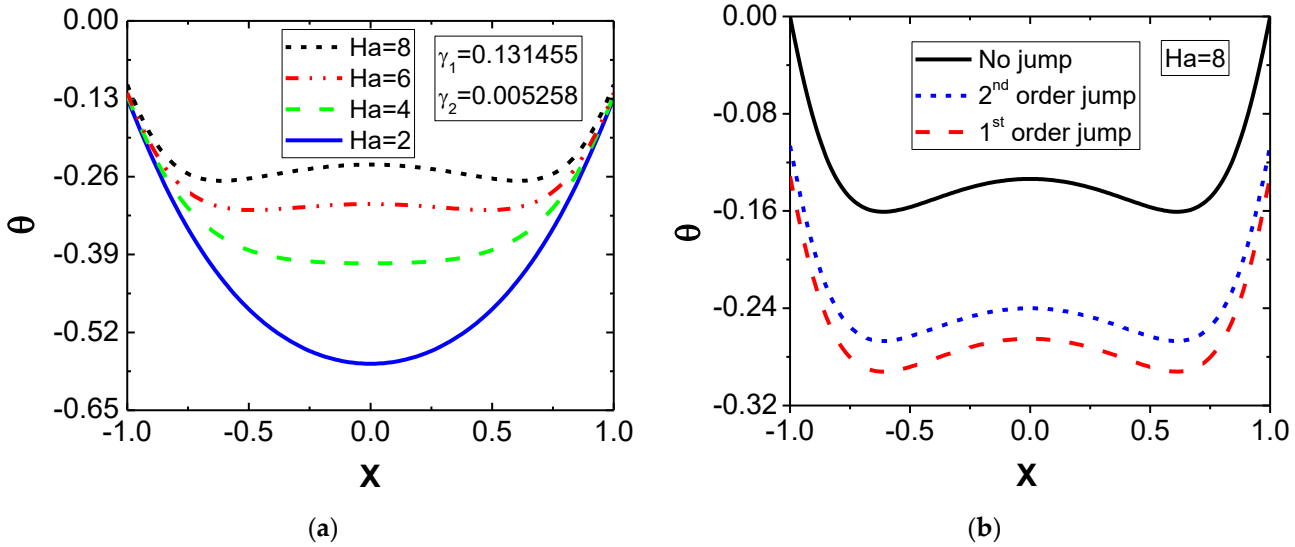

Figure 10. The temperature distribution in microchannels as a function of Hartmann number at $K = 10$, $S = 0$, $Br = 0.01$, $g_1 = 1$, $\Omega = 1$, $Nr = 1$, $\alpha_1 = 0.12$, and $\alpha_2 = 0.0048$. (**a**) Second-order jump; (**b**) Comparison of no-jump, first-order jump, and second-order jump at $Ha = 8.0$.

Here, it can be highlighted that the temperature profiles are in the plane of symmetry shown in Figures 8–10, and the set of temperature profiles are for the Knudsen number (*Kn*) = 0.08. However, the no-jump boundary condition is taken under the no-slip velocity boundary conditions. The temperature jump exists due to the presence of the Knudsen number stated above. On the other hand, the temperature difference occurs between the wall and fluid for weak thermal communication. Weak thermal communication causes due to a low number of collisions between molecules and walls and molecules themselves. Therefore, a strong temperature gradient creates near the wall. A large temperature gradient occurs for the heat transfer near wall surfaces for the first-order and second-order jump (see Figure 2b). For this reason, the temperature difference increases for the temperature jump at the boundary shown in Figures 8–10. We can also conclude that an increase in the value of the Hartmann number enhances the jump temperature.

The non-dimensional temperature distribution with the effect of the magnitude of thermal radiation (*Nr*) parameters is shown in Figure 11. One may note that thermal radiation is an important parameter that plays a vital role in temperature patterns. In the presence of Joule heating and viscous dissipation, the non-dimensional temperature decreases with an increase in the value of thermal radiation. From a physical point of view, it can be concluded that amplifying the local temperature of the fluid occurs due to radiation, as it acts as an energy source in the fluid.

Nusselt number function of *Ha* for different values of *K* with transverse electric field is depicted in Figure 12. The trend of these curves for *Nu* initially declines with *Ha*, reaches a minimum value at a particular *Ha*, and after that, it rises with *Ha*, as displayed in Figure 12. Therefore, there is a critical *Ha*rtmann number (*Hac*) at which *Nu* becomes a minimum. In other words, Nusselt number distributions with *Ha* have two distinct regimes based on the critical *Ha*. At a constant *K*, the Nusselt number decreases in the first region, whereas this trend reverses in the second region. The effect of *K* always provides a high value of *Nu*. *Nu* has also been determined numerically, and these results have been plotted in Figure 12. A comparison of analytical and numerical results shows that they are of comparable

magnitude. Therefore, the present analytical results agree well with the numerical results. The different jump-boundary conditions show that the no-jump incident involves a high value of Nu, and it has, thus, the ability to transfer heat more.

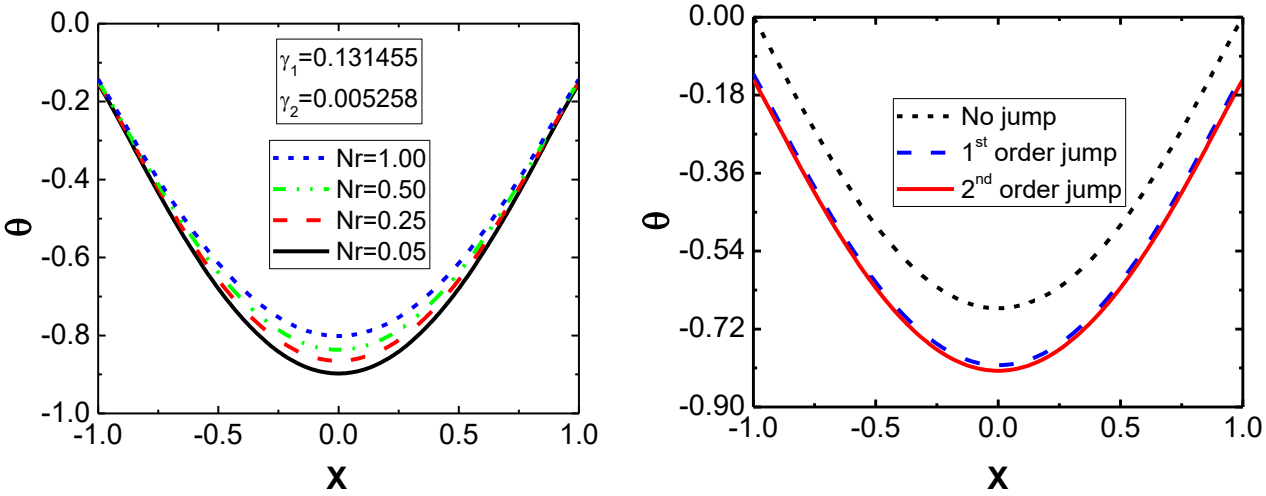

(**a**) (**b**)

Figure 11. Relationship between the Hartmann number and temperature distribution in microchannel flow at $K = 10$, $S = 10$, $Br = 0.01$, $Ha = 1.0$, $g_1 = 1$, $\Omega = 1$, $\alpha_1 = 0.12$, and $\alpha_2 = 0.0048$. (**a**) Second-order jump; (**b**) Comparison of no-jump, first-order jump, and second-order jump at $Nr = 0.75$.

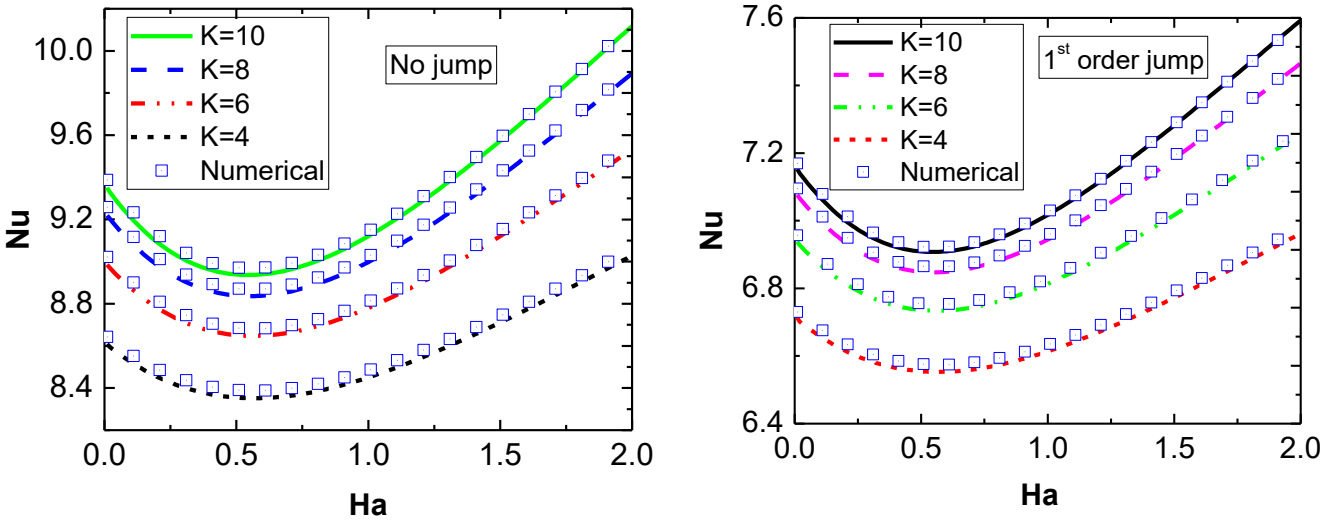

(**a**) (**b**)

Figure 12. Effects of the applied magnetic field on Nusselt number (Nu) for variation with varying electrokinetic width (K) for $Br = 0.01$ $S = 3$ $\Omega = 1$, $g_1 = 1$, $Nr = 0$, $\alpha_1 = 0.12$, and $\alpha_2 = 0.0048$. (**a**) $\gamma_1 = 0$, $\gamma_2 = 0$ and (**b**) $\gamma_1 = 0.131455$, $\gamma_2 = 0$. (**a**) No jump boundary condition; (**b**) First-order jump.

11. Conclusions

The microchannel has gained popularity in the last decade to increase heat transfer. Various applications include small-scale cooling, military hardware, microdosing system, cancer therapy, real environment analysis, etc. Miniaturization has many advantages, such as fast response, accurate results, affordability of mobile monitoring, highly sensitive analysis, etc. The existing literature finds that several analytical and numerical studies are available in electrokinetically fully developed flow in microchannels at a constant heat

flux with the no-slip and no-jump boundary conditions. However, numerical analysis was used to determine *Nu*. Electroosmotic flow in microchannels in consideration of with and without effects of zeta potential was studied by several authors. In the case of experimental works, few studies were available based on the pressure drop, friction factor, and mass flow rate across the channels. Some other works were associated with the effect of the velocity slip at the hydrophobic surface to control the velocity and to determine the region where the velocity and shear stress are comparatively low. Nevertheless, this study presents a new analysis to understand the process of calculating heat transfer for flow through microchannels in electrokinetic actions. The temperature jump condition in microchannels is included for the generalized condition to determine the temperature distribution. For critical applications of microchannels in electromagnetic radiation, radiation fields are imposed. This review paper also focuses on EMHD flow in rectangular microchannels, using second-order velocity slip and temperature jump along with the viscous dissipation, Joule heating, and thermal radiation parameters. It shows that the Hartmann number greatly influences the velocity and temperature distributions both in the presence and absence of a transverse electric field.

In the absence of a transverse electric field, the speed progressively increases with an increasing Hartmann number at a low range. Conversely, the temperature increases with an increasing Hartmann number up to value 1; it is in reversed trend at higher values of Hartmann number. The temperature also increases with an increasing Hartmann number in the presence of an electric field at its low value. Another aspect highlighted in this study is to have the effect of the rarefication in a rectangular microchannel with second-order slip and jump boundary conditions. Velocity and temperature distributions for this case differ with the first-order slip and no-slip conditions and the first-order jump and no-jump conditions, respectively. Under transverse electric fields, the Nusselt number varies with the Hartmann number with increasing values of *K*. We can conclude that up to the critical value of the Hartmann number, the Nusselt number is inversely proportional to the Hartmann number beyond the critical value, and thus, the trend alters.

Finally, it can be noted that this study is devoted to determining the best approach used from all the previously performed research works in microchannels. The whole reason to carry out this work is to prepare one single article in which all existing works are available, and the highlighted mathematical steps are helpful to formulate the analysis of the microchannel heat transfer and fluid flow. In addition, the current analytical study on electro-magneto-hydrodynamic electroosmotic flow in microchannels provides a novel mathematical analysis and unique trend of results. In a nutshell, existing methods and development and future works can be understood from the present paper without the assistance of any other published works in the open literature.

12. Scope for Future Works

Future research on electrokinetic fully developed flow related to microchannels to establish new methods can analyze heat transfer characteristics in different electromagnetic devices.

1. Electrical double layer potential in the general form should be considered in a future study. The Poisson–Boltzmann equation can predict the actual effects on the EDL potential at a high or low zeta potential.
2. An analytical model in general form for microchannels can analyze the rotating non-Newtonian fluid, using slip and jump boundary conditions in the 2D EDL potential.
3. In the non-Newtonian fluid EMHD flow in microchannels, velocity, temperature, and Nusselt number can be determined by the analytical model developed using second-order slip and jump boundary conditions.
4. A closed-form mathematical model of transient EMHD flow in non-Newtonian power-law fluids can be established by considering viscous energy dissipation, Joule heating, and thermal radiation.

Author Contributions: B.K.: Conceptualization; methodology; software; formal analysis; writing—draft preparation, review, and editing; visualization; supervision, etc. S.S.: Conceptualization; methodology; software; formal analysis; writing—original draft preparation; data curation, etc. All authors have read and agreed to the published version of the manuscript.

Funding: This research received no external funding.

Informed Consent Statement: Not applicable for this study as not involving humans.

Data Availability Statement: The data supporting this study's findings are available from the corresponding author upon reasonable request.

Conflicts of Interest: The authors declare no conflict of interest.

Nomenclature

a	half-channel height (m)
B	magnetic field (Tesla)
Br	Brinkman number, $\left(\mu v_{HS}^2\right)/(q_W a)$
c_p	heat capacity at constant pressure per unit mass $\left(\mathrm{J\ kg^{-1}K^{-1}}\right)$
d_h	hydraulic mean diameter of the channel (m)
Da	Darcy factor, $\left(R^*/\phi^N\right)^{2/(1+N)}/d_h^2$
e	electron charge (C)
$\vec{E}$	externally applied electric field per unit length $(\mathrm{Vm^{-1}})$
$\vec{F}$	volumetric electromagnetic body force $(\mathrm{Nm^{-3}})$
g_1	non-dimensional Joule heating parameter, $\left(S_J a\right)/q_w$
Ha	dimensionless magnetic field (Hartmann number), $aB_x\sqrt{\sigma/\mu}$
h	convection energy transport coefficient $\left(\mathrm{Wm^{-2}K^{-1}}\right)$
I	current flow (mA)
k	coefficient of conduction $\left(\mathrm{Wm^{-1}K^{-1}}\right)$
K	dimensionless Debye–Hückel parameter, a/λ_d
Kn	Knudsen number, λ/d_h
$k*$	Rosseland absorption coefficient $(\mathrm{m^{-1}})$
L	channel length (m)
n	ionic species concentration $(\mathrm{m^{-3}})$
n_0	bulk ionic concentration $(\mathrm{m^{-3}})$
N	flow behavior index
Nr	thermal radiation parameter, $\left(16T_3^3\sigma^*\right)/\ \left(3k^*k_T\right)$
Nu	Nusselt number based on hydraulic diameter, hd_h/k
Pe	Peclet number, vd_h/α
Pr	Prandtl number, $\mu c_p/k$
q_r	radiative heat transfer per unit area $(\mathrm{Wm^{-2}})$
q_w	heat flux at the wall imposed externally $(\mathrm{Wm^{-2}})$
R	reciprocal of Debye length, $1/\lambda_d\ \left(\mathrm{m^{-1}}\right)$
R^*	permeability for porous medium of power law fluids $\left(\mathrm{m^{N+1}}\right)$
S_J	Joule heating included as a volumetric heat generation rate $(\mathrm{Wm^{-3}})$
T	temperature (K)
T_m	bulk average temperature (K)
$\vec{U}$	velocity vector $(\mathrm{ms^{-1}})$
v	speed along the y direction $(\mathrm{ms^{-1}})$
V	dimensionless speed along the y direction, v/v_{HS}
v_{HS}	Helmholtz–Smoluchowski (reference) speed $(\mathrm{ms^{-1}})$
x	transversed coordinate (m)
X	dimensionless transverse coordinate, x/a

Greek symbols	
α	thermal diffusivity $\left(\mathrm{m}^2\mathrm{s}^{-1}\right)$
α_1	non-dimensional first-order velocity slip, $Kn(2-\sigma_v)/\sigma_v$
α_2	non-dimensional second-order velocity slip, $Kn^2(2-\sigma_v)/(2\sigma_v)$
γ_1	non-dimensional first-order temperature jump, $\left(\frac{2-\sigma_T}{\sigma_T}\right)\left(\frac{2\gamma}{\gamma+1}\right)\frac{Kn}{\mathrm{Pr}}$
γ_2	non-dimensional second-order temperature jump, $\frac{1}{2}\left(\frac{2-\sigma_T}{\sigma_T}\right)\left(\frac{2\gamma}{\gamma+1}\right)\frac{Kn^2}{\mathrm{Pr}}$
ξ	wall zeta potential (V)
ε	medium permittivity $(\mathrm{CV}^{-1}\mathrm{m}^{-1})$
ε_0	free space permittivity $(\mathrm{CV}^{-1}\mathrm{m}^{-1})$
θ	non-dimensional temperature, $k_T(T-T_w)/(q_w a)$
θ_m	dimensionless bulk mean temperature, expressed in Equation (48)
ρ	density of liquid (kgm^{-3})
ρ_e	local volumetric net charge density (Cm^{-3})
λ	Debye length dimension (m)
μ	dynamic viscosity $(\mathrm{kgm}^{-1}\mathrm{s}^{-1})$
ψ	electrical double layer (EDL) potential (V)
$\overline{\psi}$	dimensionless EDL, ψ/ζ
Ω	dimensionless relative strength of pressure driven and electroosmotic actuation, $\left(P_y a^2\right)/(\mu v_{HS})$
σ	electrical conductivity $(\Omega\mathrm{m})$
$\sigma*$	radiation heat transport (Stefan-Boltzmann) constant $(\mathrm{Wm}^{-2}\mathrm{K}^{-4})$
σ_T	thermal accommodation coefficient $(0 \le \sigma_T \le 1)$
σ_v	momentum accommodation coefficient $(0 \le \sigma_v \le 1)$
ω	valance number of ions in the electrolyte, see Equation (14)
Subscripts	
av	average
c	creep
g	gas
w	wall
x	transverse coordinate
y	axial direction (along y axis)
z	transverse direction (along z axis)

References

1. Becker, H.; Gärtner, C. Polymer microfabrication methods for microfluidic analytical applications. *Electrophoresis* **2000**, *21*, 12–26. [CrossRef]
2. Gravesen, P.; Branebjerg, J.A.; Jensen, O.S. Microfluidics—A review. *J. Micromech. Microeng.* **1993**, *3*, 168–182. [CrossRef]
3. Nguyen, N.-T.; Wu, Z. Micromixers—A review. *J. Micromech. Microeng.* **2004**, *15*, R1–R16. [CrossRef]
4. Ohno, K.-I.; Tachikawa, K.; Manz, A. Microfluidics: Applications for analytical purposes in chemistry and biochemistry. *Electrophoresis* **2008**, *29*, 4443–4453. [CrossRef] [PubMed]
5. Ziaie, B.; Baldi, A.; Lei, M.; Gu, Y.; Siegel, R.A. Hard and soft micromachining for BioMEMS: Review of techniques and examples of applications in microfluidics and drug delivery. *Adv. Drug Deliv. Rev.* **2004**, *56*, 145–172. [CrossRef]
6. Chakraborty, S. Electroosmotically driven capillary transport of typical non-Newtonian biofluids in rectangular microchannels. *Anal. Chim. Acta* **2007**, *605*, 175–184. [CrossRef]
7. Ghosal, S. Lubrication theory for electro-osmotic flow in a microfluidic channel of slowly varying cross-section and wall charge. *J. Fluid Mech.* **2002**, *459*, 103–128. [CrossRef]
8. Hardt, S.; Schönfeld, F. *Microfluidic Technologies for Miniaturized Analysis Systems*; Springer Science & Business Media: Berlin, Germany, 2007; ISBN 978-0-387-68424-6.
9. Jian, Y.; Su, J.; Chang, L.; Liu, Q.; He, G. Transient electroosmotic flow of general Maxwell fluids through a slit microchannel. *Z. Angew. Math. Phys.* **2014**, *65*, 435–447. [CrossRef]
10. Jian, Y.; Yang, L.; Liu, Q. Time periodic electro-osmotic flow through a microannulus. *Phys. Fluids* **2010**, *22*, 042001. [CrossRef]
11. Jian, Y.-J.; Liu, Q.-S.; Yang, L.-G. AC electroosmotic flow of generalized Maxwell fluids in a rectangular microchannel. *J. Non-Newton. Fluid Mech.* **2011**, *166*, 1304–1314. [CrossRef]
12. Pamme, N. Magnetism and microfluidics. *Lab Chip* **2006**, *6*, 24–38. [CrossRef]
13. Hardt, S.; Schönfeld, F. *Microfluidics: Fundamentals and Engineering Concepts*; Springer: Berlin/Heidelberg, Germany, 2007.
14. Hua, S.Z.; Sachs, F.; Yang, D.X.; Chopra, H.D. Microfluidic Actuation Using Electrochemically Generated Bubbles. *Anal. Chem.* **2002**, *74*, 6392–6396. [CrossRef] [PubMed]

15. Marmottant, P.; Hilgenfeldt, S. A bubble-driven microfluidic transport element for bioengineering. *Proc. Natl. Acad. Sci. USA* **2004**, *101*, 9523–9527. [CrossRef] [PubMed]
16. Yeo, L.Y.; Friend, J.R. Surface Acoustic Wave Microfluidics. *Annu. Rev. Fluid Mech.* **2014**, *46*, 379–406. [CrossRef]
17. Dasgupta, P.K.; Liu, S. Auxiliary Electroosmotic Pumping in Capillary Electrophoresis. *Anal. Chem.* **1994**, *66*, 3060–3065. [CrossRef]
18. Li, X.-X.; Yin, Z.; Jian, Y.-J.; Chang, L.; Su, J.; Liu, Q.-S. Transient electro-osmotic flow of generalized Maxwell fluids through a microchannel. *J. Non-Newton. Fluid Mech.* **2012**, *187*, 43–47. [CrossRef]
19. Yao, S.; Santiago, J.G. Porous glass electroosmotic pumps: Theory. *J. Colloid Interface Sci.* **2003**, *268*, 133–142. [CrossRef]
20. Harrison, D.J.; Fluri, K.; Seiler, K.; Fan, Z.; Effenhauser, C.S.; Manz, A. Micromachining a miniaturized capillary electrophoresis-based chemical analysis system on a chip. *Science* **1993**, *261*, 895–897. [CrossRef] [PubMed]
21. Santiago, J.G. Electroosmotic Flows in Microchannels with Finite Inertial and Pressure Forces. *Anal. Chem.* **2001**, *73*, 2353–2365. [CrossRef]
22. Söderman, O.; Jönsson, B. Electro-osmosis: Velocity profiles in different geometries with both temporal and spatial resolution. *J. Chem. Phys.* **1996**, *105*, 10300–10311. [CrossRef]
23. Shoji, S.; Nakagawa, S.; Esashi, M. Micropump and sample-injector for integrated chemical analyzing systems. *Sens. Actuators A Phys.* **1990**, *21*, 189–192. [CrossRef]
24. Iverson, B.; Garimella, S.V. Recent advances in microscale pumping technologies: A review and evaluation. *Microfluid. Nanofluidics* **2008**, *5*, 145–174. [CrossRef]
25. Laser, D.J.; Santiago, J.G. A review of micropumps. *J. Micromech. Microeng.* **2004**, *14*, R35–R64. [CrossRef]
26. Chakraborty, S. Dynamics of capillary flow of blood into a microfluidic channel. *Lab Chip* **2005**, *5*, 421–430. [CrossRef] [PubMed]
27. Culbertson, C.T.; Ramsey, R.S.; Ramsey, J.M. Electroosmotically Induced Hydraulic Pumping on Microchips: Differential Ion Transport. *Anal. Chem.* **2000**, *72*, 2285–2291. [CrossRef] [PubMed]
28. Dasgupta, P.K.; Liu, S. Electroosmosis: A Reliable Fluid Propulsion System for Flow Injection Analysis. *Anal. Chem.* **1994**, *66*, 1792–1798. [CrossRef]
29. Burgreen, D.; Nakache, F.R. Electrokinetic Flow in Ultrafine Capillary Slits. *J. Phys. Chem.* **1964**, *68*, 1084–1091. [CrossRef]
30. Chen, X.; Toh, K.; Chai, J.; Yang, C. Developing pressure-driven liquid flow in microchannels under the electrokinetic effect. *Int. J. Eng. Sci.* **2004**, *42*, 609–622. [CrossRef]
31. Hetsroni, G.; Mosyak, A.; Pogrebnyak, E.; Yarin, L. Fluid flow in micro-channels. *Int. J. Heat Mass Transf.* **2005**, *48*, 1982–1998. [CrossRef]
32. Mala, G.M.; Li, D.; Dale, J. Heat transfer and fluid flow in microchannels. *Int. J. Heat Mass Transf.* **1997**, *40*, 3079–3088. [CrossRef]
33. Mala, G.M.; Li, D.; Werner, C.; Jacobasch, H.-J.; Ning, Y. Flow characteristics of water through a microchannel between two parallel plates with electrokinetic effects. *Int. J. Heat Fluid Flow* **1997**, *18*, 489–496. [CrossRef]
34. Ngoma, G.D.; Erchiqui, F. Pressure gradient and electroosmotic effects on two immiscible fluids in a microchannel between two parallel plates. *J. Micromech. Microeng.* **2005**, *16*, 83–91. [CrossRef]
35. Yang, J.; Kwok, D.Y. Effect of liquid slip in electrokinetic parallel-plate microchannel flow. *J. Colloid Interface Sci.* **2003**, *260*, 225–233. [CrossRef]
36. Yang, C.; Li, D. Analysis of electrokinetic effects on the liquid flow in rectangular microchannels. *Colloids Surf. A Physicochem. Eng. Asp.* **1998**, *143*, 339–353. [CrossRef]
37. Arulanandam, S.; Li, D. Liquid transport in rectangular microchannels by electroosmotic pumping. *Colloids Surf. A Physicochem. Eng. Asp.* **2000**, *161*, 89–102. [CrossRef]
38. Chen, X.Y.; Toh, K.C.; Yang, C.; Chai, J.C. Numerical Computation of Hydrodynamically and Thermally Developing Liquid Flow in Microchannels With Electrokinetics Effects. *J. Heat Transf.* **2004**, *126*, 70–75. [CrossRef]
39. Erickson, D.; Li, D. Streaming Potential and Streaming Current Methods for Characterizing Heterogeneous Solid Surfaces. *J. Colloid Interface Sci.* **2001**, *237*, 283–289. [CrossRef]
40. Soong, C.Y.; Wang, S.H. Theoretical analysis of electrokinetic flow and heat transfer in a microchannel under asymmetric boundary conditions. *J. Colloid Interface Sci.* **2003**, *265*, 202–213. [CrossRef]
41. Yang, C.; Li, D. Electrokinetic Effects on Pressure-Driven Liquid Flows in Rectangular Microchannels. *J. Colloid Interface Sci.* **1997**, *194*, 95–107. [CrossRef]
42. Yang, C.; Li, D.; Masliyah, J.H. Modeling forced liquid convection in rectangular microchannels with electrokinetic effects. *Int. J. Heat Mass Transf.* **1998**, *41*, 4229–4249. [CrossRef]
43. Yang, R.-J.; Fu, L.-M.; Hwang, C.-C. Electroosmotic Entry Flow in a Microchannel. *J. Colloid Interface Sci.* **2001**, *244*, 173–179. [CrossRef]
44. Yang, C.; Ooi, K.; Wong, T.; Masliyah, J.H. Frequency-dependent laminar electroosmotic flow in a closed-end rectangular microchannel. *J. Colloid Interface Sci.* **2004**, *275*, 679–698.
45. Luo, W.-J.; Pan, Y.-J.; Yang, R.-J. Transient analysis of electro-osmotic secondary flow induced by dc or ac electric field in a curved rectangular microchannel. *J. Micromech. Microeng.* **2004**, *15*, 463–473. [CrossRef]
46. Yang, J.; Kwok, D.Y. Analytical treatment of electrokinetic microfluidics in hydrophobic microchannels. *Anal. Chim. Acta* **2004**, *507*, 39–53. [CrossRef]

47. Kang, Y.; Ooi, K.T.; Yang, C.; Wong, T.N. Frequency-dependent velocity and vorticity fields of electro-osmotic flow in a closed-end cylindrical microchannel. *J. Micromech. Microeng.* **2004**, *15*, 301–312.
48. Jayaraj, S.; Kang, S.; Suh, Y.K. A review on the analysis and experiment of fluid flow and mixing in micro-channels. *J. Mech. Sci. Technol.* **2007**, *21*, 536–548. [CrossRef]
49. West, J.; Karamata, B.; Lillis, B.; Gleeson, J.P.; Alderman, J.; Collins, J.K.; Lane, W.; Mathewson, A.; Berney, H. Application of magnetohydrodynamic actuation to continuous flow chemistry. *Lab Chip* **2002**, *2*, 224–230. [CrossRef]
50. Weston, M.C.; Gerner, M.D.; Fritsch, I. Magnetic Fields for Fluid Motion. *Anal. Chem.* **2010**, *82*, 3411–3418. [CrossRef]
51. Yi, M.; Qian, S.; Bau, H.H. A magnetohydrodynamic chaotic stirrer. *J. Fluid Mech.* **2002**, *468*, 153–177. [CrossRef]
52. Jang, J.; Lee, S.S. Theoretical and experimental study of MHD (magnetohydrodynamic) micropump. *Sens. Actuators A Phys.* **2000**, *80*, 84–89. [CrossRef]
53. Jian, Y.; Si, D.; Chang, L.; Liu, Q. Transient rotating electromagnetohydrodynamic micropumps between two infinite microparallel plates. *Chem. Eng. Sci.* **2015**, *134*, 12–22. [CrossRef]
54. Lemoff, A.V.; Lee, A. An AC magnetohydrodynamic micropump. *Sens. Actuators B Chem.* **2000**, *63*, 178–185. [CrossRef]
55. Nguyen, B.; Kassegne, S.K. High-current density DC magenetohydrodynamics micropump with bubble isolation and release system. *Microfluid. Nanofluidics* **2008**, *5*, 383–393. [CrossRef]
56. Xie, Z.-Y.; Jian, Y.-J. Rotating electromagnetohydrodynamic flow of power-law fluids through a microparallel channel. *Colloids Surf. A Physicochem. Eng. Asp.* **2017**, *529*, 334–345. [CrossRef]
57. Yang, C.; Jian, Y.; Xie, Z.; Li, F. Heat transfer characteristics of magnetohydrodynamic electroosmotic flow in a rectangular microchannel. *Eur. J. Mech.-B/Fluids* **2018**, *74*, 180–190. [CrossRef]
58. Debye, P.; Hückel, E. Zur theorie der elektrolyte. II. *Phys. ZfT* **1923**, *24*, 305–325.
59. Reuss, F.F. Su run nouvel effet de l'électricité galvanique. *Mem. Soc. Imp. Nat. Moscou* **1809**, *2*, 327–337.
60. Helmholtz, H.V. Studien über electrische Grenzschichten. *Ann. Phys.* **1879**, *243*, 337–382. [CrossRef]
61. Smoluchowski, M.V. Handbuch der Elektrizität und des Magnetismus. *Band II Barth-Verl. Leipz.* **1921**, 366–427. [CrossRef]
62. Gouy, M. Sur la constitution de la charge électrique à la surface d'un electrolyte. *J. Phys. Theor. Appl.* **1910**, *9*, 457–468. [CrossRef]
63. Chapman, D.L. LI. A contribution to the theory of electrocapillarity. *Lond. Edinb. Dublin Philos. Mag. J. Sci.* **1913**, *25*, 475–481. [CrossRef]
64. Stern, O. Zur theorie der elektrolytischen doppelschicht. *Z. Elektrochem. Angew. Phys. Chem.* **1924**, *30*, 508–516.
65. Cosgrove, T. *Colloid Science: Principles, Methods and Applications*; John Wiley & Sons: Hoboken, NJ, USA, 2010.
66. Hunter, R.J. *Foundations of Colloid Science*; Oxford University Press: Oxford, UK, 2001.
67. Hunter, R.J. *Zeta Potential in Colloid Science: Principles and Applications*; Academic Press: Cambridge, MA, USA, 2013.
68. Andelman, D. *Electrostatic Properties of Membranes: The Poisson-Boltzmann Theory*; Elsevier: Amsterdam, The Netherlands, 1995.
69. Wennerström, H. *The Colloidal Domain: Where Physics, Chemistry, Biology, and Technology Meet*; Wiley-VCH: Wehenheim, Germany, 1999.
70. Bayraktar, T.; Pidugu, S.B. Characterization of liquid flows in microfluidic systems. *Int. J. Heat Mass Transf.* **2006**, *49*, 815–824. [CrossRef]
71. Li, D. *Electrokinetics in Microfluidics*; Elsevier: Amsterdam, The Netherlands, 2004.
72. Alizadeh, A.; Hsu, W.; Wang, M.; Daiguji, H. Electroosmotic flow: From microfluidics to nanofluidics. *Electrophoresis* **2021**, *42*, 834–868. [CrossRef]
73. Neale, S.M. The electrical double layer, the electrokinetic potential, and the streaming current. *Trans. Faraday Soc.* **1946**, *42*, 473–478. [CrossRef]
74. Wall, S. The history of electrokinetic phenomena. *Curr. Opin. Colloid Interface Sci.* **2010**, *15*, 119–124. [CrossRef]
75. López-García, J.J.; Horno, J.; Grosse, C. Poisson–Boltzmann Description of the Electrical Double Layer Including Ion Size Effects. *Langmuir* **2011**, *27*, 13970–13974. [CrossRef]
76. Sadeghi, A.; Saidi, M.H. Viscous dissipation effects on thermal transport characteristics of combined pressure and electroosmotically driven flow in microchannels. *Int. J. Heat Mass Transf.* **2010**, *53*, 3782–3791. [CrossRef]
77. Jorgenson, J.W.; Lukacs, K.D. Capillary zone electrophoresis. *Science* **1983**, *222*, 266–274. [CrossRef]
78. Jacobson, S.C.; Hergenroder, R.; Koutny, L.B.; Ramsey, J.M. High-Speed Separations on a Microchip. *Anal. Chem.* **1994**, *66*, 1114–1118. [CrossRef]
79. Dehe, S.; Rofman, B.; Bercovici, M.; Hardt, S. Electro-osmotic flow enhancement over superhydrophobic surfaces. *Phys. Rev. Fluids* **2020**, *5*, 053701. [CrossRef]
80. Maynes, D.; Webb, B.W. Fully-Developed Thermal Transport in Combined Pressure and Electro-Osmotically Driven Flow in Microchannels. *J. Heat Transf.* **2003**, *125*, 889–895. [CrossRef]
81. Zade, A.Q.; Manzari, M.T.; Hannani, S.K. An analytical solution for thermally fully developed combined pressure-electroosmotically driven flow in microchannels. *Int. J. Heat Mass Transf.* **2007**, *50*, 1087–1096. [CrossRef]
82. Keramati, H.; Sadeghi, A.; Saidi, M.H.; Chakraborty, S. Analytical solutions for thermo-fluidic transport in electroosmotic flow through rough microtubes. *Int. J. Heat Mass Transf.* **2016**, *92*, 244–251. [CrossRef]
83. Bandopadhyay, A.; Goswami, P.; Chakraborty, S. Regimes of streaming potential in cylindrical nano-pores in presence of finite sized ions and charge induced thickening: An analytical approach. *J. Chem. Phys.* **2013**, *139*, 224503. [CrossRef]

84. Chen, C.-H. Thermal transport characteristics of mixed pressure and electro-osmotically driven flow in micro-and nanochannels with Joule heating. *J. Heat Transf.* **2009**, *131*, 022401. [CrossRef]
85. Ferrás, L.L.; Afonso, A.; Alves, M.; Nóbrega, J.; Pinho, F. Analytical and numerical study of the electro-osmotic annular flow of viscoelastic fluids. *J. Colloid Interface Sci.* **2013**, *420*, 152–157. [CrossRef]
86. Yavari, H.; Sadeghi, A.; Saidi, M.H.; Chakraborty, S. Combined influences of viscous dissipation, non-uniform Joule heating and variable thermophysical properties on convective heat transfer in microtubes. *Int. J. Heat Mass Transf.* **2012**, *55*, 762–772. [CrossRef]
87. Yoshida, H.; Kinjo, T.; Washizu, H. Analysis of electro-osmotic flow in a microchannel with undulated surfaces. *Comput. Fluids* **2016**, *124*, 237–245. [CrossRef]
88. Babaie, A.; Sadeghi, A.; Saidi, M.H. Combined electroosmotically and pressure driven flow of power-law fluids in a slit microchannel. *J. Non-Newton. Fluid Mech.* **2011**, *166*, 792–798. [CrossRef]
89. Chen, C.-H. Fully-developed thermal transport in combined slit microchannel electroosmotic and pressure driven flow of power-law fluids in microchannels. *Int. J. Heat Mass Transf.* **2012**, *55*, 2173–2183. [CrossRef]
90. Deng, S.Y.; Jian, Y.; Bi, Y.; Chang, L.; Wang, H.; Liu, Q. Unsteady electroosmotic flow of power-law fluid in a rectangular microchannel. *Mech. Res. Commun.* **2012**, *39*, 9–14. [CrossRef]
91. Tang, G.H.; Li, X.; He, Y.; Tao, W. Electroosmotic flow of non-Newtonian fluid in microchannels. *J. Non-Newton. Fluid Mech.* **2009**, *157*, 133–137. [CrossRef]
92. Vakili, M.A.; Saidi, M.H.; Sadeghi, A. Thermal transport characteristics pertinent to electrokinetic flow of power-law fluids in rectangular microchannels. *Int. J. Therm. Sci.* **2014**, *79*, 76–89. [CrossRef]
93. Vasu, N.; De, S. Electroosmotic flow of power-law fluids at high zeta potentials. *Colloids Surf. A Physicochem. Eng. Asp.* **2010**, *368*, 44–52. [CrossRef]
94. Zhao, C.; Zholkovskij, E.; Masliyah, J.H.; Yang, C. Analysis of electroosmotic flow of power-law fluids in a slit microchannel. *J. Colloid Interface Sci.* **2008**, *326*, 503–510. [CrossRef]
95. Choi, D.-S.; Yun, S.; Choi, W. An Exact Solution for Power-Law Fluids in a Slit Microchannel with Different Zeta Potentials under Electroosmotic Forces. *Micromachines* **2018**, *9*, 504. [CrossRef]
96. Yu, S.; Ameel, T.A. Slip-flow heat transfer in rectangular microchannels. *Int. J. Heat Mass Transf.* **2001**, *44*, 4225–4234. [CrossRef]
97. Chein, R.; Yang, Y.C.; Lin, Y. Estimation of Joule heating effect on temperature and pressure distribution in electrokinetic-driven microchannel flows. *Electrophoresis* **2006**, *27*, 640–649. [CrossRef]
98. Tang, G.; Yan, D.; Yang, C.; Gong, H.; Chai, C.; Lam, Y. Joule heating and its effects on electrokinetic transport of solutes in rectangular microchannels. *Sens. Actuators A Phys.* **2007**, *139*, 221–232. [CrossRef]
99. Xuan, X. Joule heating in electrokinetic flow. *Electrophoresis* **2008**, *29*, 33–43. [CrossRef] [PubMed]
100. Hu, G.; Xiang, Q.; Fu, R.; Xu, B.; Venditti, R.; Li, D. Electrokinetically controlled real-time polymerase chain reaction in microchannel using Joule heating effect. *Anal. Chim. Acta* **2006**, *557*, 146–151. [CrossRef]
101. Xuan, X.; Sinton, D.; Li, D. Thermal end effects on electroosmotic flow in a capillary. *Int. J. Heat Mass Transf.* **2004**, *47*, 3145–3157. [CrossRef]
102. Cetin, B.; Li, D. Effect of Joule heating on electrokinetic transport. *Electrophoresis* **2008**, *29*, 994–1005. [CrossRef]
103. Das, S.; Das, T.; Chakraborty, S. Modeling of coupled momentum, heat and solute transport during DNA hybridization in a microchannel in the presence of electro-osmotic effects and axial pressure gradients. *Microfluid. Nanofluid* **2006**, *2*, 37–49. [CrossRef]
104. Elazhary, A.; Soliman, H. Analytical solutions of fluid flow and heat transfer in parallel-plate micro-channels at high zeta-potentials. *Int. J. Heat Mass Transf.* **2009**, *52*, 4449–4458. [CrossRef]
105. Horiuchi, K.; Dutta, P. Joule heating effects in electroosmotically driven microchannel flows. *Int. J. Heat Mass Transf.* **2004**, *47*, 3085–3095. [CrossRef]
106. Jain, A.; Jensen, M.K. Analytical modeling of electrokinetic effects on flow and heat transfer in microchannels. *Int. J. Heat Mass Transf.* **2007**, *50*, 5161–5167. [CrossRef]
107. Su, J.; Jian, Y.; Chang, L. Thermally fully developed electroosmotic flow through a rectangular microchannel. *Int. J. Heat Mass Transf.* **2012**, *55*, 6285–6290. [CrossRef]
108. Tang, G.Y.; Yang, C.; Chai, C.J.; Gong, H.Q. Modeling of Electroosmotic Flow and Capillary Electrophoresis with the Joule Heating Effect: The Nernst−Planck Equation versus the Boltzmann Distribution. *Langmuir* **2003**, *19*, 10975–10984. [CrossRef]
109. Xuan, X.; Xu, B.; Sinton, D.; Li, D. Electroosmotic flow with Joule heating effects. *Lab Chip* **2004**, *4*, 230–236. [CrossRef] [PubMed]
110. Xuan, X.; Li, D. Analytical study of Joule heating effects on electrokinetic transportation in capillary electrophoresis. *J. Chromatogr. A* **2005**, *1064*, 227–237. [CrossRef] [PubMed]
111. Lizardi, J.J.; Ramos, E.; Mendez, F. Numerical Analysis for Temperature Changes in an Electro-Osmotic Flow in a Microchannel. *J. Thermophys. Heat Transf.* **2019**, *33*, 663–672. [CrossRef]
112. Erickson, D.; Sinton, D.; Li, D. Joule heating and heat transfer in poly(dimethylsiloxane) microfluidic systems. *Lab Chip* **2003**, *3*, 141–149. [CrossRef] [PubMed]
113. Petersen, N.J.; Nikolajsen, R.P.H.; Mogensen, K.B.; Kutter, J.P. Effect of Joule heating on efficiency and performance for microchip-based and capillary-based electrophoretic separation systems: A closer look. *Electrophoresis* **2004**, *25*, 253–269. [CrossRef]

114. Xuan, X.; Li, D. Joule heating effects on peak broadening in capillary zone electrophoresis. *J. Micromech. Microeng.* **2004**, *14*, 1171–1180. [CrossRef]
115. Tang, G.; Yan, D.; Yang, C.; Gong, H.; Chai, J.C.; Lam, Y.C. Assessment of Joule heating and its effects on electroosmotic flow and electrophoretic transport of solutes in microfluidic channels. *Electrophoresis* **2006**, *27*, 628–639. [CrossRef]
116. Grushka, E.; McCormick, R.M.; Kirkland, J.J. Effect of temperature gradients on the efficiency of capillary zone electrophoresis separations. *Anal. Chem.* **1989**, *61*, 241–246. [CrossRef]
117. Jones, A.E.; Grushka, E. Nature of temperature gradients in capillary zone electrophoresis. *J. Chromatogr. A* **1989**, *466*, 219–225. [CrossRef]
118. Knox, J.H.; Grant, I.H. Miniaturisation in pressure and electroendosmotically driven liquid chromatography: Some theoretical considerations. *Chromatographia* **1987**, *24*, 135–143. [CrossRef]
119. Knox, H.; McCormack, K.A. Temperature effects in capillary electrophoresis. 1: Internal capillary temperature and effect upon performance. *Chromatographia* **1994**, *38*, 207–214. [CrossRef]
120. Mondal, M.; Misra, R.P.; De, S. Combined electroosmotic and pressure driven flow in a microchannel at high zeta potential and overlapping electrical double layer. *Int. J. Therm. Sci.* **2014**, *86*, 48–59. [CrossRef]
121. Tripathi, D.; Sharma, A.; Bég, O.A. Joule heating and buoyancy effects in electro-osmotic peristaltic transport of aqueous nanofluids through a microchannel with complex wave propagation. *Adv. Powder Technol.* **2018**, *29*, 639–653. [CrossRef]
122. Noreen, S.; Waheed, S.; Lu, D.C. Influence of Joule heating and wall slip in electroosmotic flow via peristalsis: Second law analysis. *J. Braz. Soc. Mech. Sci. Eng.* **2020**, *42*, 1–19. [CrossRef]
123. Nayak, A.K.; Haque, A.; Weigand, B. Analysis of electroosmotic flow and Joule heating effect in a hydrophobic channel. *Chem. Eng. Sci.* **2018**, *176*, 165–179. [CrossRef]
124. Shit, G.G.; Mondal, A.; Sinha, A.; Kundu, P. Electro-osmotic flow of power-law fluid and heat transfer in a micro-channel with effects of Joule heating and thermal radiation. *Phys. A Stat. Mech. Its Appl.* **2016**, *462*, 1040–1053. [CrossRef]
125. Sánchez, S.; Ascanio, G.; Méndez, F.; Bautista, O. Theoretical analysis of non-linear Joule heating effects on an electroosmotic flow with patterned surface charges. *Phys. Fluids* **2018**, *30*, 112002. [CrossRef]
126. Vargas, C.; Bautista, O.; Méndez, F. Effect of temperature-dependent properties on electroosmotic mobility at arbitrary zeta potentials. *Appl. Math. Model.* **2018**, *68*, 616–628. [CrossRef]
127. Del Giudice, S.; Nonino, C.; Savino, S. Effects of viscous dissipation and temperature dependent viscosity in thermally and simultaneously developing laminar flows in microchannels. *Int. J. Heat Fluid Flow* **2006**, *28*, 15–27. [CrossRef]
128. Morini, G.L. Viscous heating in liquid flows in micro-channels. *Int. J. Heat Mass Transf.* **2005**, *48*, 3637–3647. [CrossRef]
129. Morini, G.L.; Spiga, M. The Role of the Viscous Dissipation in Heated Microchannels. *J. Heat Transf.* **2006**, *129*, 308–318. [CrossRef]
130. Tso, C.P.; Mahulikar, S. The role of the Brinkman number in analysing flow transitions in microchannels. *Int. J. Heat Mass Transf.* **1999**, *42*, 1813–1833. [CrossRef]
131. Tso, C.P.; Mahulikar, S. Experimental verification of the role of Brinkman number in microchannels using local parameters. *Int. J. Heat Mass Transf.* **2000**, *43*, 1837–1849. [CrossRef]
132. Lawal, A.; Mujumdar, A.S. Viscous dissipation effects on thermal entrance heat transfer to power-law fluids in arbitrary cross-sectional ducts. *Chem. Eng. J.* **1989**, *41*, 57–66. [CrossRef]
133. Xu, B.; Ooi, K.T.; Mavriplis, C.; E Zaghloul, M. Evaluation of viscous dissipation in liquid flow in microchannels. *J. Micromech. Microeng.* **2002**, *13*, 53. [CrossRef]
134. Nonino, C.; Del Giudice, S.; Savino, S. Temperature-Dependent Viscosity and Viscous Dissipation Effects in Simultaneously Developing Flows in Microchannels With Convective Boundary Conditions. *J. Heat Transf.* **2006**, *129*, 1187–1194. [CrossRef]
135. Nonino, C.; Del Giudice, S.; Savino, S. Temperature-Dependent Viscosity and Viscous Dissipation Effects in Microchannel Flows with Uniform Wall Heat Flux. *Heat Transf. Eng.* **2010**, *31*, 682–691. [CrossRef]
136. Baranov, A.V.; Yunitskii, S.A. Influence of Dissipation on Heat Transfer During Flow of a Non-Newtonian Fluid in a Porous Channel. *J. Eng. Phys.* **2017**, *90*, 1003–1009. [CrossRef]
137. Barletta, A. Fully developed laminar forced convection in circular ducts for power-law fluids with viscous dissipation. *Int. J. Heat Mass Transf.* **1996**, *40*, 15–26. [CrossRef]
138. Chen, G.M.; Tso, C. Effects of viscous dissipation on forced convective heat transfer in a channel embedded in a power-law fluid saturated porous medium. *Int. Commun. Heat Mass Transf.* **2011**, *38*, 57–62. [CrossRef]
139. Chiba, R.; Izumi, M.; Sugano, Y. An analytical solution to non-axisymmetric heat transfer with viscous dissipation for non-Newtonian fluids in laminar forced flow. *Ingenieur-Archiv* **2007**, *78*, 612008. [CrossRef]
140. Kolitawong, C.; Kananai, N.; Giacomin, J.; Nontakaew, U. Viscous dissipation of a power law fluid in axial flow between isothermal eccentric cylinders. *J. Non-Newton. Fluid Mech.* **2011**, *166*, 133–144. [CrossRef]
141. Lawal, A.; Mujumdar, A.S. The effects of viscous dissipation on heat transfer to power law fluids in arbitrary cross-sectional ducts. *Wärme Stoffübertrag.* **1992**, *27*, 437–446. [CrossRef]
142. Tso, C.P.; Sheela-Francisca, J.; Hung, Y.-M. Viscous dissipation effects of power-law fluid flow within parallel plates with constant heat fluxes. *J. Non-Newton. Fluid Mech.* **2010**, *165*, 625–630. [CrossRef]
143. Koo, J.; Kleinstreuer, C. Viscous dissipation effects in microtubes and microchannels. *Int. J. Heat Mass Transf.* **2004**, *47*, 3159–3169. [CrossRef]

144. Koo, J.; Kleinstreuer, C. Liquid flow in microchannels: Experimental observations and computational analyses of microfluidics effects. *J. Micromech. Microeng.* **2003**, *13*, 568–579. [CrossRef]
145. Tso, C.P.; Mahulikar, S. The use of the Brinkman number for single phase forced convective heat transfer in microchannels. *Int. J. Heat Mass Transf.* **1998**, *41*, 1759–1769. [CrossRef]
146. Tunc, G.; Bayazitoglu, Y. Heat transfer in microtubes with viscous dissipation. *Int. J. Heat Mass Transf.* **2001**, *44*, 2395–2403. [CrossRef]
147. Sheela-Francisca, J.; Tso, C.; Hung, Y.M.; Rilling, D. Heat transfer on asymmetric thermal viscous dissipative Couette–Poiseuille flow of pseudo-plastic fluids. *J. Non-Newton. Fluid Mech.* **2012**, *169–170*, 42–53. [CrossRef]
148. Chee, Y.S.; Ting, T.W.; Hung, Y.M. Entropy generation of viscous dissipative flow in thermal non-equilibrium porous media with thermal asymmetries. *Energy* **2015**, *89*, 382–401. [CrossRef]
149. Hung, Y.M.; Tso, C.P. Temperature Variations of Forced Convection in Porous Media for Heating and Cooling Processes: Internal Heating Effect of Viscous Dissipation. *Transp. Porous Media* **2008**, *75*, 319–332. [CrossRef]
150. Hung, Y.-M.; Tso, C. Effects of viscous dissipation on fully developed forced convection in porous media. *Int. Commun. Heat Mass Transf.* **2009**, *36*, 597–603. [CrossRef]
151. Mukherjee, S.; Biswal, P.; Chakraborty, S.; DasGupta, S. Effects of viscous dissipation during forced convection of power-law fluids in microchannels. *Int. Commun. Heat Mass Transf.* **2017**, *89*, 83–90. [CrossRef]
152. Mah, W.H.; Hung, Y.M.; Guo, N. Entropy generation of viscous dissipative nanofluid flow in microchannels. *Int. J. Heat Mass Transf.* **2012**, *55*, 4169–4182. [CrossRef]
153. Ting, T.W.; Hung, Y.M.; Guo, N. Entropy generation of viscous dissipative nanofluid flow in thermal non-equilibrium porous media embedded in microchannels. *Int. J. Heat Mass Transf.* **2015**, *81*, 862–877. [CrossRef]
154. Ting, T.W.; Hung, Y.M.; Guo, N. Viscous dissipative forced convection in thermal non-equilibrium nanofluid-saturated porous media embedded in microchannels. *Int. Commun. Heat Mass Transf.* **2014**, *57*, 309–318. [CrossRef]
155. Haddout, Y.; Lahjomri, J. The extended Graetz problem for a gaseous slip flow in micropipe and parallel-plate microchannel with heating section of finite length: Effects of axial conduction, viscous dissipation and pressure work. *Int. J. Heat Mass Transf.* **2015**, *80*, 673–687. [CrossRef]
156. Jing, D.; Pan, Y.; Wang, X. Joule heating, viscous dissipation and convective heat transfer of pressure-driven flow in a microchannel with surface charge-dependent slip. *Int. J. Heat Mass Transf.* **2017**, *108*, 1305–1313. [CrossRef]
157. Zanchini, E. Effect of viscous dissipation on mixed convection in a vertical channel with boundary conditions of the third kind. *Int. J. Heat Mass Transf.* **1998**, *41*, 3949–3959. [CrossRef]
158. Şen, S.; Darici, S. Transient conjugate heat transfer in a circular microchannel involving rarefaction, viscous dissipation and axial conduction effects. *Appl. Therm. Eng.* **2017**, *111*, 855–862. [CrossRef]
159. Lalami, A.A.; Afrouzi, H.H.; Moshfegh, A.; Omidi, M.; Javadzadegan, A. Investigation of nanofluid heat transfer in a microchannel under magnetic field via Lattice Boltzmann method: Effects of surface hydrophobicity, viscous dissipation, and Joule heating. *J. Heat Transf.* **2019**, *141*, 062403. [CrossRef]
160. Rad, P.M.; Aghanajafi, C. The Effect of Thermal Radiation on Nanofluid Cooled Microchannels. *J. Fusion Energy* **2008**, *28*, 91–100.
161. Cortell, R. Fluid flow and radiative nonlinear heat transfer over a stretching sheet. *J. King Saud Univ.-Sci.* **2014**, *26*, 161–167. [CrossRef]
162. Farooq, M.; Khan, M.I.; Waqas, M.; Hayat, T.; Alsaedi, A. MHD stagnation point flow of viscoelastic nanofluid with non-linear radiation effects. *J. Mol. Liq.* **2016**, *221*, 1097–1103. [CrossRef]
163. Gorla, R.S.R.; Bakier, A. Thermal analysis of natural convection and radiation in porous fins. *Int. Commun. Heat Mass Transf.* **2011**, *38*, 638–645. [CrossRef]
164. López, A.; Ibáñez, G.; Pantoja, J.; Moreira, J.; Lastres, O. Entropy generation analysis of MHD nanofluid flow in a porous vertical microchannel with nonlinear thermal radiation, slip flow and convective-radiative boundary conditions. *Int. J. Heat Mass Transf.* **2017**, *107*, 982–994. [CrossRef]
165. Kundu, B.; Bhanja, D.; Lee, K.-S. A model on the basis of analytics for computing maximum heat transfer in porous fins. *Int. J. Heat Mass Transf.* **2012**, *55*, 7611–7622. [CrossRef]
166. Kundu, B.; Bhanja, D. An analytical prediction for performance and optimum design analysis of porous fins. *Int. J. Refrig.* **2011**, *34*, 337–352. [CrossRef]
167. Das, R.; Kundu, B. Simultaneous estimation of heat generation and magnetic field in a radial porous fin from surface temperature information. *Int. Commun. Heat Mass Transf.* **2021**, *127*, 105497. [CrossRef]
168. He, Y.; Shirazaki, M.; Liu, H.; Himeno, R.; Sun, Z. A numerical coupling model to analyze the blood flow, temperature, and oxygen transport in human breast tumor under laser irradiation. *Comput. Biol. Med.* **2005**, *36*, 1336–1350. [CrossRef]
169. Pal, D.; Mondal, H. Influence of temperature-dependent viscosity and thermal radiation on MHD forced convection over a non-isothermal wedge. *Appl. Math. Comput.* **2009**, *212*, 194–208. [CrossRef]
170. Pal, D.; Mondal, H. Influence of thermophoresis and Soret–Dufour on magnetohydrodynamic heat and mass transfer over a non-isothermal wedge with thermal radiation and Ohmic dissipation. *J. Magn. Magn. Mater.* **2013**, *331*, 250–255. [CrossRef]
171. Sinha, A.; Shit, G. Electromagnetohydrodynamic flow of blood and heat transfer in a capillary with thermal radiation. *J. Magn. Magn. Mater.* **2014**, *378*, 143–151. [CrossRef]

172. Nazeer, M.; Ali, N.; Ahmad, F.; Ali, W.; Saleem, A.; Ali, Z.; Sarfraz, A. Effects of radiative heat flux and joule heating on electro-osmotically flow of non-Newtonian fluid: Analytical approach. *Int. Commun. Heat Mass Transf.* **2020**, *117*, 104744. [CrossRef]
173. Thompson, P.A.; Troian, S.M. A general boundary condition for liquid flow at solid surfaces. *Nature* **1997**, *389*, 360–362. [CrossRef]
174. Helmholtz, H. *Über Reibung Tropfbarer Flüssigkeiten: Von H. Helmholtz Und G.V. Piotrowski. (Mit 2 Taff.) (Aus d. XL. Bd. S. 607. 1860. Der Sitzgsber. Der Math-Nat. Cl. Der k. Ak. Der Wiss. Bes. Dbg)*; Hof-& Stts.-Druck: Singapore, 1860; p. 607.
175. Ng, C.-O.; Sun, R. Pressure loss in channel flow resulting from a sudden change in boundary condition from no-slip to partial-slip. *Phys. Fluids* **2017**, *29*, 103603. [CrossRef]
176. Shu, J.-J.; Teo, J.B.M.; Chan, W.K. Fluid Velocity Slip and Temperature Jump at a Solid Surface. *Appl. Mech. Rev.* **2017**, *69*, 020801. [CrossRef]
177. Navier, C. *Memoirs de l'Academie Royale Des Sciences de l'Institut de France*; Academie Royale des Sciences de l'Institut de France: Paris, France, 1823; Volume 1.
178. Leger, L.; Hervet, H.; Massey, G.; Durliat, E. Wall slip in polymer melts. *J. Phys. Condens. Matter* **1997**, *9*, 7719. [CrossRef]
179. Neto, C.; Evans, D.; Bonaccurso, E.; Butt, H.-J.; Craig, V. Boundary slip in Newtonian liquids: A review of experimental studies. *Rep. Prog. Phys.* **2005**, *68*, 2859–2897. [CrossRef]
180. Ala-Nissila, T.; Ferrando, R.; Ying, S.C. Collective and single particle diffusion on surfaces. *Adv. Phys.* **2002**, *51*, 949–1078. [CrossRef]
181. Maxwell, J.C. VII. On stresses in rarified gases arising from inequalities of temperature. *Philos. Trans. R. Soc. London* **1879**, 231–256. [CrossRef]
182. Smoluchowski, M. Über den Temperatursprung bei Wärmeleitung in Gasen. *Pisma Marian. Smoluchowskiego* **1924**, *1*, 113–138.
183. Deissler, R.G. An analysis of second-order slip flow and temperature-jump boundary conditions for rarefied gases. *Int. J. Heat Mass Transf.* **1964**, *7*, 681–694. [CrossRef]
184. Karniadakis, G.E.M.; Beskok, A.; Gad-El-Hak, M. Micro Flows: Fundamentals and Simulation. *Appl. Mech. Rev.* **2002**, *55*, B61–B82. [CrossRef]
185. Bataineh, K.M.; Moh'd A, A.-N. 2D Navier–Stokes simulations of microscale viscous pump with slip flow. *J. Fluids Eng.* **2009**, *131*, 051105. [CrossRef]
186. Sharatchandra, M.C.; Sen, M.; Gad-El-Hak, M. Thermal Aspects of a Novel Viscous Pump. *J. Heat Transf.* **1998**, *120*, 99–107. [CrossRef]
187. Cahill, D.G.; Ford, W.K.; Goodson, K.E.; Mahan, G.D.; Majumdar, A.; Maris, H.J.; Merlin, R.; Phillpot, S.R. Nanoscale thermal transport. *J. Appl. Phys.* **2003**, *93*, 793–818. [CrossRef]
188. Pollack, G.L. Kapitza resistance. *Rev. Mod. Phys.* **1969**, *41*, 48–61. [CrossRef]
189. Swartz, E.T.; Pohl, R.O. Thermal boundary resistance. *Rev. Mod. Phys.* **1989**, *61*, 605–668. [CrossRef]
190. Kapitza, P.L. The study of heat transfer in helium II. *J. Phys. (Mosc.)* **1941**, *4*, 181.
191. Gad-El-Hak, M. The Fluid Mechanics of Microdevices—The Freeman Scholar Lecture. *J. Fluids Eng.* **1999**, *121*, 5–33. [CrossRef]
192. Colin, S.; Lalonde, P.; Caen, R. Validation of a Second-Order Slip Flow Model in Rectangular Microchannels. *Heat Transf. Eng.* **2004**, *25*, 23–30. [CrossRef]
193. Colin, C.A.S. High-order boundary conditions for gaseous flows in rectangular microducts. *Microscale Thermophys. Eng.* **2001**, *5*, 41–54. [CrossRef]
194. Spiga, G.L.M.M. Slip flow in rectangular microtubes. *Microscale Thermophys. Eng.* **1998**, *2*, 273–282. [CrossRef]
195. Barron, R.F.; Wang, X.; Ameel, T.A.; Warrington, R.O. The Graetz problem extended to slip-flow. *Int. J. Heat Mass Transf.* **1997**, *40*, 1817–1823. [CrossRef]
196. Barron, R.F.; Wang, X.; Warrington, R.O.; Ameel, T. Evaluation of the eigenvalues for the graetz problem in slip-flow. *Int. Commun. Heat Mass Transf.* **1996**, *23*, 563–574. [CrossRef]
197. Ebert, W.A.; Sparrow, E.M. Slip Flow in Rectangular and Annular Ducts. *J. Basic Eng.* **1965**, *87*, 1018–1024. [CrossRef]
198. Yang, J.; Kwok, D.Y. A New Method to Determine Zeta Potential and Slip Coefficient Simultaneously. *J. Phys. Chem. B* **2002**, *106*, 12851–12855. [CrossRef]
199. Park, H.M.; Kim, T. Simultaneous estimation of zeta potential and slip coefficient in hydrophobic microchannels. *Anal. Chim. Acta* **2007**, *593*, 171–177. [CrossRef]
200. Yang, J.; Kwok, D.Y. Time-dependent laminar electrokinetic slip flow in infinitely extended rectangular microchannels. *J. Chem. Phys.* **2003**, *118*, 354–363. [CrossRef]
201. Tretheway, D.C.; Meinhart, C.D. Apparent fluid slip at hydrophobic microchannel walls. *Phys. Fluids* **2002**, *14*, L9–L12. [CrossRef]
202. Jamaati, J.; Niazmand, H.; Renksizbulut, M. Pressure-driven electrokinetic slip-flow in planar microchannels. *Int. J. Therm. Sci.* **2010**, *49*, 1165–1174. [CrossRef]
203. Soong, C.Y.; Hwang, P.W.; Wang, J.C. Analysis of pressure-driven electrokinetic flows in hydrophobic microchannels with slip-dependent zeta potential. *Microfluid. Nanofluidics* **2009**, *9*, 211–223. [CrossRef]
204. Goswami, P.; Chakraborty, S. Energy Transfer through Streaming Effects in Time-Periodic Pressure-Driven Nanochannel Flows with Interfacial Slip. *Langmuir* **2009**, *26*, 581–590. [CrossRef]
205. Jing, D.; Bhushan, B. Effect of boundary slip and surface charge on the pressure-driven flow. *J. Colloid Interface Sci.* **2013**, *392*, 15–26. [CrossRef]

206. Tan, Z.; Qi, H.-T.; Jiang, X.-Y. Electroosmotic flow of Eyring fluid in slit microchannel with slip boundary condition. *Appl. Math. Mech.* **2014**, *35*, 689–696. [CrossRef]
207. Bhattacharjee, S.; Mondal, M.; De, S. Effects of overlapping electric double layer on mass transport of a macro-solute across porous wall of a micro/nanochannel for power law fluid. *Electrophoresis* **2017**, *38*, 1301–1309. [CrossRef]
208. Sun, Q.; Wu, Y.; Liu, L.; Wiwatanapataphee, B. Study of a Newtonian Fluid through Circular Channels with Slip Boundary Taking into Account Electrokinetic Effect. *Abstr. Appl. Anal.* **2013**, *2013*, 718603. [CrossRef]
209. Yang, J.; Kwok, D.Y. Analytical treatment of flow in infinitely extended circular microchannels and the effect of slippage to increase flow efficiency. *J. Micromech. Microeng.* **2002**, *13*, 115–123. [CrossRef]
210. Yang, J.; Kwok, D.Y. Microfluid flow in circular microchannel with electrokinetic effect and Navier's slip condition. *Langmuir* **2003**, *19*, 1047–1053. [CrossRef]
211. Zhu, J.; Chu, P.; Sui, J. Exact Analytical Nanofluid Flow and Heat Transfer Involving Asymmetric Wall Heat Fluxes with Nonlinear Velocity Slip. *Math. Probl. Eng.* **2018**, *2018*, 1–12. [CrossRef]
212. Hooman, K.; Hooman, F.; Famouri, M. Scaling effects for flow in micro-channels: Variable property, viscous heating, velocity slip, and temperature jump. *Int. Commun. Heat Mass Transf.* **2009**, *36*, 192–196. [CrossRef]
213. Hooman, K. Entropy generation for microscale forced convection: Effects of different thermal boundary conditions, velocity slip, temperature jump, viscous dissipation, and duct geometry. *Int. Commun. Heat Mass Transf.* **2007**, *34*, 945–957. [CrossRef]
214. Hooman, K. Heat transfer and entropy generation for forced convection through a microduct of rectangular cross-section: Effects of velocity slip, temperature jump, and duct geometry. *Int. Commun. Heat Mass Transf.* **2008**, *35*, 1065–1068. [CrossRef]
215. Ranjit, N.K.; Shit, G.C.; Tripathi, D. Entropy generation and Joule heating of two layered electroosmotic flow in the peristaltically induced micro-channel. *Int. J. Mech. Sci.* **2019**, *153*, 430–444. [CrossRef]
216. Jiang, H.; Fan, N.; Peng, B.; Weng, X. Characterization of an induced pressure pumping force for microfluidics. *Appl. Phys. Lett.* **2017**, *110*, 184102. [CrossRef]
217. Eringen, A.C.; Maugin, G.A. *Kinematics of Material Continua*; Springer: Berlin/Heidelberg, Germany, 1990.
218. Oosawa, F. *Polyelectrolytes*; Marcel Dekker: New York, NY, USA, 1971.
219. Volkenstein, M.V.; Bell, G.I. Molecular biophysics. *Phys. Today* **1979**, *32*, 79. [CrossRef]
220. Hendricks, C.D., Jr.; Pfeifer, R.J. Parametric studies of electrohydrodynamic spraying. *Aiaa J.* **1968**, *6*, 496–502.
221. Joffre, R.L. Devices for Cleaning, Dusting, Mopping and Applying Liquid to Floors. Google Patents No. 4,184,224, 22 January 1980.
222. Richter, A.; Plettner, A.; Hofmann, K.A.; Sandmaier, H. A micro-machined electrohydrodynamic (EHD) pump. *Sens. Actuat. A Phys.* **1991**, *29*, 159–168. [CrossRef]
223. Zhong, J.; Yi, M.; Bau, H.H. Magneto hydrodynamic (MHD) pump fabricated with ceramic tapes. *Sens. Actuators A Phys.* **2002**, *96*, 59–66. [CrossRef]
224. Chen, G.; Das, S. Streaming potential and electroviscous effects in soft nanochannels beyond Debye–Hückel linearization. *J. Colloid Interface Sci.* **2015**, *445*, 357–363. [CrossRef] [PubMed]
225. Haiwang, L.; Wong, T.N.; Nguyen, N.-T. Analytical model of mixed electroosmotic/pressure driven three immiscible fluids in a rectangular microchannel. *Int. J. Heat Mass Transf.* **2009**, *52*, 4459–4469. [CrossRef]
226. Matin, M.H.; Ohshima, H. Combined electroosmotically and pressure driven flow in soft nanofluidics. *J. Colloid Interface Sci.* **2015**, *460*, 361–369. [CrossRef] [PubMed]
227. Matin, M.H.; Ohshima, H. Thermal transport characteristics of combined electroosmotic and pressure driven flow in soft nanofluidics. *J. Colloid Interface Sci.* **2016**, *476*, 167–176. [CrossRef]
228. Zhao, L.; Liu, L. Effect of Joule heating on electro-osmotic flow in a closedend micro-channel with isothermal and convective boundary conditions. *Front. Energy Power Eng. China* **2009**, *3*, 381–388. [CrossRef]
229. Lorenzini, M. Electro-osmotic non-isothermal flow in rectangular channels with smoothed corners. *Therm. Sci. Eng. Prog.* **2020**, *19*, 100617. [CrossRef]
230. Tan, D.K.; Liu, Y. Combined effects of streaming potential and wall slip on flow and heat transfer in microchannels. *Int. Commun. Heat Mass Transf.* **2014**, *53*, 39–42. [CrossRef]
231. Zhao, C.; Yang, C. On the competition between streaming potential effect and hydrodynamic slip effect in pressure-driven microchannel flows. *Colloids Surf. A Physicochem. Eng. Asp.* **2011**, *386*, 191–194. [CrossRef]
232. Moyers-Gonzalez, M.; Owens, R.G.; Fang, J. A non-homogeneous constitutive model for human blood. Part 1. Model derivation and steady flow. *J. Fluid Mech.* **2008**, *617*, 327–354. [CrossRef]
233. Owens, R.G. A new microstructure-based constitutive model for human blood. *J. Non-Newton. Fluid Mech.* **2006**, *140*, 57–70. [CrossRef]
234. Vissink, A.; Waterman, H.A.; s-Gravenmade, E.J.; Panders, A.K.; Vermey, A. Rheological properties of saliva substitutes containing mucin, carboxymethylcellulose or polyethylenoxide. *J. Oral Pathol Med.* **1984**, *13*, 22–28. [CrossRef] [PubMed]
235. Fam, H.; Bryant, J.T.; Kontopoulou, M. Rheological properties of synovial fluids. *Biorheology* **2007**, *44*, 59–74. [PubMed]
236. Thurston, G.B.; Greiling, H. Viscoelastic properties of pathological synovial fluids for a wide range of oscillatory shear rates and frequencies. *Rheol. Acta* **1978**, *17*, 433–445. [CrossRef]
237. Afonso, A.M.; Alves, M.; Pinho, F. Analytical solution of mixed electro-osmotic/pressure driven flows of viscoelastic fluids in microchannels. *J. Non-Newton. Fluid Mech.* **2009**, *159*, 50–63. [CrossRef]

238. Afonso, A.M.; Alves, M.A.; Pinho, F.T. Electro-osmotic flow of viscoelastic fluids in microchannels under asymmetric zeta potentials. *J. Eng. Math.* **2010**, *71*, 15–30. [CrossRef]
239. Bautista, O.; Sánchez, S.; Arcos, J.C.; Méndez, F. Lubrication theory for electro-osmotic flow in a slit microchannel with the Phan-Thien and Tanner model. *J. Fluid Mech.* **2013**, *722*, 496–532. [CrossRef]
240. Coelho, P.M.; Alves, M.A.; Pinho, F.T. Forced convection in electro-osmotic/Poiseuille micro-channel flows of viscoelastic fluids: Fully developed flow with imposed wall heat flux. *Microfluid. Nanofluidics* **2011**, *12*, 431–449. [CrossRef]
241. Dhinakaran, S.; Afonso, A.M.; Alves, M.A.; Pinho, F.T. Steady viscoelastic fluid flow between parallel plates under electro-osmotic forces: Phan-Thien–Tanner model. *J. Colloid Interface Sci.* **2010**, *344*, 513–520. [CrossRef]
242. Escandón, J.P.; Bautista, O.; Mendez, F.; Bautista, E. Theoretical conjugate heat transfer analysis in a parallel flat plate microchannel under electro-osmotic and pressure forces with a Phan-Thien-Tanner fluid. *Int. J. Therm. Sci.* **2011**, *50*, 1022–1030. [CrossRef]
243. Ferrás, L.L.; Afonso, A.M.; Alves, M.A.; Nóbrega, J.M.; Pinho, F.T. Electro-osmotic and pressure-driven flow of viscoelastic fluids in microchannels: Analytical and semi-analytical solutions. *Phys. Fluids* **2016**, *28*, 093102. [CrossRef]
244. Sadeghi, A.; Saidi, M.H.; Mozafari, A.A. Heat transfer due to electroosmotic flow of viscoelastic fluids in a slit microchannel. *Int. J. Heat Mass Transf.* **2011**, *54*, 4069–4077. [CrossRef]
245. Ferrás, L.L.; Afonso, A.; Alves, M.; Nóbrega, J.; Pinho, F. Annular flow of viscoelastic fluids: Analytical and numerical solutions. *J. Non-Newton. Fluid Mech.* **2014**, *212*, 80–91. [CrossRef]
246. Sadeghi, A.; Veisi, H.; Saidi, M.H.; Mozafari, A.A. Electroosmotic Flow of Viscoelastic Fluids Through a Slit Microchannel With a Step Change in Wall Temperature. *J. Heat Transf.* **2013**, *135*, 021706. [CrossRef]
247. Reshadi, M.; Saidi, M.H.; Ebrahimi, A. Pure axial flow of viscoelastic fluids in rectangular microchannels under combined effects of electro-osmosis and hydrodynamics. *Theor. Comput. Fluid Dyn.* **2017**, *32*, 1–21. [CrossRef]
248. Martínez, L.; Bautista, O.; Escandón, J.; Méndez, F. Electroosmotic flow of a Phan-Thien–Tanner fluid in a wavy-wall microchannel. *Colloids Surf. A Physicochem. Eng. Asp.* **2016**, *498*, 7–19. [CrossRef]
249. Afonso, A.M.; Ferrás, L.L.; Nóbrega, J.M.; Alves, M.A.; Pinho, F. Pressure-driven electrokinetic slip flows of viscoelastic fluids in hydrophobic microchannels. *Microfluid. Nanofluidics* **2013**, *16*, 1131–1142. [CrossRef]
250. Matías, A.; Sánchez, S.; Mendez, F.; Bautista, O. Influence of slip wall effect on a non-isothermal electro-osmotic flow of a viscoelastic fluid. *Int. J. Therm. Sci.* **2015**, *98*, 352–363. [CrossRef]
251. Sarma, R.; Deka, N.; Sarma, K.; Mondal, P.K. Electroosmotic flow of Phan-Thien–Tanner fluids at high zeta potentials: An exact analytical solution. *Phys. Fluids* **2018**, *30*, 062001. [CrossRef]
252. Mukherjee, S.; Goswami, P.; Dhar, J.; Dasgupta, S.; Chakraborty, S. Ion-size dependent electroosmosis of viscoelastic fluids in microfluidic channels with interfacial slip. *Phys. Fluids* **2017**, *29*, 072002. [CrossRef]
253. Bandopadhyay, A.; Ghosh, U.; Chakraborty, S. Time periodic electroosmosis of linear viscoelastic liquids over patterned charged surfaces in microfluidic channels. *J. Non-Newton. Fluid Mech.* **2013**, *202*, 1–11. [CrossRef]
254. Yang, J.; Bhattacharyya, A.; Masliyah, J.; Kwok, D. Oscillating laminar electrokinetic flow in infinitely extended rectangular microchannels. *J. Colloid Interface Sci.* **2003**, *261*, 21–31. [CrossRef]
255. Peralta, M.; Arcos, J.; Mendez, F.; Bautista, O. Oscillatory electroosmotic flow in a parallel-plate microchannel under asymmetric zeta potentials. *Fluid Dyn. Res.* **2017**, *49*, 035514. [CrossRef]
256. Arcos, J.C.; Méndez, F.; Bautista, E.G.; Bautista, O. Dispersion coefficient in an electro-osmotic flow of a viscoelastic fluid through a microchannel with a slowly varying wall zeta potential. *J. Fluid Mech.* **2018**, *839*, 348–386. [CrossRef]
257. Hoshyargar, V.; Talebi, M.; Ashrafizadeh, S.N.; Sadeghi, A. Hydrodynamic dispersion by electroosmotic flow of viscoelastic fluids within a slit microchannel. *Microfluid. Nanofluidics* **2017**, *22*, 4. [CrossRef]
258. Sadeghi, M.; Saidi, M.H.; Moosavi, A.; Adeghi, A. Unsteady solute dispersion by electrokinetic flow in a polyelectrolyte layer-grafted rectangular microchannel with wall absorption. *J. Fluid Mech.* **2020**, *887*, A13. [CrossRef]
259. Chakraborty, D.; Madou, M.; Chakraborty, S. Anomalous mixing behaviour in rotationally actuated microfluidic devices. *Lab Chip* **2011**, *11*, 2823–2826. [CrossRef]
260. Leung, W.W.-F.; Ren, Y. Crossflow and mixing in obstructed and width-constricted rotating radial microchannel. *Int. J. Heat Mass Transf.* **2013**, *64*, 457–467. [CrossRef]
261. Ren, Y.; Leung, W.W.-F. Flow and mixing in rotating zigzag microchannel. *Chem. Eng. J.* **2013**, *215*, 561–578. [CrossRef]
262. Chang, C.-C.; Wang, C.-Y. Rotating electro-osmotic flow over a plate or between two plates. *Phys. Rev. E* **2011**, *84*, 056320. [CrossRef]
263. Ng, C.-O.; Qi, C. Electro-osmotic flow in a rotating rectangular microchannel. *Proc. R. Soc. A Math. Phys. Eng. Sci.* **2015**, *471*, 20150200. [CrossRef]
264. Kaushik, P.; Mandal, S.; Chakraborty, S. Transient electroosmosis of a Maxwell fluid in a rotating microchannel. *Electrophoresis* **2017**, *38*, 2741–2748. [CrossRef] [PubMed]
265. Yang, X.; Qi, H.; Jiang, X. Numerical analysis for electroosmotic flow of fractional Maxwell fluids. *Appl. Math. Lett.* **2018**, *78*, 1–8. [CrossRef]
266. Patel, M.; Kruthiventi, S.S.H.; Kaushik, P. Polyelectrolyte layer grafting effect on the rotational electroosmotic flow of viscoplastic material. *Microfluid. Nanofluid.* **2021**, *25*, 1. [CrossRef]
267. Gheshlaghi, B.; Nazaripoor, H.; Kumar, A.; Sadrzadeh, M. Analytical solution for transient electroosmotic flow in a rotating microchannel. *RSC Adv.* **2016**, *6*, 17632–17641. [CrossRef]

268. Li, S.-X.; Jian, Y.-J.; Xie, Z.-Y.; Liu, Q.-S.; Li, F.-Q. Rotating electro-osmotic flow of third grade fluids between two microparallel plates. *Colloids Surf. A Physicochem. Eng. Asp.* **2015**, *470*, 240–247. [CrossRef]
269. Liu, Y.; Jian, Y. Rotating electroosmotic flows in soft parallel plate microchannels. *Appl. Math. Mech.* **2019**, *40*, 1017–1028. [CrossRef]
270. Qi, C.; Ng, C.-O. Rotating electroosmotic flow of viscoplastic material between two parallel plates. *Colloids Surf. A Physicochem. Eng. Asp.* **2017**, *513*, 355–366. [CrossRef]
271. Sinha, A.; Mondal, A.; Shit, G.C.; Kundu, P.K. Effect of heat transfer on rotating electroosmotic flow through a micro-vessel: Haemodynamical applications. *Heat Mass Transf.* **2016**, *52*, 1549–1557. [CrossRef]
272. Zheng, J.; Jian, Y. Rotating electroosmotic flow of two-layer fluids through a microparallel channel. *Int. J. Mech. Sci.* **2018**, *136*, 293–302. [CrossRef]
273. Cao, L.; Zhang, P.; Li, B.; Zhu, J.; Si, X. Numerical study of rotating electro-osmotic flow of double layers with a layer of fractional second-order fluid in a microchannel. *Appl. Math. Lett.* **2021**, *111*, 106633. [CrossRef]
274. Siva, T.; Kumbhakar, B.; Jangili, S.; Mondal, P.K. Unsteady electro-osmotic flow of couple stress fluid in a rotating microchannel: An analytical solution. *Phys. Fluids* **2020**, *32*, 102013. [CrossRef]
275. Siginer, D.A.; Akyildiz, F.T.; Boutaous, M. Unsteady gaseous Poiseuille slip flow in rectangular microchannels. *J. Braz. Soc. Mech. Sci. Eng.* **2019**, *41*, 286. [CrossRef]
276. Shit, G.C.; Mondal, A.; Sinha, A.; Kundu, P.K. Effects of slip velocity on rotating electro-osmotic flow in a slowly varying micro-channel. *Colloids Surf. A Physicochem. Eng. Asp.* **2016**, *489*, 249–255. [CrossRef]
277. Yavari, H.; Sadeghi, A.; Saidi, M.H.; Chakraborty, S. Temperature Rise in Electroosmotic Flow of Typical Non-Newtonian Biofluids Through Rectangular Microchannels. *J. Heat Transf.* **2013**, *136*, 031702. [CrossRef]
278. Xie, Z.-Y.; Jian, Y.-J. Rotating electroosmotic flow of power-law fluids at high zeta potentials. *Colloids Surf. A Physicochem. Eng. Asp.* **2014**, *461*, 231–239. [CrossRef]
279. Babaie, A.; Saidi, M.H.; Sadeghi, A. Heat transfer characteristics of mixed electroosmotic and pressure driven flow of power-law fluids in a slit microchannel. *Int. J. Therm. Sci.* **2011**, *53*, 71–79. [CrossRef]
280. Chen, C.-H. Electro-Osmotic Heat Transfer of Non-Newtonian Fluid Flow in Microchannels. *J. Heat Transf.* **2011**, *133*, 071705. [CrossRef]
281. Sadeghi, A.; Saidi, M.H.; Veisi, H.; Fattahi, M. Thermally developing electroosmotic flow of power-law fluids in a parallel plate microchannel. *Int. J. Therm. Sci.* **2012**, *61*, 106–117. [CrossRef]
282. Zhao, C.; Yang, C. An exact solution for electroosmosis of non-Newtonian fluids in microchannels. *J. Non-Newton. Fluid Mech.* **2011**, *166*, 1076–1079. [CrossRef]
283. Vakili, M.A.; Sadeghi, A.; Saidi, M.H.; Mozafari, A.A. Electrokinetically driven fluidic transport of power-law fluids in rectangular microchannels. *Colloids Surf. A Physicochem. Eng. Asp.* **2012**, *414*, 440–456. [CrossRef]
284. Choi, W.; Yun, S.; Choi, D.-S. Electroosmotic Flows of Power-Law Fluids with Asymmetric Electrochemical Boundary Conditions in a Rectangular Microchannel. *Micromachines* **2017**, *8*, 165. [CrossRef]
285. Moghadam, A.J.; Akbarzadeh, P. Non-Newtonian fluid flow induced by pressure gradient and time-periodic electroosmosis in a microtube. *J. Braz. Soc. Mech. Sci. Eng.* **2017**, *39*, 5015–5025. [CrossRef]
286. Dey, R.; Chakraborty, D.; Chakraborty, S. Analytical Solution for Thermally Fully Developed Combined Electroosmotic and Pressure-Driven Flows in Narrow Confinements with Thick Electrical Double Layers. *J. Heat Transf.* **2010**, *133*, 024503. [CrossRef]
287. Dey, R.; Ghonge, T.; Chakraborty, S. Steric-effect-induced alteration of thermal transport phenomenon for mixed electroosmotic and pressure driven flows through narrow confinements. *Int. J. Heat Mass Transf.* **2013**, *56*, 251–262. [CrossRef]
288. Ban, H.; Lin, B.; Song, Z. Effect of electrical double layer on electric conductivity and pressure drop in a pressure-driven microchannel flow. *Biomicrofluidics* **2010**, *4*, 014104. [CrossRef] [PubMed]
289. Dutta, P.; Beskok, A. Analytical Solution of Combined Electroosmotic/Pressure Driven Flows in Two-Dimensional Straight Channels: Finite Debye Layer Effects. *Anal. Chem.* **2001**, *73*, 1979–1986. [CrossRef]
290. Bandopadhyay, A.; Chakraborty, S. Electrokinetically induced alterations in dynamic response of viscoelastic fluids in narrow confinements. *Phys. Rev. E* **2012**, *85*, 056302. [CrossRef]
291. Ng, C.-O.; Qi, C. Electroosmotic flow of a power-law fluid in a non-uniform microchannel. *J. Non-Newton. Fluid Mech.* **2014**, *208–209*, 118–125. [CrossRef]
292. Shojaeian, M.; Koşar, A. Convective heat transfer of non-Newtonian power-law slip flows and plug flows with variable thermophysical properties in parallel-plate and circular microchannels. *Int. J. Therm. Sci.* **2016**, *100*, 155–168. [CrossRef]
293. Saravani, M.S.; Kalteh, M. Heat transfer investigation of combined electroosmotic/pressure driven nanofluid flow in a microchannel: Effect of heterogeneous surface potential and slip boundary condition. *Eur. J. Mech. B Fluids* **2020**, *80*, 13. [CrossRef]
294. Gaikwad, H.S.; Roy, A.; Mondal, P.K.; Chimres, N.; Wongwises, S. Irreversibility analysis in a slip aided electroosmotic flow through an asymmetrically heated microchannel: The effects of joule heating and the conjugate heat transfer. *Anal. Chim. Acta* **2018**, *1045*, 85–97. [CrossRef] [PubMed]
295. Gaikwad, H.S.; Mondal, P.K.; Basu, D.N.; Chimres, N.; Wongwises, S. Analysis of the effects of Joule heating and viscous dissipation on combined pressure-driven and electrokinetic flows in a two-parallel plate channel with unequal constant temperatures, Proceedings of the Institution of Mechanical Engineers. *Part E J. Process Mech. Eng.* **2019**, *233*, 871. [CrossRef]

296. Sharma, A.; Chakraborty, S. Semi-analytical solution of the extended Graetz problem for combined electroosmotically and pressure-driven microchannel flows with step-change in wall temperature. *Int. J. Heat Mass Transf.* **2008**, *51*, 4875–4885. [CrossRef]
297. Dey, R.; Chakraborty, D.; Chakraborty, S. Extended Graetz problem for combined electroosmotic and pressure-driven flows in narrow confinements with thick electric double layers. *Int. J. Heat Mass Transf.* **2012**, *55*, 4724–4733. [CrossRef]
298. Krishnaveni, T.; Renganathan, T.; Picardo, J.R.; Pushpavanam, S. Numerical study of enhanced mixing in pressure-driven flows in microchannels using a spatially periodic electric field. *Phys. Rev. E* **2017**, *96*, 033117. [CrossRef] [PubMed]
299. Hoshyargar, V.; Ashrafizadeh, S.N.; Sadeghi, A. Diffusioosmotic flow in rectangular microchannels. *Electrophoresis* **2016**, *37*, 809–817. [CrossRef]
300. Zhu, Q.; Deng, S.; Chen, Y. Periodical pressure-driven electrokinetic flow of power-law fluids through a rectangular microchannel. *J. Non-Newton. Fluid Mech.* **2014**, *203*, 38–50. [CrossRef]
301. Jiménez, E.; Escandón, J.; Bautista, O.; Méndez, F. Start-up electroosmotic flow of Maxwell fluids in a rectangular microchannel with high zeta potentials. *J. Non-Newton. Fluid Mech.* **2016**, *227*, 17–29. [CrossRef]
302. Wang, X.; Xu, H.; Qi, H. Numerical analysis for rotating electro-osmotic flow of fractional Maxwell fluids. *Appl. Math. Lett.* **2019**, *103*, 106179. [CrossRef]
303. Jimenez, E.; Escandón, J.; Méndez, F.; Bautista, O. Combined viscoelectric and steric effects on the electroosmotic flow in a microchannel under induced high zeta potentials. *Colloids Surf. A Physicochem. Eng. Asp.* **2017**, *531*, 221–233. [CrossRef]
304. Xing, J.; Jian, Y. Steric effects on electroosmotic flow in soft nanochannels. *Meccanica* **2017**, *53*, 135–144. [CrossRef]
305. Ramos, E.A.; Bautista, O.; Lizardi, J.J.; Méndez, F. A perturbative thermal analysis for an electro-osmotic flow in a slit microchannel based on a Lubrication theory. *Int. J. Therm. Sci.* **2017**, *111*, 499–510. [CrossRef]
306. Kaushik, P.; Chakraborty, S. Startup electroosmotic flow of a viscoelastic fluid characterized by Oldroyd-B model in a rectangular microchannel with symmetric and asymmetric wall zeta potentials. *J. Non-Newton. Fluid Mech.* **2017**, *247*, 41–52. [CrossRef]
307. Jiang, Y.; Qi, H.; Xu, H.; Jiang, X. Transient electroosmotic slip flow of fractional Oldroyd-B fluids. *Microfluid. Nanofluidics* **2017**, *21*, 7. [CrossRef]
308. Kaushik, P.; Abhimanyu, P.; Mondal, P.K.; Chakraborty, S. Confinement effects on the rotational microflows of a viscoelastic fluid under electrical double layer phenomenon. *J. Non-Newton. Fluid Mech.* **2017**, *244*, 123–137. [CrossRef]
309. Liang, P.; Wang, S.; Zhao, M. Numerical study of rotating electroosmotic flow of Oldroyd-B fluid in a microchannel with slip boundary condition. *Chin. J. Phys.* **2020**, *65*, 459–471. [CrossRef]
310. Wang, X.; Qi, H.; Yu, B.; Xiong, Z.; Xu, H. Analytical and numerical study of electroosmotic slip flows of fractional second grade fluids. *Commun. Nonlinear Sci. Numer. Simul.* **2017**, *50*, 77–84. [CrossRef]
311. Dey, P.; Shit, G.C. Electroosmotic flow of a fractional second-grade fluid with interfacial slip and heat transfer in the microchannel when exposed to a magnetic field. *Heat Transf.* **2021**, *50*, 2643–2666. [CrossRef]
312. Huang, H.-F.; Yang, P.-W. Electrokinetic streaming power generation using squeezing liquid flows in slit channels with wall slip. *Colloids Surf. A Physicochem. Eng. Asp.* **2017**, *514*, 192–208. [CrossRef]
313. Matin, M.H. Electroviscous effects on thermal transport of electrolytes in pressure driven flow through nanoslit. *Int. J. Heat Mass Transf.* **2017**, *106*, 473–481. [CrossRef]
314. Sadeghi, A.; Yavari, H.; Saidi, M.H.; Chakraborty, S. Mixed electroosmotically and pressure- driven flow with temperature-dependent properties. *J. Thermophys. Heat Transf.* **2011**, *25*, 432–442. [CrossRef]
315. Zhao, Q.; Xu, H.; Tao, L. Nanofluid flow and heat transfer in a microchannel with interfacial electrokinetic effects. *Int. J. Heat Mass Transf.* **2018**, *124*, 158–167. [CrossRef]
316. Mondal, A.; Shit, G.C. Electro-osmotic flow and heat transfer in a slowly varying asymmetric micro-channel with Joule heating effects. *Fluid Dyn. Res.* **2018**, *50*, 065502. [CrossRef]
317. Nadeem, S.; Kiani, M.N.; Saleem, A.; Issakhov, A. Microvascular blood flow with heat transfer in a wavy channel having electroosmotic effects. *Electrophoresis* **2020**, *41*, 1198–1205. [CrossRef] [PubMed]
318. Bag, N.; Bhattacharyya, S. Electroosmotic flow of a non-Newtonian fluid in a microchannel with heterogeneous surface potential. *J. Non-Newton. Fluid Mech.* **2018**, *259*, 48–60. [CrossRef]
319. Chen, X.; Jian, Y. Streaming potential analysis on the hydrodynamic transport of pressure-driven flow through a rotational microchannel. *Chin. J. Phys.* **2018**, *56*, 1296–1307. [CrossRef]
320. Qi, C.; Ng, C.-O. Electroosmotic flow of a two-layer fluid in a slit channel with gradually varying wall shape and zeta potential. *Int. J. Heat Mass Transf.* **2018**, *119*, 52–64. [CrossRef]
321. Nekoubin, N. Electroosmotic flow of power-law fluids in curved rectangular microchannel with high zeta potentials. *J. Non-Newton. Fluid Mech.* **2018**, *260*, 54–68. [CrossRef]
322. Kamali, R.; Soloklou, M.N.; Hadidi, H. Numerical simulation of electroosmotic flow in rough microchannels using the lattice Poisson-Nernst-Planck methods. *Chem. Phys.* **2018**, *507*, 1–9. [CrossRef]
323. Sadek, S.H.; Pinho, F.T. Electro-osmotic oscillatory flow of viscoelastic fluids in a microchannel. *J. Non-Newton. Fluid Mech.* **2019**, *266*, 46–58. [CrossRef]
324. Rice, C.L.; Whitehead, R. Electrokinetic Flow in a Narrow Cylindrical Capillary. *J. Phys. Chem.* **1965**, *69*, 4017–4024. [CrossRef]
325. Levine, S.; Marriott, J.R.; Robinson, K. Theory of electrokinetic flow in a narrow parallel-plate channel. *J. Chem. Soc. Faraday Trans. 2* **1975**, *71*, 1–11. [CrossRef]

326. Kang, Y.; Yang, C.; Huang, X. Dynamic aspects of electroosmotic flow in a cylindrical microcapillary. *Int. J. Eng. Sci.* **2002**, *40*, 2203–2221. [CrossRef]
327. Maynes, D.; Webb, B. Fully developed electro-osmotic heat transfer in microchannels. *Int. J. Heat Mass Transf.* **2003**, *46*, 1359–1369. [CrossRef]
328. Najjaran, S.; Rashidi, S.; Valipour, M.S. Heat transfer intensification in microchannel by induced-charge electrokinetic phenomenon: A numerical study. *J. Therm. Anal. Calorim.* **2021**, *145*, 1849–1861. [CrossRef]
329. Liechty, B.; Webb, B.; Maynes, R. Convective heat transfer characteristics of electro-osmotically generated flow in microtubes at high wall potential. *Int. J. Heat Mass Transf.* **2005**, *48*, 2360–2371. [CrossRef]
330. Aydın, O.; Avcı, M. Heat and fluid flow characteristics of gases in micropipes. *Int. J. Heat Mass Transf.* **2006**, *49*, 1723–1730. [CrossRef]
331. Tang, G.Y.; Yang, C.; Chai, J.C.; Gong, H.Q. Joule heating effect on electroosmotic flow and mass species transport in a microcapillary. *Int. J. Heat Mass Transf.* **2004**, *47*, 215–227. [CrossRef]
332. Kang, Y.; Yang, C.; Huang, X. Electroosmotic Flow in a Capillary Annulus with High Zeta Potentials. *J. Colloid Interface Sci.* **2002**, *253*, 285–294. [CrossRef]
333. Moghadam, A.J. Effect of periodic excitation on alternating current electroosmotic flow in a microannular channel. *Eur. J. Mech.-B/Fluids* **2014**, *48*, 1–12. [CrossRef]
334. Tsao, H.-K. Electroosmotic Flow through an Annulus. *J. Colloid Interface Sci.* **2000**, *225*, 247–250. [CrossRef]
335. Bhattacharyya, A.; Masliyah, J.; Yang, J. Oscillating laminar electrokinetic flow in infinitely extended circular microchannels. *J. Colloid Interface Sci.* **2003**, *261*, 12–20. [CrossRef]
336. Chakraborty, S.; Ray, S. Mass flow-rate control through time periodic electro-osmotic flows in circular microchannels. *Phys. Fluids* **2008**, *20*, 083602. [CrossRef]
337. Yang, J.; Masliyah, J.H.; Kwok, D.Y. Streaming potential and electroosmotic flow in heterogeneous circular microchannels with non-uniform zeta potentials: Requirements of flow rate and current continuities. *Langmuir* **2004**, *20*, 3863. [CrossRef] [PubMed]
338. Zhao, M.; Wang, S.; Wei, S. Transient electro-osmotic flow of Oldroyd-B fluids in a straight pipe of circular cross section. *J. Non-Newton. Fluid Mech.* **2013**, *201*, 135–139. [CrossRef]
339. Prakash, J.; Ramesh, K.; Tripathi, D.; Kumar, R. Numerical simulation of heat transfer in blood flow altered by electroosmosis through tapered micro-vessels. *Microvasc. Res.* **2018**, *118*, 162–172. [CrossRef]
340. Hsu, J.-P.; Kao, C.-Y.; Tseng, S.; Chen, C.-J. Electrokinetic Flow through an Elliptical Microchannel: Effects of Aspect Ratio and Electrical Boundary Conditions. *J. Colloid Interface Sci.* **2002**, *248*, 176–184. [CrossRef]
341. Deng, S.; Xiao, T.; Wu, S. Two-layer combined electroosmotic and pressure-driven flow of power-law fluids in a circular microcapillary. *Colloids Surf. A Physicochem. Eng. Asp.* **2020**, *610*, 125727. [CrossRef]
342. Prakash, J.; Tripathi, D.; Bég, O.A. Comparative study of hybrid nanofluids in microchannel slip flow induced by electroosmosis and peristalsis. *Appl. Nanosci.* **2020**, *10*, 1693–1706. [CrossRef]
343. Narla, V.K.; Tripathi, D.; Sekhar, G.P.R. Time-dependent analysis of electroosmotic fluid flow in a microchannel. *J. Eng. Math.* **2019**, *114*, 177–196. [CrossRef]
344. Ren, L.; Li, D. Electroosmotic Flow in Heterogeneous Microchannels. *J. Colloid Interface Sci.* **2001**, *243*, 255–261. [CrossRef]
345. Masilamani, K.; Ganguly, S.; Feichtinger, C.; Bartuschat, D.; Rüde, U. Effects of surface roughness and electrokinetic heterogeneity on electroosmotic flow in microchannel. *Fluid Dyn. Res.* **2015**, *47*, 035505. [CrossRef]
346. Chakraborty, S. Analytical solutions of Nusselt number for thermally fully developed flow in microtubes under a combined action of electroosmotic forces and imposed pressure gradients. *Int. J. Heat Mass Transf.* **2006**, *49*, 810–813. [CrossRef]
347. Azari, M.; Sadeghi, A.; Chakraborty, S. Electroosmotic flow and heat transfer in a heterogeneous circular microchannel. *Appl. Math. Model.* **2020**, *87*, 640–654. [CrossRef]
348. Matías, A.; Méndez, F.; Bautista, O. Interfacial Electric Effects on a Non-Isothermal Electroosmotic Flow in a Microcapillary Tube Filled by Two Immiscible Fluids. *Micromachines* **2017**, *8*, 232. [CrossRef]
349. Azari, M.; Sadeghi, A.; Chakraborty, S. Graetz problem for combined pressure-driven and electroosmotic flow in microchannels with distributed wall heat flux. *Int. J. Heat Mass Transf.* **2018**, *128*, 150–160. [CrossRef]
350. Chang, L.; Jian, Y.; Buren, M.; Liu, Q.; Sun, Y. Electroosmotic flow through a microtube with sinusoidal roughness. *J. Mol. Liq.* **2016**, *220*, 258–264. [CrossRef]
351. Monazami, R.; Manzari, M.T. Analysis of combined pressure-driven electroosmotic flow through square microchannels. *Microfluid. Nanofluidics* **2006**, *3*, 123–126. [CrossRef]
352. Cetin, B.; Travis, B.; Li, D. Analysis of the electro-viscous effects on pressure-driven liquid flow in a two-section heterogeneous microchannel. *Electrochim. Acta* **2008**, *54*, 660–664. [CrossRef]
353. Bharti, R.P.; Harvie, D.; Davidson, M.R. Electroviscous effects in steady fully developed flow of a power-law liquid through a cylindrical microchannel. *Int. J. Heat Fluid Flow* **2009**, *30*, 804–811. [CrossRef]
354. Deng, S. The Parametric Study of Electroosmotically Driven Flow of Power-Law Fluid in a Cylindrical Microcapillary at High Zeta Potential. *Micromachines* **2017**, *8*, 344. [CrossRef] [PubMed]
355. Sun, Z.-Y.; Gao, Y.-T.; Yu, X.; Liu, Y. Formation of vortices in a combined pressure-driven electro-osmotic flow through the insulated sharp tips under finite Debye length effects. *Colloids Surf. A Physicochem. Eng. Asp.* **2010**, *366*, 1–11. [CrossRef]

356. Moghadam, A.J. An exact solution of AC electro-kinetic-driven flow in a circular micro-channel. *Eur. J. Mech.-B/Fluids* **2012**, *34*, 91–96. [CrossRef]
357. Basati, Y.; Mohammadipour, O.R.; Niazmand, H. Numerical investigation and simultaneous optimization of geometry and zeta-potential in electroosmotic mixing flows. *Int. J. Heat Mass Transf.* **2019**, *133*, 786–799. [CrossRef]
358. Peralta, M.; Arcos, J.; Méndez, F.; Bautista, O. Mass transfer through a concentric-annulus microchannel driven by an oscillatory electroosmotic flow of a Maxwell fluid. *J. Non-Newton. Fluid Mech.* **2020**, *279*, 104281. [CrossRef]
359. Cho, C.-C.; Chen, C.-L. Characteristics of combined electroosmotic flow and pressure-driven flow in microchannels with complex-wavy surfaces. *Int. J. Therm. Sci.* **2012**, *61*, 94–105. [CrossRef]
360. Guo, X.; Qi, H. Analytical Solution of Electro-Osmotic Peristalsis of Fractional Jeffreys Fluid in a Micro-Channel. *Micromachines* **2017**, *8*, 341. [CrossRef]
361. Cho, C.-C.; Chen, C.-L. Electrokinetically-driven non-Newtonian fluid flow in rough microchannel with complex-wavy surface. *J. Non-Newton. Fluid Mech.* **2012**, *173*, 13–20. [CrossRef]
362. Ng, C.-O.; Zhou, Q. Dispersion due to electroosmotic flow in a circular microchannel with slowly varying wall potential and hydrodynamic slippage. *Phys. Fluids* **2012**, *24*, 112002. [CrossRef]
363. Baños, R.D.; Arcos, J.C.; Bautista, O.; Méndez, F.; Merchán-Cruz, E.A. Mass transport by an oscillatory electroosmotic flow of power-law fluids in hydrophobic slit microchannels. *J. Braz. Soc. Mech. Sci. Eng.* **2021**, *43*, 1–15. [CrossRef]
364. Karabi, M.; Moghadam, A.J. Non-Newtonian Fluid Flow and Heat Transfer in a Semicircular Microtube Induced by Electroosmosis and Pressure Gradient. *J. Heat Transf.* **2018**, *140*, 122403. [CrossRef]
365. Peralta, M.; Bautista, O.; Méndez, F. Pulsatile electroosmotic flow of a Maxwell fluid in a parallel flat plate microchannel with asymmetric zeta potentials. *Appl. Math. Mech.* **2018**, *39*, 667–684. [CrossRef]
366. Yavari, H.; Sadeghi, A.; Saidi, M.H. Hydrodynamic and Thermal Characteristics of Combined Electroosmotic and Pressure Driven Flow in a Microannulus. *J. Heat Transf.* **2012**, *134*, 101703. [CrossRef]
367. Vocale, P.; Geri, M.; Cattani, L.; Morini, G.; Spiga, M. Electro-osmotic heat transfer in elliptical microchannels under H1 boundary condition. *Int. J. Therm. Sci.* **2013**, *72*, 92–101. [CrossRef]
368. Srinivas, B. Electroosmotic flow of a power law fluid in an elliptic microchannel. *Colloids Surf. A Physicochem. Eng. Asp.* **2016**, *492*, 144–151. [CrossRef]
369. Zhao, G.; Jian, Y.J.; Li, F.Q. Heat transfer of nanofluids in microtubes under the effects of streaming potential. *Appl. Therm. Eng.* **2016**, *100*, 1299–1307. [CrossRef]
370. Tan, Z.; Liu, J. Electro-osmotic flow of Eyring fluids in a circular microtube with Navier's slip boundary condition. *Phys. Lett. A* **2017**, *381*, 2573–2577. [CrossRef]
371. Qi, C.; Ng, C.-O. Rotating electroosmotic flow of an Eyring fluid. *Acta Mech. Sin.* **2017**, *33*, 295–315. [CrossRef]
372. Nayak, A.K.; Haque, A.; Banerjee, A.; Weigand, B. Flow mixing and electric potential effect of binary fluids in micro/nano channels. *Colloids Surf. A Physicochem. Eng. Asp.* **2017**, *512*, 145–157. [CrossRef]
373. Gaikwad, H.S.; Basu, D.N.; Mondal, P.K. Slip driven micro-pumping of binary system with a layer of non-conducting fluid under electrical double layer phenomenon. *Colloids Surf. A Physicochem. Eng. Asp.* **2017**, *518*, 166–172. [CrossRef]
374. Tanveer, T.; Salahuddin, T.; Khan, M.; Malik, M.; Alqarni, M. Theoretical analysis of non-Newtonian blood flow in a microchannel. *Comput. Methods Programs Biomed.* **2019**, *191*, 105280. [CrossRef] [PubMed]
375. Saleem, A.; Kiani, M.N.; Nadeem, S.; Akhtar, S.; Ghalambaz, M.; Issakhov, A. Electroosmotically driven flow of micropolar bingham viscoplastic fluid in a wavy microchannel: Application of computational biology stomach anatomy. *Comput. Methods Biomech. Biomed. Eng.* **2021**, *24*, 289–298. [CrossRef] [PubMed]
376. Saleem, A.; Kiani, M.N.; Nadeem, S.; Issakhov, A. Heat transfer and Helmholtz-Smoluchowski velocity in Bingham fluid flow. *Appl. Math. Mech.* **2020**, *41*, 1167–1178. [CrossRef]
377. Rojas, G.; Arcos, J.; Peralta, M.; Méndez, F.; Bautista, O. Pulsatile electroosmotic flow in a microcapillary with the slip boundary condition. *Colloids Surf. A Physicochem. Eng. Asp.* **2016**, *513*, 57–65. [CrossRef]
378. Cramer, K.R.; Pai, S.-I. *Magnetofluid Dynamics for Engineers and Applied Physicists*; McGraw-Hill Book Company: New York, NY, USA, 1973.
379. Ritchie, W. XIII. Experimental researches in voltaic electricity and electro-magnetism. *Philos. Trans. R. Soc. Lond.* **1832**, *122*, 279–289.
380. Woodson, H.H.; Melcher, J.R. *Electromechanical Dynamics: Elastic and Fluid Media*; Wiley: Hoboken, NJ, USA, 1968.
381. Davidson, P.A. *An Introduction to Magnetohydrodynamics*; Peter, A., Ed.; Davidson Cambridge U. Press: New York, NY, USA, 2001.
382. Davidson, P.A.; Thess, A. *Magnetohydrodynamics*; Springer Science & Business Media: Berlin, Germany, 2002.
383. Mitra, S.; Maity, S.; Sutradhar, S.; Bandyopadhyay, D. Electroosmosis with Augmented Mixing in Rigid to Flexible Microchannels with Surface Patterns. *Ind. Eng. Chem. Res.* **2019**, *59*, 3717–3792. [CrossRef]
384. Bera, S.; Bhattacharyya, S. Effects of geometric modulation and surface potential heterogeneity on electrokinetic flow and solute transport in a microchannel. *Theor. Comput. Fluid Dyn.* **2017**, *32*, 201–214. [CrossRef]
385. SVerardi, S.; Cardoso, J.R.; Motta, C. A solution of two-dimensional magnetohydrodynamic flow using the finite element method. *IEEE Trans. Magn.* **1998**, *34*, 3134–3137. [CrossRef]
386. Bau, H.H.; Zhong, J.; Yi, M. A minute magneto hydro dynamic (MHD) mixer. *Sens. Actuators B Chem.* **2001**, *79*, 207–215. [CrossRef]

387. Qian, S.; Zhu, J.; Bau, H.H. A stirrer for magnetohydrodynamically controlled minute fluidic networks. *Phys. Fluids* **2002**, *14*, 3584–3592. [CrossRef]
388. Woodson, H.H.; Melcher, J.R. *Electromechanical Dynamics: Part 2: Fields, Forces, and Motion*; John Wiley and Sons Ltd.: Hoboken, NJ, USA, 1968.
389. Vilkner, T.; Janasek, D.; Manz, A. Micro total analysis systems: Recent developments. *Anal. Chem.* **2004**, *76*, 3373–3386. [CrossRef] [PubMed]
390. Reyes, D.R.; Iossifidis, D.; Auroux, P.-A.; Manz, A. Micro total analysis systems. 1. Introduction, theory, and technology. *Anal. Chem.* **2002**, *74*, 2623–2636. [CrossRef] [PubMed]
391. Auroux, P.-A.; Iossifidis, D.; Reyes, D.R.; Manz, A. Micro Total Analysis Systems. 2. Analytical Standard Operations and Applications. *Anal. Chem.* **2002**, *74*, 2637–2652. [CrossRef] [PubMed]
392. Dallakehnejad, M.; Mirbozorgi, S.A.; Niazmand, H. A numerical investigation of magnetic mixing in electroosmotic flows. *J. Electrost.* **2019**, *100*, 103354. [CrossRef]
393. Chakraborty, R.; Dey, R.; Chakraborty, S. Thermal characteristics of electromagnetohydrodynamic flows in narrow channels with viscous dissipation and Joule heating under constant wall heat flux. *Int. J. Heat Mass Transf.* **2013**, *67*, 1151–1162. [CrossRef]
394. Chakraborty, S.; Paul, D. Microchannel flow control through a combined electromagnetohydrodynamic transport. *J. Phys. D Appl. Phys.* **2006**, *39*, 5364–5371. [CrossRef]
395. Sarkar, S.; Ganguly, S. Fully developed thermal transport in combined pressure and electroosmotically driven flow of nanofluid in a microchannel under the effect of a magnetic field. *Microfluid. Nanofluidics* **2014**, *18*, 623–636. [CrossRef]
396. Xie, Z.-Y.; Jian, Y.-J. Entropy generation of two-layer magnetohydrodynamic electroosmotic flow through microparallel channels. *Energy* **2017**, *139*, 1080–1093. [CrossRef]
397. Zhao, G.; Jian, Y.; Chang, L.; Buren, M. Magnetohydrodynamic flow of generalized Maxwell fluids in a rectangular micropump under an AC electric field. *J. Magn. Magn. Mater.* **2015**, *387*, 111–117. [CrossRef]
398. Liu, Y.; Jian, Y.; Liu, Q.; Li, F. Alternating current magnetohydrodynamic electroosmotic flow of Maxwell fluids between two micro-parallel plates. *J. Mol. Liq.* **2015**, *211*, 784–791. [CrossRef]
399. Liu, Y.; Jian, Y. Electroviscous effect on electromagnetohydrodynamic flows of Maxwell fluids in parallel plate microchannels. *Appl. Math. Mech.* **2019**, *40*, 1457–1470. [CrossRef]
400. Sarkar, S.; Ganguly, S.; Dutta, P. Electrokinetically induced thermofluidic transport of power-law fluids under the influence of superimposed magnetic field. *Chem. Eng. Sci.* **2017**, *171*, 391–403. [CrossRef]
401. Sarkar, S.; Ganguly, S. Characterization of electromagnetohydrodynamic transport of power law fluids in microchannel. *J. Non-Newton. Fluid Mech.* **2017**, *250*, 18–30. [CrossRef]
402. Zhao, G.; Jian, Y.; Li, F. Streaming potential and heat transfer of nanofluids in microchannels in the presence of magnetic field. *J. Magn. Magn. Mater.* **2016**, *407*, 75–82. [CrossRef]
403. Ganguly, S.; Sarkar, S.; Hota, T.K.; Mishra, M. Thermally developing combined electroosmotic and pressure-driven flow of nanofluids in a microchannel under the effect of magnetic field. *Chem. Eng. Sci.* **2015**, *126*, 10–21. [CrossRef]
404. Xie, Z.; Jian, Y. Entropy generation of magnetohydrodynamic electroosmotic flow in two-layer systems with a layer of non-conducting viscoelastic fluid. *Int. J. Heat Mass Transf.* **2018**, *127*, 600–615. [CrossRef]
405. Patel, M.; Kruthiventi, S.H.; Kaushik, P. Rotating electroosmotic flow of power-law fluid through polyelectrolyte grafted microchannel. *Colloids Surf. B Biointerfaces* **2020**, *193*, 111058. [CrossRef]
406. Li, F.; Jian, Y.J.; Xie, Z.Y.; Liu, Y.B.; Liu, Q.S. Transient alternating current electroosmotic flow of a Jeffrey fluid through a polyelectrolyte-grafted nanochannel. *RSC Adv.* **2017**, *7*, 782–790. [CrossRef]
407. Hoshyargar, V.; Khorami, A.; Ashrafizadeh, S.N.; Sadeghi, A. Solute dispersion by electroosmotic flow through soft microchannels. *Sens. Actuators B Chem.* **2018**, *255*, 3585–3600. [CrossRef]
408. Sun, R.; Hu, W.; Jiao, B.; Qi, C. Heat transfer characteristics and entropy generation of electroosmotic flow in a rotating rectangular microchannel. *Int. J. Therm. Sci.* **2019**, *140*, 238–254. [CrossRef]
409. Sarkar, S.; Ganguly, S.; Dutta, P. Thermofluidic characteristics of combined electroosmotic and pressure driven flows in narrow confinements in presence of spatially non-uniform magnetic field. *Int. J. Heat Mass Transf.* **2017**, *104*, 1325–1340. [CrossRef]
410. Qi, C.; Wu, C. Electromagnetohydrodynamic flow in a rectangular microchannel. *Sens. Actuators B Chem.* **2018**, *263*, 643–660. [CrossRef]
411. Vargas, C.; Arcos, J.; Bautista, O.; Mendez, F. Hydrodynamic dispersion in a combined magnetohydrodynamic- electroosmotic-driven flow through a microchannel with slowly varying wall zeta potentials. *Phys. Fluids* **2017**, *29*, 092002. [CrossRef]
412. Mirza, I.A.; Abdulhameed, M.; Vieru, D.; Shafie, S. Transient electro-magneto-hydrodynamic two-phase blood flow and thermal transport through a capillary vessel. *Comput. Methods Programs Biomed.* **2016**, *137*, 149–166. [CrossRef] [PubMed]
413. Xie, Z.-Y.; Jian, Y.-J.; Li, F.-Q. Thermal transport of magnetohydrodynamic electroosmotic flow in circular cylindrical microchannels. *Int. J. Heat Mass Transf.* **2018**, *119*, 355–364. [CrossRef]
414. Chen, X.; Jian, Y.; Xie, Z.; Ding, Z. Thermal transport of electromagnetohydrodynamic in a microtube with electrokinetic effect and interfacial slip. *Colloids Surf. A Physicochem. Eng. Asp.* **2018**, *540*, 194–206. [CrossRef]
415. Zhao, G.; Wang, Z.; Jian, Y. Heat transfer of the MHD nanofluid in porous microtubes under the electrokinetic effects. *Int. J. Heat Mass Transf.* **2018**, *130*, 821–830. [CrossRef]

416. Ali, F.; Iftikhar, M.; Khan, I.; Sheikh, N.A.; Nisar, K.S. Time fractional analysis of electro-osmotic flow of Walters' sB fluid with time-dependent temperature and concentration. *Alex. Eng. J.* **2020**, *59*, 25–38. [CrossRef]
417. Tso, C.P.; Sundaravadivelu, K. Capillary flow between parallel plates in the presence of an electromagnetic field. *J. Phys. D Appl. Phys.* **2001**, *34*, 3522–3527. [CrossRef]
418. Duwairi, H.; Abdullah, M. Thermal and flow analysis of a magneto-hydrodynamic micropump. *Microsyst. Technol.* **2006**, *13*, 33–39. [CrossRef]
419. Shit, G.C.; Mondal, A.; Sinha, A.; Kundu, P. Electro-osmotically driven MHD flow and heat transfer in micro-channel. *Phys. A Stat. Mech. Its Appl.* **2016**, *449*, 437–454. [CrossRef]
420. Buren, M.; Jian, Y.; Chang, L.; Li, F.; Liu, Q. Combined electromagnetohydrodynamic flow in a microparallel channel with slightly corrugated walls. *Fluid Dyn. Res.* **2017**, *49*, 025517. [CrossRef]
421. Li, F.; Jian, Y.; Buren, M.; Chang, L. Effects of three-dimensional surface corrugations on electromagnetohydrodynamic flow through microchannel. *Chin. J. Phys.* **2019**, *60*, 345–361. [CrossRef]
422. Munshi, F.; Chakraborty, S. Hydroelectrical energy conversion in narrow confinements in the presence of transverse magnetic fields with electrokinetic effects. *Phys. Fluids* **2009**, *21*, 122003. [CrossRef]
423. Das, S.; Chakraborty, S.; Mitra, S.K. Magnetohydrodynamics in narrow fluidic channels in presence of spatially non-uniform magnetic fields: Framework for combined magnetohydrodynamic and magnetophoretic particle transport. *Microfluid. Nanofluidics* **2012**, *13*, 799–807. [CrossRef]
424. Jian, Y.; Chang, L. Electromagnetohydrodynamic (EMHD) micropumps under a spatially non-uniform magnetic field. *AIP Adv.* **2015**, *5*, 057121. [CrossRef]
425. Moghaddam, S. MHD micropumping of power-law fluids: A numerical solution. *Korea-Aust. Rheol. J.* **2013**, *25*, 29–37. [CrossRef]
426. Jian, Y. Transient MHD heat transfer and entropy generation in a microparallel channel combined with pressure and electroosmotic effects. *Int. J. Heat Mass Transf.* **2015**, *89*, 193–205. [CrossRef]
427. Shit, G.C.; Ranjit, N.K.; Sinha, A. Electro-magnetohydrodynamic Flow of Biofluid Induced by Peristaltic Wave: A Non-newtonian Model. *J. Bionic Eng.* **2016**, *13*, 436–448. [CrossRef]
428. Ranjit, N.K.; Shit, G. Entropy generation on electro-osmotic flow pumping by a uniform peristaltic wave under magnetic environment. *Energy* **2017**, *128*, 649–660. [CrossRef]
429. Kiyasatfar, M.; Pourmahmoud, N. Laminar MHD flow and heat transfer of power-law fluids in square microchannels. *Int. J. Therm. Sci.* **2016**, *99*, 26–35. [CrossRef]
430. Liu, Y.; Jian, Y.; Tan, W. Entropy generation of electromagnetohydrodynamic (EMHD) flow in a curved rectangular microchannel. *Int. J. Heat Mass Transf.* **2018**, *127*, 901–913. [CrossRef]
431. Mondal, A.; Mandal, P.K.; Weigand, B.; Nayak, A.K. Entropic and heat-transfer analysis of EMHD flows with temperature-dependent properties. *Fluid Dyn. Res.* **2020**, *52*, 065503. [CrossRef]
432. Ranjit, N.K.; Shit, G. Entropy generation on electromagnetohydrodynamic flow through a porous asymmetric micro-channel. *Eur. J. Mech.-B/Fluids* **2019**, *77*, 135–147. [CrossRef]
433. Ramesh, K.; Kumar, D.; Devakar, M. Electrokinetically modulated flow of couple stress magneto-nanofluids in a microfluidic channel. *Heat Transf.—Asian Res.* **2018**, *48*, 379–397. [CrossRef]
434. Noreen, S.; Waheed, S.; Lu, D.; Hussanan, A. Entropy generation in electromagnetohydrodynamic water based three Nano fluids via porous asymmetric microchannel. *Eur. J. Mech.-B/Fluids* **2020**, *85*, 458–466. [CrossRef]
435. Ghosh, U. Electro-magneto-hydrodynamics of non-linear viscoelastic fluids. *J. Non-Newton. Fluid Mech.* **2020**, *277*, 104234. [CrossRef]
436. Wang, X.; Xu, H.; Qi, H. Transient magnetohydrodynamic flow and heat transfer of fractional Oldroyd-B fluids in a microchannel with slip boundary condition. *Phys. Fluids* **2020**, *32*, 103104. [CrossRef]
437. Elmaboud, Y.A. Electroosmotic flow of generalized Burgers' fluid with Caputo–Fabrizio derivatives through a vertical annulus with heat transfer. *Alex. Eng. J.* **2020**, *59*, 4563–4575. [CrossRef]
438. Khan, M.; Farooq, A.; Khan, W.A.; Hussain, M. Exact solution of an electroosmotic flow for generalized Burgers fluid in cylindrical domain. *Results Phys.* **2016**, *6*, 933–939. [CrossRef]
439. Turkyilmazoglu, M. Analytic heat and mass transfer of the mixed hydrodynamic/thermal slip MHD viscous flow over a stretching sheet. *Int. J. Mech. Sci.* **2011**, *53*, 886–896. [CrossRef]
440. Turkyilmazoglu, M. Multiple solutions of heat and mass transfer of MHD slip flow for the viscoelastic fluid over a stretching sheet. *Int. J. Therm. Sci.* **2011**, *50*, 2264–2276. [CrossRef]
441. Turkyilmazoglu, M. The analytical solution of mixed convection heat transfer and fluid flow of a MHD viscoelastic fluid over a permeable stretching surface. *Int. J. Mech. Sci.* **2013**, *77*, 263–268. [CrossRef]
442. Chamkha, A.J.; Dogonchi, A.S.; Ganji, D.D. Magneto-hydrodynamic flow and heat transfer of a hybrid nanofluid in a rotating system among two surfaces in the presence of thermal radiation and Joule heating. *AIP Adv.* **2019**, *9*, 025103. [CrossRef]
443. Turkyilmazoglu, M. An analytical treatment for the exact solutions of MHD flow and heat over two–three dimensional deforming bodies. *Int. J. Heat Mass Transf.* **2015**, *90*, 781–789. [CrossRef]
444. Turkyilmazoglu, M. Magnetic Field and Slip Effects on the Flow and Heat Transfer of Stagnation Point Jeffrey Fluid over Deformable Surfaces. *Z. Nat. A* **2016**, *71*, 549–556. [CrossRef]

445. Turkyilmazoglu, M. Magnetohydrodynamic Moving Liquid Plug within a Microchannel: Analytical Solutions. *J. Biomech. Eng.* **2020**, *143*, 011012. [CrossRef]
446. Sheikholeslami, M.; Ganji, D.D. Numerical investigation of nanofluid melting heat transfer between two pipes. *Alex. Eng. J.* **2018**, *57*, 1261–1269. [CrossRef]
447. Salehi, S.; Nori, A.; Hosseinzadeh, K.; Ganji, D. Hydrothermal analysis of MHD squeezing mixture fluid suspended by hybrid nanoparticles between two parallel plates. *Case Stud. Therm. Eng.* **2020**, *21*, 100650. [CrossRef]
448. Hosseinzadeh, K.; Roghani, S.; Mogharrebi, A.R.; Asadi, A.; Ganji, D.D. Optimization of hybrid nanoparticles with mixture fluid flow in an octagonal porous medium by effect of radiation and magnetic field. *J. Therm. Anal.Calorim.* **2021**, *143*, 1413–1424. [CrossRef]
449. Sheikholeslami, M.; Ganji, D. Nanofluid hydrothermal behavior in existence of Lorentz forces considering Joule heating effect. *J. Mol. Liq.* **2016**, *224*, 526–537. [CrossRef]
450. Dogonchi, A.S.; Ganji, D.D. Thermal radiation effect on the Nano-fluid buoyancy flow and heat transfer over a stretching sheet considering Brownian motion. *J. Mol. Liq.* **2016**, *223*, 521–527. [CrossRef]
451. Mahapatra, B.; Bandopadhyay, A. Numerical analysis of combined electroosmotic-pressure driven flow of a viscoelastic fluid over high zeta potential modulated surfaces. *Phys. Fluids* **2021**, *33*, 012001. [CrossRef]
452. Yuan, S.; Jiang, B.; Peng, T.; Zhou, M.; Drummer, D. Investigation of efficient mixing enhancement in planar micromixers with short mixing length. *Chem. Eng. Process. Process Intensif.* **2021**, *171*, 108747. [CrossRef]
453. Mehta, S.K.; Pati, S. Enhanced Electroosmotic Mixing in a Wavy Micromixer Using Surface Charge Heterogeneity. *Ind. Eng. Chem. Res.* **2022**, *61*, 2904–2914. [CrossRef]
454. Wu, Y.; Hu, B.; Ma, X.; Zhang, H.; Li, W.; Wang, Y.; Wang, S. Generation of droplets with adjustable chemical concentrations based on fixed potential induced-charge electro-osmosis. *Lab Chip* **2021**, *22*, 403–412. [CrossRef]
455. Saha, S.; Kundu, B. Electroosmotic pressure-driven oscillatory flow and mass transport of Oldroyd-B fluid under high zeta potential and slippage conditions in microchannels. *Colloids Surf. A Physicochem. Eng. Asp.* **2022**, *647*, 129070. [CrossRef]
456. Li, Z.; Zhang, B.; Dang, D.; Yang, X.; Yang, W.; Liang, W. A review of microfluidic-based mixing methods. *Sens. Actuators A Phys.* **2022**, *344*, 113757. [CrossRef]
457. Liu, M.; Li, N.; Cui, S.; Li, G.; Yang, F. Biochemical Reaction Acceleration by Electrokinetic Mixing in a Microfluidic Chip. *J. Phys. Chem. Lett.* **2022**, *13*, 5633–5637. [CrossRef]
458. Nady, E.; Nagy, G.; Huszánk, R. Improvement in mixing efficiency of microfluidic passive mixers functionalized by microstructures created with proton beam lithography. *Chem. Eng. Sci.* **2022**, *247*, 117006. [CrossRef]
459. Zhao, S.; Huang, J.; Lei, J.; Huo, D.; Huang, Q.; Tan, J.; Li, Y.; Hou, C.; Tian, F. A portable and automatic dual-readout detector integrated with 3D-printed microfluidic nanosensors for rapid carbamate pesticides detection. *Sens. Actuators B Chem.* **2021**, *346*, 130454. [CrossRef]
460. Gopi, R.; Thangarasu, V.; Ramanathan, A. A critical review of recent advancements in continuous flow reactors and prominent integrated microreactors for biodiesel production. *Renew. Sustain. Energy Rev.* **2021**, *154*, 111869.
461. Granados-Ortiz, F.J.; Garcia-Cardosa, M.; Ortega-Casanova, J. Effect of wall modifications in a vortex shedding-based mechanical micromixer for heat/mass exchange. *Eur. J. Mech. B Fluids* **2022**, *92*, 174–190. [CrossRef]
462. Wu, M.; Gao, Y.; Ghaznavi, A.; Zhao, W.; Xu, J. AC electroosmosis micromixing on a lab-on-a-foil electric microfluidic device. *Sens. Actuators B Chem.* **2022**, *359*, 131611. [CrossRef]
463. Bai, C.; Zhou, W.; Yu, S.; Zheng, T.; Wang, C. A surface acoustic wave-assisted micromixer with active temperature control. *Sens. Actuators A Phys.* **2022**, *346*, 113833. [CrossRef]
464. Gimondi, S.; Guimarães, C.F.; Vieira, S.F.; Gonçalves, V.M.; Tiritan, M.E.; Reis, R.L.; Ferreira, H.; Neves, N.M. Microfluidic mixing system for precise PLGA-PEG nanoparticles size control. Nanomedicine: Nanotechnology. *Biol. Med.* **2022**, *40*, 102482.
465. Qamareen, A.; Ansari, M.A.; Alam, S.S. Mixing enhancement using the aiding and opposing flow effects in curved micro channel. *Chem. Eng. Process. Process Intensif.* **2022**, *176*, 108945. [CrossRef]
466. Hong, H.; Yeom, E. Numerical and experimental analysis of effective passive mixing via a 3D serpentine channel. *Chem. Eng. Sci.* **2022**, *261*, 117972. [CrossRef]
467. Banerjee, A.; Nayak, A.K. Influence of varying zeta potential on non-Newtonian flow mixing in a wavy patterned microchannel. *J. Non-Newton. Fluid Mech.* **2019**, *269*, 17–27. [CrossRef]
468. Rashidi, S.; Bafekr, H.; Valipour, M.S.; Esfahani, J.A. A review on the application, simulation, and experiment of the electrokinetic mixers. *Chem. Eng. Process* **2018**, *126*, 108–122. [CrossRef]
469. Mondal, B.; Mehta, S.K.; Pati, S.; Patowari, P.K. Numerical analysis of electroosmotic mixing in a heterogeneous charged micromixer with obstacles. *Chem. Eng. Process. Process Intensif.* **2021**, *168*, 108585. [CrossRef]
470. Channon, R.B.; Menger, R.F.; Wang, W.; Carrão, D.B.; Vallabhuneni, S.; Kota, A.K.; Henry, C.S. Design and application of a self-pumping microfluidic staggered herringbone mixer. *Microfluid. Nanofluidics* **2021**, *25*, 1–8. [CrossRef]
471. Cheng, Y.; Jiang, Y.; Wang, W. Numerical simulation for electro-osmotic mixing under three types of periodic potentials in a T-shaped micro-mixer. *Chem. Eng. Process. Process Intensif.* **2018**, *127*, 93–102. [CrossRef]
472. Shah, I.; Kim, S.W.; Kim, K.; Doh, Y.H.; Choi, K.H. Experimental and numerical analysis of Y-shaped split and recombination micro-mixer with different mixing units. *Chem. Eng. J.* **2018**, *358*, 691–706. [CrossRef]

473. Wang, X.; Liu, Z.; Yang, Y.; Cai, Y.; Song, Q.; Wang, B. Effects of sidewall roughness on mixing performance of zigzag microchannels. *Chem. Eng. Process* **2022**, *179*, 109057. [CrossRef]
474. Seo, H.-S.; Kim, Y.-J. A study on the mixing characteristics in a hybrid type microchannel with various obstacle configurations. *Mater. Res. Bull.* **2012**, *47*, 2948–2951. [CrossRef]
475. Nazari, M.; Rashidi, S.; Esfahani, J.A. Mixing process and mass transfer in a novel design of induced-charge electrokinetic micromixer with a conductive mixing-chamber. *Int. Commun. Heat Mass Transf.* **2019**, *108*, 104293. [CrossRef]
476. Vasista, K.N.; Mehta, S.K.; Pati, S. Electroosmotic mixing in a microchannel with heterogeneous slip dependent zeta potential. *Chem. Eng. Process. Process Intensif.* **2022**, *176*, 108940. [CrossRef]
477. Alipanah, M.; Hatami, M.; Ramiar, A. Thermal and rheological investigation of non-Newtonian fluids in an induced-charge electroosmotic micromixer. *Eur. J. Mech.-B/Fluids* **2021**, *88*, 178–190. [CrossRef]
478. Al-Ali, A.; Waheed, W.; Abu-Nada, E.; Alazzam, A. A review of active and passive hybrid systems based on Dielectrophoresis for the manipulation of microparticles. *J. Chromatogr. A* **2022**, *1676*, 463268. [CrossRef]
479. Kwon, T.; Choi, K.; Han, J. Separation of Ultra-High-Density Cell Suspension via Elasto-Inertial Microfluidics. *Small* **2021**, *17*, 2101880. [CrossRef] [PubMed]
480. Ghasemi, A.; Ramiar, A. Numerical investigation of continuous acoustic particle separation using electrothermal pumping in a point of care microfluidic device. *Chem. Eng. Process. Process Intensif.* **2022**, *176*, 108964. [CrossRef]
481. Ebrahimi, S.; Shamloo, A.; Alishiri, M.; Mofrad, Y.M.; Akherati, F. Targeted pulmonary drug delivery in coronavirus disease (COVID-19) therapy: A patient-specific in silico study based on magnetic nanoparticles-coated microcarriers adhesion. *Int. J. Pharm.* **2021**, *609*, 121133. [CrossRef] [PubMed]
482. Poncelet, L.; Malic, L.; Clime, L.; Geissler, M.; Morton, K.J.; Nassif, C.; Da Fonte, D.; Veilleux, G.; Veres, T. Multifunctional magnetic nanoparticle cloud assemblies for in situ capture of bacteria and isolation of microbial DNA. *Anal.* **2021**, *146*, 7491–7502. [CrossRef] [PubMed]
483. Jia, L.; Li, X.; Liu, H.; Xia, J.; Shi, X.; Shen, M. Ultrasound-enhanced precision tumor theranostics using cell membrane-coated and pH-responsive nanoclusters assembled from ultrasmall iron oxide nanoparticles. *Nano Today* **2021**, *36*, 101022. [CrossRef]
484. Mohammadi, S.; Rafii-Tabar, H.; Sasanpour, P. Contribution of the dipole–dipole interaction to targeting efficiency of magnetite nanoparticles inside the blood vessel: A computational modeling analysis with different magnet geometries. *Phys. Fluids* **2022**, *34*, 033601. [CrossRef]
485. Das, D.; Al-Rjoub, M.F.; Heineman, W.R.; Banerjee, R.K. Efficient capture of magnetic microbeads by sequentially switched electroosmotic flow—An experimental study. *J. Micromech. Microeng.* **2016**, *26*, 55013. [CrossRef]
486. Alipanah, M.; Hafttananian, M.; Hedayati, N.; Ramiar, A.; Alipanah, M. Microfluidic on-demand particle separation using induced charged electroosmotic flow and magnetic field. *J. Magn. Magn. Mater.* **2021**, *537*, 168156. [CrossRef]
487. Teodoro, C.; Bautista, O.; Mendez, F. Mass transport and separation of species in an oscillating electro-osmotic flow caused by distinct periodic electric fields. *Phys. Scr.* **2019**, *94*, 115012. [CrossRef]
488. Cao, L.; Zhang, P.; Si, X. Electroosmotic flow of two-layer fluid containing Oldroyd-B fluid with fractional derivative in a rotating microparallel channel. *Microfluid. Nanofluidics* **2022**, *26*, 1–12. [CrossRef]
489. Xiao, B.; Wang, W.; Zhang, X.; Long, G.; Fan, J.; Chen, H.; Deng, L. A novel fractal solution for permeability and Kozeny-Carman constant of fibrous porous media made up of solid particles and porous fibers. *Powder Technol.* **2019**, *349*, 92–98. [CrossRef]
490. Liang, M.; Fu, C.; Xiao, B.; Luo, L.; Wang, Z. A fractal study for the effective electrolyte diffusion through charged porous media. *Int. J. Heat Mass Transf.* **2019**, *137*, 365–371. [CrossRef]
491. Villarroel-Schneider, J.; Malmquist, A.; Araoz, J.A.; Martí-Herrero, J.; Martin, A. Performance Analysis of a Small-Scale Biogas-Based Trigeneration Plant: An Absorption Refrigeration System Integrated to an Externally Fired Microturbine. *Energies* **2019**, *12*, 3830. [CrossRef]
492. Fraga-Lamas, P.; Fernández-Caramés, T.M.; Suárez-Albela, M.; Castedo, L.; González-López, M. A Review on Internet of Things for Defense and Public Safety. *Sensors* **2016**, *16*, 1644. [CrossRef]
493. Bußmann, A.B.; Grünerbel, L.M.; Durasiewicz, C.P.; Thalhofer, T.A.; Wille, A.; Richter, M. Microdosing for drug delivery application—A review. *Sens. Actuator A Phys.* **2021**, *330*, 112820. [CrossRef]
494. Kundu, B. Exact analysis for propagation of heat in a biological tissue subject to different surface conditions for therapeutic applications. *Appl. Math. Comput.* **2016**, *285*, 204–216. [CrossRef]
495. Kundu, B.; Dewanjee, D. A new method for non-Fourier thermal response in a single layer skin tissue. *Case Stud. Therm. Eng.* **2015**, *5*, 79–88. [CrossRef]